学位論文　（要約）

Petrology and geochemistry of mafic rocks in the Acasta Gneiss Complex: Implications for the Hadean mantle evolution

（アカスタ片麻岩体苦鉄質岩の岩石学的・地球化学的特徴
から示唆される冥王代マントル進化）

平成 28 年 12 月博士（理学）申請

東京大学大学院理学系研究科
地球惑星科学専攻
越田　渓子

Abstract

The first billion years' history of the earth is still poorly understood because terrestrial rocks with the ages are scarcely preserved. Especially, a period of the first 500 million years is named the Hadean, and no Hadean rocks are preserved over the world. The Hadean is well known as the most dramatic period that many drastic events such as magma-ocean, fore-formation and late heavy bombardment occurred based on geochemistry of meteorites, planetary science and numerical simulation. However, it is necessary to study the Eoarchean crusts to quantitatively unravel the early Earth's history. The Acasta Gneiss Complex (AGC) is one of the rare Eoarchean geologic bodies, located in the western margin of the Slave Craton, Canada, and is composed of felsic to intermediate gneisses with subordinate amounts of mafic rocks. The felsic to intermediate gneisses are relatively well understood, and comprise 4.03-3.6 Ga orthogneisses, including the oldest terrestrial rocks with 4.03 Ga age. On the other hand, the mafic rocks are still enigmatic because they suffered from intense metamorphisms and deformations. This study aims to obtain physico-chemical constraints on the Hadean mantle and propose a new picture of early mantle evolution based on geological, petrological and geochemical investigations of the oldest mafic rocks in AGC.

We conducted a petrographic study of over 100 mafic rocks all over the AGC to estimate the metamorphic grade and to select the least altered samples for whole-rock analyses of major and trace element compositions. The mafic rocks mainly consist of fine to coarse-grained hornblende and plagioclase with small amount of quartz, chlorite and ilmenite. Especially, garnet-bearing mafic rocks occur at the northeastern part of the AGC. The modal amounts of the hornblende and plagioclase are variable and some samples contain quite large amounts, over 90%, of hornblende. They commonly suffered from amphibolite to upper amphibolite facies metamorphism, and differences of mineral assemblages and compositions among mafic rocks are due to difference of their whole-rock compositions, rather than difference of metamorphic grade. The mafic rocks show

large variations in the major and trace element compositions, possibly due to later partial melting and infiltration of metamorphic fluids/melts derived from mafic rocks and/or surrounding granitoids. The mafic rocks are subdivided into three groups based on the rare earth element (REE) patterns: highly variable light REE-enriched pattern, flat REE pattern and slightly light REE-enriched pattern with positive Eu anomaly, respectively. The samples, which have flat REE patterns and whose high field strength element (HFSE) and REE contents are well correlated with immobile Zr contents, were selected as the least altered samples to estimate their source mantle because the infiltration of metamorphic fluids/melts increases the light REE contents relative to the middle and heavy REE contents and more severely disturbs other trace element contents than Zr contents. The least altered mafic rocks have chondritic trace element relative abundances with negative Nb and Ta anomalies. This implies that the Nb and Ta were partitioned into the metallic core to form a Nb and Ta-deficit primitive mantle.

The least altered mafic rocks show a positive correlation on a $^{187}Re/^{188}Os$ vs $^{187}Os/^{188}Os$ diagram, yielding a formation age of 4272±300 Ma. The age is consistent with the field occurrence of mafic rocks because they were intruded by orthogneisses with 4.03 to 3.6 Ga ages. The highly radiogenic initial $^{187}Os/^{188}Os$ ratio suggests that their source material was a pre-late veneer mantle with a high Re/Os ratio. However, geochemical signatures, which the initial $^{187}Os/^{188}Os$ ratio overlaps with a chondritic value within the error and their highly siderophile element (HSE) abundances are similar to those of modern basalts, indicate that their source mantle had modern mantle-like high HSE contents, implying that the late veneer event and later homogenization took place before 4.3 Ga.

Two ^{147}Sm-^{143}Nd and ^{176}Lu-^{176}Hf isotope systems of the least altered samples yield young metamorphic ages of 2020±290 Ma and 3016±560 Ma, respectively. On the other hand, their $^{142}Nd/^{144}Nd$ ratios are identical to those of a modern mantle with a suprachondritic value. Their chondritic initial $^{143}Nd/^{144}Nd$ ratio and REE patterns, and suprachondritic $^{142}Nd/^{144}Nd$ ratios

indicate that their source material had a chondritic Sm/Nd ratio and a suprachondritic (modern mantle value) $^{142}Nd/^{144}Nd$ ratio at 4.3 Ga. This is the first evidence that > 3.7 Ga source mantle had a modern mantle-like (normal) $^{142}Nd/^{144}Nd$ ratio. Two possible scenarios account for the Hadean mantle with the primitive mantle-like trace element contents and normal $^{142}Nd/^{144}Nd$ ratio at 4.3 Ga. One is that the early mantle convection was rapid enough to homogenize large-scale mantle heterogeneity due to a magma ocean until 4.3 Ga. The Acasta mafic rocks was derived from the homogenized primitive mantle, whereas the 3.8-3.7 Ga Isua mafic rocks with excess $\mu^{142}Nd$ values were formed from a shallow depleted mantle possibly due to progressive extraction of primitive crusts. This scenario is supported by the HSE contents and ^{187}Re-^{187}Os isotopes. Another model suggests that the extent of a magma ocean was limited and non-melting primitive parts remained in the deep mantle, and that the Acasta mafic rocks were formed from the deep primitive mantle, whereas the Isua mafic rocks were derived from the early differentiated upper mantle.

CONTENTS

Chapter 1

Introduction

The Hadean is defined as a period when no rock record is preserved in the world, and ranges from the beginning of the solar system (~4.567 Ga: Connelly et al., 2012) to the age of the oldest terrestrial rock (4.03 Ga: Bowring and Williams, 1999). The Earth was highly active in the dawn so that many large-scaled structural differentiations occurred in the early earth. Our planet, Earth, was formed through aggregation of dusts in a circumstellar protoplanetary disk. When the objects were larger than a kilometer in diameter, gravitational force became strong enough for gravitationally driven runaway growth to begin. After Earth's size reached about 10% of its current size (Stevenson, 1981), significant melting started to occur on surface of the earth to form an extensively-molten outer layer, namely magma ocean. Droplets of liquid metal were formed and fell in the magma ocean (Rubie et al., 2003). Based on a deep magma ocean model, the droplets kept equilibrated with surrounding silicate melts during the fall to the bottom of a magma ocean and were accumulated at the bottom. And then, they were segregated as large falling diapirs to form the core at the center of the earth (Karato and Murthy, 1997). Short-lived ^{182}Hf-^{182}W isotope systematic observations indicate very early formation of the planetary cores separated from their silicate mantles, and estimated the earliest possible age of core formation at *ca.* 30 million years after the Solar system formation (Kleine et al., 2002; Yin et al., 2002). At the last stage of the accretion, collision(s) of mars-sized embryo(s), named "giant impact(s)", resulted in large-scale melting of, possibly up to the entire, mantle and early silicate differentiation (e.g. Solomatov and Stevenson 1993; Caro et al. 2005, Corgne et al. 2005).

It is considered that major events to form the solid earth with present characteristics had already taken place in the Hadean, but there remain numerous unresolved crucial issues about the early earth's evolution: (1) the composition of the

Bulk Silicate Earth, (2) the structure and chemical composition of the mantle after the magma ocean, and (3) timing and duration of the late accretion related to abundances of highly siderophile elements in early terrestrial mantle.

No preservation of the Hadean terrestrial rocks is the most important reason why an early history of the earth is still unresolved. The accessible Hadean terrestrial materials are only detrital zircons, dated up to 4.37 Ga, from the Jack Hills conglomerates in Australia (Wilde et al., 2001; Valley et al., 2014). The fact that the source rocks or magmas from which the zircons were crystallized are missed also makes it difficult to elucidate the early evolution. However, the Hadean zircons provide some essential information about the early Earth. For example, their oxygen isotope compositions suggested the presence of liquid water on the Earth's surface (Mojzsis et al., 2001; Valley et al., 2002). But, because zircons are generally crystallized from an evolved magma (Belousova et al., 2002; Crowley et al., 2005), they have little information about mantle composition and evolution. As a result, most of previous studies about the early Earth worked on meteorites and theoretical calculations.

There are very few Eoarchean rocks on the earth: the Acasta Gneiss Complex, Canada (4.03 Ga; Bowring and Williams, 1999), the Itsaq Gneiss Complex, Greenland (3.85-3.60 Ga; Nutman et al. 1996), the Napier complex, Antarctica (3.95-3.8 Ga; Williams et al. 1986; Harley et al., 2007), Saglek-Hebron block, Labrador (3.95 Ga; Shimojo et al., 2016), Nuvvuagittuq Supracrustal Belt in Quebec, Canada (3.8 or 4.3 Ga; Cates and Mojzsis, 2007; O'Neil et al., 2008) and the Anshan area, China (3.8 Ga; Song et al. 1996). Those terrains have suffered from multiple phases of deformation and metamorphism so that primary geochemical signatures were erased. In addition, they mainly consist of felsic gneisses, and the supracrustal rocks, accompanied with

the felsic rocks, are much lesser than the felsic rocks even in the Inukjuak Block of the Hudson Bay Terrane, where the Nuvvuagittuq supracrustal belt occurs, as well as the Itsaq Gneiss Complex, Napier complex and Saglek Block. The felsic gneisses commonly contain many igneous zircons so that the magmatic ages can be determined relatively easily and precisely. But, they are, generally, formed due to remelting of mafic rocks rather than mantle melting so that they have little information of the mantle. On the other hand, mafic rocks are directly produced by the mantle melting so that they still possess characteristics of their mantle sources. A variety of isotope analyses including ^{146,147}Sm-^{143,142}Nd, ^{176}Lu-^{176}Hf and ^{18}7Re-^{187}Os systematics of the numerous old mafic rocks provided much information of the early Earth and many possible scenarios about the early mantle evolution (e.g. Frei et al., 2004; Rizo et al., 2011; Rizo et al., 2016; O'Neil et al., 2016; Guitreau et al., 2013; O'Neil et al., 2012). However, almost all of the mafic rocks are only from the Itsaq Gneiss Complex and Nuvvuagittuq supracrustal belt, which are relatively less metamorphosed and contain large amount of mafic rocks among other old terrains. It still remains unknown whether the obtained geochemical signatures were derived from global features in the Hadean because the accessible rocks are limited to only the tow supracrustal belts. Therefore, it is quite significant to study the mafic rocks in other terrains to understand the global mantle evolution.

The Acasta Gneiss Complex, Canada, is one of the oldest terrains, and mainly consists of 4.0-3.6 Ga felsic to intermediate gneisses with minor mafic rocks (e.g. Bowring et al., 1990; Iizuka et al., 2007). Numerous previous studies carried on petrological and geochronological investigations on felsic and intermediate gneisses, providing their precise ages, formation processes and the characteristics of source materials (e.g. Bowring et al., 1990; Iizuka et al., 2007; Mojzsis et al., 2014; Reimink

et al., 2014). On the other hand, there are only few studies about the mafic rocks so that even their ages have not been determined yet. Recent more advanced geochemical analyses of ^{142}Nd and ^{182}W isotopes of a few mafic rocks were conducted to obtain geochemical signatures of the source mantle (Roth et al., 2014; Willbold et al., 2015). However, it is a key issue to obtain the original geochemical signatures from the mafic rocks because the AGC underwent multiple metamorphisms and deformations so that the mafic rocks were modified in the compositions.

The main purpose of this thesis is to obtain constraints on the Hadean mantle evolution from Acasta mafic rocks: petrology of the Acasta mafic rocks over the AGC to understand the geochemical variations of the mafic rocks due to petrological and metamorphic processes and select the least modified samples with original geochemical signatures, and comprehensive isotope geochemistry of ^{187}Re-^{187}Os, ^{176}Lu-^{176}Hf and ^{147,146}Sm-^{143,142}Nd systems to obtain their magmatic age(s) and geochemical signatures of their source mantle(s).

References

Belousova, E.A., Griffin, W.L., O'Reilly, S.Y., and Fisher, N.I., 2002. Igneous zircon: Trace element composition as an indicator of source rock type: Contributions to Mineralogy and Petrology, v. 143, p. 602–622.

Bowring S. A., Housh T. B. and Isachsen C. E., 1990. The Acasta Gneisses: remnant of Earth's early crust. In Origin of the Earth (eds. H. E. Newsom and J. H. Jones). Oxford University Press, New York, pp. 319–343.

Bowring, S.A., Williams, I.S., 1999. Priscoan (4.00–4.03Ga) orthogneisses from northwestern Canada.Contrib.Mineral.Petrol.134,3–16.

Bowring S. A., Housh T. B. and Isachsen C. E. 1990. The Acasta Gneisses: remnant of Earth's early crust. In Origin of the Earth (eds. H. E. Newsom and J. H. Jones). Oxford University Press, New York, pp. 319–343.

Caro G, Bourdon B, Wood BJ, Corgne A. 2005. Trace element fractionation generated by melt segregation from a magma ocean. Nature 436:246–49.

Cates, N.L. and Mojzsis, S.J., 2007. Pre-3750 Ma supracrustal rocks from the Nuvvuagittuq supracrustal belt, northern Quebec. Earth and Planetary Science Letters, 255, 9-21.

Connelly J. N., Bizarro M., Krot A. N., Nordlund A., Wielandt D. and Ivanova M. A., 2012. The absolute chronology and thermal processing of solids in the solar protoplanetary disk. Science 338 , 651 - 655.

Corgne A, Liebske C, Wood BJ, Rubie DC, Frost DJ. 2005. Silicate perovskite-melt partitioning of trace elements and geochemical signature of a deep perovskitic reservoir. Geochim. Cosmochim. Acta 69:485–96

Crowley, J.L., Myers, J.S., Sylvester, P.J., and Cox, R.A., 2005, Detrital zircons from the Jack Hills and Mount Narryer, Western Australia: Evidence for diverse .4.0

Ga source rocks: Journal of Geology, v. 113, p. 239–263.

Frei, R., Polat, A., Meibom, A., 2004. The Hadean upper mantle conundrum: evidence for source depletion and enrichment from Sm–Nd, Re–Os, and Pb isotopic com-positions in 3.71Gy boninite-like metabasalts from the Isua Supracrustal Belt, Greenland. Geochim. Cosmochim. Acta68 (7), 1645–1660.

Karato S-I and Rama Murthy V 1997. Core formation and chemical equilibrium in the Earth. Part I: Physical considerations. Physics of the Earth and Planetary Interiors 100(1–4): 61–79.

Kleine T, Munker C, Mezger K, and Palme H 2002. Rapid accretion and early core formation on asteroids and the terrestrial planets from Hf–W chronometry. Nature 418: 952–955.

Nutman, A. P., McGregor, V. R., Friend, C. R. L., Bennett, V. C., Kinny, P. D., 1996. The Itsaq gneiss complex of southern West Greenland; the world's most extensive record of early crustal evolution (3900-3600 Ma). Precambrian Research 78, 1-39.

Harley, S.L., Kelly, N.M., Martin, J., van Kranendonk, R.H.S., and Vickie, C.B. 2007 Ancient Antarctica: The Archaean of the East Antarctic Shield, Developments in Precambrian Geology, Elsevier, pp. 149–186

Guitreau, M., Blichert-Toft, J., Mojzsis, S. J., Roth, A. S., & Bourdon, B. (2013). A legacy of Hadean silicate differentiation inferred from Hf isotopes in Eoarchean rocks of the Nuvvuagittuq supracrustal belt (Québec, Canada). Earth and Planetary Science Letters, 362, 171-181.

Iizuka T., Komiya T., Ueno Y., Katayama I., Uehara Y., Maruyama S., Hirata T., Johnson S. P. and Dunkley D. J. 2007. Geology and zircon geochronology of the Acasta Gneiss Complex, northwestern Canada: new constraints on its

tectonothermal history. Precambrian Research. 153, 179–208.

Iizuka T., Komiya T., Ueno Y., Katayama I., Uehara Y., Maruyama S., Hirata T., Johnson S.P. Dunkley D.J., 2007. Geology and zircon geochronology of the Acasta Gneiss Complex, northwestern Canada: new constraints on its tectonothermal history. Precamb. Res. 153, 179–208.

Li, X.H., Li, Z.X., Zhou, H., Liu, Y., Kinny, P.D. 2002. U–Pb zircon geochronology, geochemistry and Nd isotopic study of Neoproterozoic bimodal volcanic rocks in the Kangdian Rift of South China: implications for the initial rifting of Rodinia. Precambrian Research, 113(1), 135-154.

Mojzsis, S.J., Cates, N.L., Caro, G., Trail, D., Abramov, O., Guitreau, M., Bleeker, W., 2014. Component geochronology in the polyphase ca. 3920Ma Acasta Gneiss. Geochimica et Cosmochimica Acta, 133, 68-96.

O'Neil, J., Carlson, R.W., Francis, D., Stevenson, R.K., 2008. Neodymium-142 Evidence for Hadean Mafic Crust., Science, 321, pp.1828-1831.

O'Neil, J., Carlson, R.W., Paquette, J.-L., Francis, D., 2012. Formation age and meta-morphic history of the Nuvvuagittuq greenstone belt. Precambrian Res.220–221, 23–44.

Reimink, J.R., Chacko, T., Stern, R.A., Heaman, L.M., 2014. Earth [rsquor] s earliest evolved crust generated in an Iceland-like setting. Nature Geoscience, 7(7), 529-533.

Rizo, H., Boyet, M., Blichert-Toft, J., Rosing, M., 2011. Combined Nd and Hf iso-tope evidence for deep-seated source of Isua lavas. Earth Planet. Sci. Lett.312, 267–279.

Rizo, H., Walker, R.J., Carlson, R.W., Touboul, M., Horan, M.F., Puchtel, I.S., Boyet, M., Rosing, M.T., 2016. Early Earth differentiation investigated through 142Nd,

182W, and highly siderophile element abundances in samples from Isua, Greenland. Geochim. Cosmochim. Acta175, 319–336.

Rubie DC, Melosh HJ, Reid JE, Liebske C, and Righter K 2003. Mechanisms of metal-silicate equilibration in the terrestrial magma ocean. Earth and Planetary Science Letters 205: 239–255.

Shimojo, M., Yamamoto, S., Sakata, S., Yokoyama, T. D., Maki, K., Sawaki, Y., Ishikawa, A., Aoki, K., Aoki, S., Koshida, K., Tashiro, T., Hirata, T., Collerson, K. D. & Komiya, T., 2016. Occurrence and geochronology of the Eoarchean, ~3.9 Ga, Iqaluk Gneiss in the Saglek Block, northern Labrador, Canada: Evidence for the oldest supracrustal rocks in the world. Precambrian Research, 278, 218-243.

Solomatov VS, Stevenson DJ. 1993. Nonfractional crystallization of a terrestrial magma ocean. J. Geophys. Res. 98:5391–406

Song B., Nutman, A. P., Liu D., Wu J., 1996. 3800 to 2500 Ma crustal evolution in the Anshan area of Liaoning Province, northeastern China. Precambrian Research 78, 79-94.

Stevenson, DJ (1981) Models of the Earth's core. Science 214: 611–619.

Valley, J. W., Cavosie, A. J., Ushikubo, T., Reinhard, D. A., Lawrence, D. F., Larson, D. J., Clifton, P., Kelly, T., Wilde, S., Moser, D., & Spicuzza, M. J. 2014. Hadean age for a post-magma-ocean zircon confirmed by atom-probe tomography. Nature Geoscience, 7(3), 219-223.

Wilde, S. A., Valley, J. W., Peck, W. H., & Graham, C. M. 2001. Evidence from detrital zircons for the existence of continental crust and oceans on the Earth 4.4 Gyr ago. Nature, 409(6817), 175-178.

Willbold, M., Mojzsis, S. J., Chen, H. W., & Elliott, T. 2015. Tungsten isotope

composition of the Acasta Gneiss Complex. Earth and Planetary Science Letters, 419, 168-177.

Williams, I.S., Black, L.P., Compston, W., 1986. Four zircon ages from one rock: the evolution of a 3930 Ma-old granulite from Mount Sones, Antarctica, Contributions to Mineralogy and Petralogy 94, 427-437

Yin, Q., Jacobsen, S. B., Yamashita, K., Blichert-Toft, J., Télouk, P., & Albarede, F. 2002. A short timescale for terrestrial planet formation from Hf–W chronometry of meteorites. Nature, 418(6901), 949-952.

Chapter 2

Petrology and geochemistry of mafic rocks in the Acasta Gneiss Complex: Implications for the oldest mafic rocks and their origin

Abstract

The Acasta Gneiss Complex, located in the western part of the Slave Province, Canada, is widely recognized as the oldest Eoarchean terrane. In addition to felsic gneisses with the ages of 3.6-4.0 Ga, minor mafic rocks occur as rounded to elliptical enclaves and inclusions within the felsic gneisses. Despite serving as potential sources of geochemical information on the Hadean mantle, the mafic rocks have received less attention in previous studies. Thus, we conducted a comprehensive geological petrological and geochemical investigation on the Acasta mafic rocks to constrain their petrogenesis and geodynamic setting.

The mafic rocks comprise massive to weakly foliated amphibolite, garnet amphibolite and hornblendite, with variable abundances of hornblende, plagioclase, chlorite and quartz and subordinate clinopyroxene, garnet and cummingtonite. They commonly underwent high-grade metamorphic recrystallization under amphibolite to upper-amphibolite facies conditions. The observed variations in mineral assemblages, abundances and compositions reflect large differences in whole-rock compositions, likely caused by crustal anatexis during the Eoarchean thermal events responsible for the generation of the surrounding felsic gneisses. Infiltration or extraction of felsic melts formed due to partial melting of precursor rocks can account for an overall negative correlation between Al_2O_3 and MgO contents and variable enrichments in the incompatible elements.

Despite the widespread influence of anatexis on the geochemistry of Acasta mafic rocks, we identified the precursor compositions of the least-modified amphibolites as basaltic magmas. They are characterized by intermediate Al_2O_3 and

MgO contents on the observed array and by near chondritic patterns for incompatible trace elements, except for slightly negative Nb and Ta anomalies. We considered two scenarios to explain the origin of Eoarchean basaltic rocks with Nb-Ta anomalies: (1) generation of Nb-Ta deficient basaltic magma in a suprasubduction setting, analogous to modern arcs-derived magmas, and (2) generation of Nb-Ta deficient basaltic magma from the melting of a Nb-Ta deficient primitive mantle, possible if the core contains significant proportions of the Earth's Nb and Ta budget. Although the operation of plate tectonics and the presence of subduction zones at the end of Hadean may be an attractive explanation for the observed Nb-Ta depletions, the chondritic relative proportions of other immobile trace elements for Acasta mafic rocks leave open the possibility of their formation from an Nb-Ta deficient primitive mantle.

1. Introduction

The Hadean is the earliest period of Earth's history, from its birth to the beginning of Eoarchean at 4.03 Ga, which is the age of the oldest terrestrial rock (Bowring and Wiliams, 1999). A global magma ocean was thought to be present in the first hundred million years of the Hadean Earth, as a natural consequence of planetary evolution due to the gravitational energy released by core formation, as well as highly energetic collisions of Moon-to Mars-sized bodies (e.g. Rubie et al., 2011). To unravel the nature and timing of early differentiation processes via crystallization of magma ocean, several short-lived nuclide systems have been utilized. For example, the application of ^{182}Hf-^{182}W short-lived radioisotope system suggests that metallic core was rapidly separated from the silicate mantles in the first 30 million years of Solar system history (Kleine et al., 2002). Furthermore, ^{146}Sm-^{142}Nd isotope systematics of Archean igneous and sedimentary rocks suggest that the mantle underwent a rapid differentiation in the early Earth and that the differentiated mantle was not completely homogenized until at least the Eoarchean (e.g. Boyet and Carlson et al., 2005; Bennett et al., 2007; O'Neil et al., 2011; Rizo et al., 2013). However, details of the early differentiation of the solid Earth due to crystallization of magma ocean and the subsequent evolution of mantle-crust system still remain obscure (Caro et al. 2005, Labrosse et al. 2007; Caro, 2011)

Scarce Eoarchean rocks are preserved on Earth, possibly because subsequent mantle convection and plate tectonics have removed all Hadean rocks and almost all Eoarchean rocks. They include the Acasta Gneiss Complex, Canada (4.03 Ga; Bowring & Williams, 1999), the Itsaq Gneiss Complex, Greenland (3.85-3.60 Ga; Nutman et al. 1996), the Napier Complex, Antarctica (3.95-3.8 Ga; Williams et al., 1986), Saglek-Hebron block, Labrador (3.95 Ga; Komiya et al., 2015), the Nuvvuagittuq

supracrustal belt, Canada (3.75 Ga; Cates & Mojzsis, 2007) and the Anshan area, North China (3.8 Ga; Song et al., 1996). Most of these terranes are predominantly composed of felsic rocks, including tonalite, trondhjemite and granodiorite (TTG), with minor ultramafic and mafic rocks and metasedimentary rocks. They have suffered severe deformation and metamorphism such that primary geological and geochemical signatures are poorly preserved. Many studies of the Earth's early crusts focus on felsic rocks because they commonly contain igneous zircons providing precise U-Pb ages (e.g. Bowring et al., 1989; Mojzsis et al., 2014; Reimink et al., 2014). However, mafic rocks, directly derived from the mantle, can be expected to provide more information on solid Earth evolution. Studies on mafic rocks in the Itsaq Gneiss Complex and Nuvvuagittuq supracrustal belt suggest that plate tectonics and the modern style of recycling of oceanic crust could go back to at least 3.8 Ga (e.g. Nutman et al., 1996; Komiya et al., 1999, 2004; Polat et al., 2002; Polat et al., 2003; Jenner et al., 2009; Furnes et al., 2009; Polat et al., 2011; Polat et al., 2012). Therefore, in order to decode the characteristics and evolution of the solid Earth before 3.8 Ga, it is necessary to clarify the origin of older mafic rocks.

The Acasta Gneiss Complex (AGC) is one of the oldest Eoarchean terranes and is dominated by felsic rocks composed of tonalitic, granodioritic and granitic gneisses (e.g. Bowring et al., 1990; Iizuka et al., 2007a). Geochronological studies show different generations of felsic plutonic rocks, with the oldest suites formed at 3.92 to 4.03 Ga (Bowring et al., 1990; Bowring & Williams, 1999; Bowring and Housh, 1995; Iizuka et al., 2007a; Reimink et al., 2014). Zircons extracted from these have sub-chondritic initial $^{176}Hf/^{177}Hf$ values, suggesting that they were formed from a Hadean crustal component (Amelin et al., 1999, 2000; Iizuka et al., 2009). The presence of a 4200 Ma inherited zircon core also supports the presence of Hadean

granitoid crust in the area (Iizuka et al., 2006). Although previous studies analyzed whole-rock geochemistry mainly from felsic rocks (Bowring et al., 1990; Mojzsis et al., 2014; Reimink et al., 2014), the AGC also contains mafic rocks (e.g. Bowring et al., 1990; Bowring & Housh, 1995; Bleeker and Stern, 1997). A detailed geological study showed some of these mafic rocks are structurally cut by felsic gneisses, implying they are the Hadean fragments (Iizuka et al., 2007a). However, because of numerous metamorphic events and deformation, little is known about mafic rocks from the AGC (Moorbath et al., 1997). This work presents the petrology and geochemistry of these mafic rocks in an attempt to understand Eoarchean mantle evolution based on the least altered rocks.

2. Geological outline of the Acasta Gneiss Complex

2-1. Slave province

The Slave province is an Archean granite greenstone terrane located in the northwestern part of the Canadian Shield with an area of approximately 190,000 km2 (Hoffman, 1989). It is bounded on the east by the 2.0-1.9 Ga Thelon orogen, and on the west by the 1.9-1.8 Ga Wopmay orogen. The slave province mainly consists of pre-2.8 Ga basement rocks, metavolcanic rocks erupted between 2.66 and 2.72 Ga, metaturbidites largely derived from the 2.72–2.65 Ga volcanic and plutonic rocks intruded into the supracrustal sequence between 2.62 and 2.58 Ga (van Breemen et al., 1992; Villeneuve and van Breemen, 1994). The Slave Province can be broadly subdivided along a north–south-trending Nd-Pb isotopic boundary that separates an eastern juvenile Neoarchean-dominated domain from a central and western region characterized by pre-2.8 Ga (4.03-2.80 Ga) basement rocks. The pre-2.8 Ga basement gneisses consist of amphibolite-grade granitic gneisses, granitoids and supracrustal

rocks comprising quartzite, banded iron formation, conglomerate and volcanic rocks that pre-date the deposition of supracrustal rocks. Except for Acasta gneiss complex, most basement occurrences yield only post-3.5 Ga crustal histories. A summary of the Slave basement protolith ages obtained by combining the detrital zircon age populations from pre-2.8 Ga supracrustal rocks and the few direct age determinations of exposed basement indicates at least four significant periods of Mesoarchean crustal growth at 3.40, 3.15, 2.95, and 2.83 Ga (Bleeker and Davis, 1999; Sircombe et al., 2001).

2-2. Geological and geochronological background of the Acasta Gneiss Complex

The Acasta Gneiss Complex (AGC) is located on the western margin of the Slave Province (Figure 2-1, e.g. Bowring et al., 1990). The AGC consists of banded/layered and massive TTG gneisses, and foliated to massive granite sheets with subordinate amphibolites and ultramafic rocks (Bowring et al., 1990; Bowring & Williams, 1999). Iizuka et al. (2007) showed that the AGC is divided into two domains by a northeast-trending fault. In the eastern part, relatively massive tonalitic, granodioritic and granitic gneisses (felsic gneiss series) and gabbroic, dioritic and quartz-dioritic gneisses (mafic-intermediate gneiss series) are predominant. The western part is dominated by layered gneiss with continuous and rhythmic layering of felsic and mafic layers on a centimeter to meter-scale, subsequently intruded by foliated granite sheets. Some young northwest-trending mafic dikes occur in both areas, and cut the central fault (Figure 2-1).

Based on U-Pb dating of zircons from the orthogneisses, the eastern felsic gneiss series comprises orthogneisses with at least four ages of 4.03-3.94 Ga, 3.74-3.72 Ga, 3.66 Ga and 3.6-3.58 Ga (Bowring et al., 1989; Bowring & Housh, 1995; Iizuka et

al., 2006, 2007), whereas the granitic protoliths of the western layered gneisses were formed at 4.0-3.94 Ga and 3.74 Ga, and the foliated granite at 3.58 Ga (Bowring et al., 1989; Bowring & Housh, 1995; Iizuka et al., 2007a; Mojzsis et al., 2014). However, the ages of protoliths are still controversial because it is difficult to distinguish inherited zircons from magmatic zircons (Bowring and Williams, 1999; Mojzsis et al., 2014). Recently, Reimink et al. (2014) described five major rock units in the northern part of the AGC. One of the units, the Idiwhaa Tonalitic Gneiss, contains abundant igneous zircons with 4.02 Gyr age, and has a distinctive geochemistry of high Fe contents, low Mg numbers, relatively flat REE pattern and negative Eu anomaly compared to other Archean TTGs. Based on these features, Reimink et al. (2014) suggested that they were formed due to plume-related magmatic processes, including assimilation of rocks altered by surface waters. Some are considered to preserve the primary whole-rock Lu–Hf isotope systematics, and their mantle sources had negative to near-chondritic values (Guitreau et al., 2014). In addition, they show a negative μ^{142}Nd anomaly, indicating a Hadean mantle differentiation event (Roth et al. 2014).

On the other hand, ages of zircon overgrowths from the Acasta gneisses indicate that they underwent intense metamorphisms in the Eoarchean, especially at 3.65 and 3.6 Ga, coeval with the intrusion of the foliated granites (Bleeker and Stern, 1997; Iizuka et al., 2007a). Whole-rock ^{147}Sm-^{143}Nd isotope data of 51 rocks, with a large compositional variation from 74 to 43 wt% SiO_2, from both the eastern and western portions of the AGC yield a regression age of 3371 Ma (Bowring et al., 1990; Bowring & Housh, 1995; Moorbath et al., 1997; Roth et al., 2014), this age is interpreted as a metamorphic event that homogenized Nd isotopes across the area. Subsequently, the AGC experienced multiple metamorphic events, caused by the

intrusion of granitic sheets at 2.88 and 2.6 Ga and syenites at 1.8 Ga, and the 1.9 Ga Wopmay Orogeny (Stern and Bleeker, 1998; Hodges et al., 1995; Sano et al., 1999).

2-3. Field occurrence of mafic rocks

Previous works described the mafic rocks as an assortment of amphibolites and ultramafic rocks (Bowring and Williams, 1999). However, Iizuka et al. (2007) subsequently reappraised them as a series of gabbroic, dioritic and quartz dioritic gneisses (mafic-intermediate gneiss series). These mafic-intermediate rocks are ubiquitously scattered over the AGC, and occur as map-scale discordant blocks within the felsic gneisses with ages from 3.6 to 4.03 Ga (Figure 2-1). They can be clearly discriminated from young mafic dykes based on their field occurrence. In the eastern area, the mafic rocks occur mainly as rounded to elliptical, kilometer to centimeter sized enclaves and inclusions within the felsic gneisses, and are intruded by numerous granitic veins and sheets (Figure 2-2a-f). Figures 2-2a and b show that the mafic rocks are surrounded or intruded by felsic gneisses. The gneissosity of the mafic gneisses is cut by the felsic gneisses, and white pegmatites occur along the boundary between mafic and felsic gneisses and within the mafic gneiss (Figure 2-2b). Because the felsic gneisses and white pegmatite shown have a U-Pb zircon age of 3.6 Ga, the geological and geochronological observations indicate that the mafic rocks were formed before 3.6 Ga (Iizuka et al., 2007a). Moreover, Figure 2-2c shows a mafic rock intruded by a 3.94 Ga granitic gneiss, indicating that some mafic enclaves were formed before the Eoarchean (Iizuka et al., 2007a). In addition, pegmatite veins occur within the mafic enclaves or within the peripheries of the granite intrusions, and massive hornblendite inclusions are present within some mafic-intermediate gneisses. Some of mafic rocks break down into leucosomes and melanosomes, forming migmatite (Figure 2-2f). In

the western area, layered gneisses (Figure 2-2gh) dominate. These have similar mineralogical and whole-rock compositions to the felsic and mafic-intermediate gneiss series in the eastern area (Iizuka et al., 2007a), suggesting that the layered gneisses represent more severely deformed equivalents of the mafic enclaves and felsic rocks in the eastern area (Figure 2-2g h).

3. Sample preparation and analytical methods

We collected 137 massive or weakly banded mafic rocks (Figure 2-3), and carried out a petrological study. Mineral compositions were determined by electron probe micro-analysis (EPMA: JEOL-JXA8800) at the Tokyo Institute of Technology. All analyses were performed with an accelerating voltage of 15 kV, 12 nA beam current and a counting time of 10-40s. A ZAF correction was applied. Representative mineral compositions are summarized in Table 2-1. For amphiboles, Fe^{3+} was calculated stoichiometrically (Leake et al., 1997).

Sample localities for whole-rock chemical analyses are shown in Figure 1. The samples were selected to cover a variety of grain sizes, mineral assemblages and textures. Silica and carbonate vein-free portions of the samples were sliced into centimeters-thick slabs. The slabs were polished on all sides using a SiC sandpaper to remove saw marks, and crushed into small pieces using a hammer wrapped in a plastic bag. Alteration-free pieces were crushed again using a cleaned alumina stamp mill into 1~2 mm sands. The sand samples were pre-ground in an agate ball mill, and then re-ground into fine powder with an agate mortar and pestle.

Major element compositions were analyzed with X-ray fluorescence spectrometry (XRF: RIGAKU XRF3550 and RIGAKU RIX-2100) at the Tokyo Institute of Technology using fused glass beads. Fused glass beads were made from 0.4

g sample powder mixed with 4 g lithium tetraborate. A drop of LiI solution was added as an absorber. The major element compositions were calibrated using 16 to geochemical reference materials whose maximum and minimum values cover the compositions of all samples. The reproducibilities of major elements were calculated based on duplicate analyses of JB-3. Their average and standard deviation (2σ) values are shown along with the recommended values in Table 2-2. The detailed analytical methods were described elsewhere (Goto and Tatsumi, 1994; Komiya et al., 2002a, 2004).

Trace elements were analyzed with an inductively coupled plasma mass spectrometer (ICP-MS: Agilent 7500s) housed at Komaba, the University of Tokyo. We performed two different decomposition procedures: conventional HF-$HClO_4$ digestion and glass fusion bead digestion, respectively in order to evaluate the complete decomposition of acid-resistant minerals such as a zircon. Basaltic reference material W-2 (USGS) was analyzed as unknowns to estimate reproducibility (Table 2-1).

For the HF-$HClO_4$ digestion, approximately 100 mg of sample powders were weighed into Teflon PFA screw-cap vessels, and then 0.5 ml of 48% HF and 0.5 ml of $HClO_4$ were added. The tightly capped vessels were agitated in an ultrasonic bath for 30 minutes and then heated for over 24 hours at 80 ˚C. They were dried at 100 to 160 ˚C for overnight. To dissolve the fluoride 0.5 ml of $HClO_4$ and 0.5 ml of Milli-Q water were added again. Samples were completely evaporated at 100 to 160 ˚C, followed by addition of 0.25 ml of 20% HCl and 0.25 ml of Milli-Q water and complete evaporation at 100 ˚C. The dried residue was dissolved in 10 ml of 2% HNO_3 with trace amounts of HF (to be 0.1%) to increase the solubility of high field strength

elements (HFSE). Finally, indium (In) and bismuth (Bi) were added as internal standards, and they were diluted 2000 times by 2% HNO_3.

For glass bead digestion, glass beads used for XRF analyses were crushed into pieces, and *ca.* 30 mg of the fragments were weighed into 30 ml polypropylene bottles. After adding 30 ml of 2% HNO_3, the tightly capped bottles were left overnight after agitating in an ultrasonic bath for 30 minutes. Finally, In and Bi were added as internal standards. A blank bead, made from only the lithium tetraborate and a drop of Lil solution, was also decomposed by the same method for a blank analysis.

JB-3, issued by the Geological Survey of Japan, was used as a calibration standard for determining concentrations of twenty-six elements (Rb, Sr, Y, Zr, Nb, Cs, Ba, Hf, Pb, Th, U and fourteen REEs). For Nb determination, BIR-1, issued by U.S. Geological Survey (USGS), was also used as a secondary standard. Reproducibility and the difference between the recommended value and our averaged value of the trace element analyses were calculated from replicate analyses of W-2, issued by the USGS (Table 2-3). The reproducibilities of the bead digestion method are within 6.0% except for Cr, Ni, Zn and Ta, whereas 6.7-10.5% for Cr, Ni and Zn, and 17% for Ta, respectively. The differences between the recommended values and our averaged values of the bead digestion method are within 6.0% except for Rb and Y (8.2% Rb;12%), respectively. The reproducibilities of the HF-$HClO_4$ digestion method are within 8% except for Cr Y, Ta, Th and U (8-12%; Ta= 17%) respectively. The differences between the recommended values and our averaged values are within 10% except for Cu and Y (12% for Cu, 13% for Y; Table 2-3).

The two methods provide consistent data within analytical errors except for Zr and Hf (Figure 2-4, Table 2- 4 and 5). The Zr and Hf concentrations obtained using the bead digestion method are higher than those from the HF-$HClO_4$ digestion method in

almost all samples (Figure 2-4). The differences between the two decomposition methods are not uniform, indicating that the HF-$HClO_4$ digestion method fails to completely decompose the mafic samples. Therefore, we use the trace element compositions obtained using the bead digestion method hereafter.

4. Results

4-1. Petrography

The mafic rocks contain no relict igneous minerals, and all of them contain amphibole, plagioclase and quartz. However, but they are highly variable in their mineral assemblage, texture and mineral compositions. Mineral compositions of representative and other samples are presented in Table 2-1 and 6, respectively. Although some minerals partially broke down to secondary minerals and have rims that may reflect retrograde metamorphism, most minerals are homogeneous in their compositions not only within individual grains but also among minerals in individual samples. We subdivide the mafic samples into three groups based on their mineral assemblages and modal compositions: amphibolite, hornblendite and garnet-amphibolite groups. The garnet-amphibolite group is defined by presence of garnet (Figure 2-5gh), whereas the hornblendite group has over 90 vol. % amphibole, and shows coarse-grained textures (Figure 2-5e f). All the remaining samples belong to the amphibolite group, although these show varying textures from fine- to coarse-grained (Figure 2-5a-d). The spatial distributions of each rock group are displayed in Figure A1.

Amphibolite group

The amphibolites, most abundant among the three groups, are distributed over the AGC (Figure 2-3). The amphibolites are highly variable in their mineralogy,which

is uncorrelated with sample locality. Calcic amphibole, plagioclase and quartz predominate, with small amounts of biotite, chlorite, titanite, apatite and clinopyroxene (Figure 2-5a-d, 2-6c-f). Plagioclase is occasionally broken down to fine-grained epidote and albite (Figure 2-6h). The amphibolites are highly variable in the texture, displaying fine- to coarse-grained (Figure 2-5a-d) and massive to weakly banded textures. The fine-grained samples generally contain elongate calcic amphibole grains (Figure 2-5a-d), whereas the medium- to coarse-grained samples contain anhedral, granoblastic or elongate calcic amphiboles (Figure 2-5c). Many of them are massive while some samples show weak bands defined by calcic amphiboles-rich and plagioclase- or quartz-rich, mm to cm-thick layers.

The compositions of amphiboles are variable, irrespective of texture, ranging between the magnesio-hornblende and ferro-tschermakite (Figure 2-7a; $Mg^{\#}$ 0.43 to 0.60 in; Table 2-1, 6). Plagioclases range from oligoclase to labradorite. Only two samples (AC279 and AC477) contain clinopyroxene, which has been altered to chlorite in some grains (Figure 2-6c), or ilmenite and primary chlorite at the rim or along fractures within amphiboles (Figure 2-6d). Some ilmenites are elliptically surrounded by titanites or rarely pyrites as reaction rims (Figure 2-6f). A few samples contain discontinuously aligned titanite grains, crosscutting calcic amphibole and plagioclase grains (Figure 2-6ef). Also, numerous small ilmenite inclusions, probably exsolved from the calcic amphibole, are observed in some amphibole crystals (Figure 2-6g). Two calcic amphibolites have anhedral clinopyroxene rims, suggesting that they were formed due to amphibole-consuming reaction (Figure 2-5b). The clinopyroxenes have salite compositions and 0.66 in $Mg^{\#}$ values (Figure 2-7b).

Hornblendite group

Hornblendites are also distributed widely in the AGC (Figure 2-3). They are coarse-grained, and some of them have granoblastic texture (Figure 2-5ef). The calcic amphiboles commonly have high MgO and low Al_2O_3 contents, ranging from actinolite to tremolite compositions (Figure 2-7a). The hornblendites also include fewer amounts of other minerals. One sample (AY259) contains a few tiny biotites and Mg-rich chlorites ($Mg^{\#}$ = 0.54, Table 2-1) along calcic-amphibole grain boundaries, and quartz and apatite as inclusions within the calcic amphiboles (Figure 2-5e). Sample AC283 contains numerous, oriented, small ilmenites, probably due to exsolution from the amphiboles (Figure 2-6b). Sample AC148 contains calcites and clinopyroxenes (Figure 2-5f), which have similar compositions to those of amphibolite group, but relatively higher $Mg^{\#}$ value of 0.86 and diopside compositions (Table 2-1, Figure 2-7b). Some of the clinopyroxene grains enclose calcites and calcic amphiboles, which have similar compositions to discrete calcic amphibole grains. The calcite is mostly present along the boundaries among the calcic amphibole grains (Figure 2-6a).

Garnet-amphibolite group

Garnet-amphibolite occurs only in the northern part of the eastern area (Figure 2-3). They are medium-grained, and contain mainly calcic-amphiboles and plagioclases with subordinate amounts of quartz, garnet, ilmenite and apatite (Figure 2-5gh). A few grains of biotite, chlorite and cummingtonite can be recognized in some samples. The chlorites in the garnet-amphibolites have a lower $Mg^{\#}$ value than those in the amphibolites and hornblendites (Table 2- 1). The calcic amphiboles within the garnt amphibolites have high Al_2O_3 contents, and are plotted in the magnesio-tschermakite to ferro-tschermakite fields on an amphibole quadrangle diagram (Leak et al., 1997, Figure 2-7a). The cummingtonites are intimately intergrown with the calcic amphibole or occur at their rims (Figure 2-5h). The garnets

are pinkish, rounded, up to *ca.* 5 mm in diameter, and irregularly fractured (Figure 2-5g). They are commonly enriched in grossular component. Garnets associated with cummingtonite have relatively higher pyrope and lower spessartine components than those in cummingtonite-free samples (Table 2-1, Figure 2-7c). The amounts and sizes of ilmenite and apatite grains are significantly larger than those in other groups. The ilmenites are anhedral and up to 1 mm long, whereas the apatites are elliptical and up to 300 μm across (Figure 2-5gh).

4-2. Geochemistry

We selected thirty-seven amphibolites, five hornblendites, and six garnet-amphibolites for whole-rock analysis (Figure 2-1). Major and trace element compositions of these samples are given in Table 2-5. Figure 2-8 shows major element variations with MgO for these mafic rocks, compared to modern mid-ocean ridge basalts (MORBs) and ocean island basalts (OIBs). The mafic rocks have broadly similar compositions to the modern basalts. Figure 2-9 displays chondrite-normalized rare earth element (REE) and primitive mantle (PM)-normalized trace element patterns (Sun & McDonough, 1989). Values of Nb^*, Ta^*, Eu^*, Zr^* and Hf^* were calculated with respect to the neighboring elements (Table 2-3). Based on replicate analyses performed on a basaltic reference material W-2, analytical errors for Nb/Nb^*, Ta/Ta^*, Eu/Eu^*, Zr/Zr^*, and Hf/Hf^* values can be estimated within 10% (Table 2-3). Therefore, if their values fall outside a range from 0.9 to 1.1, we considered them as anomalies, except for Ta/Ta* value for a range from 0.82 to 1.18 because the reproducibility of Ta/Ta* measurement for W-2 is relatively poor (18%).

Both major and trace element compositions are systematically different among the groups. The amphibolites have large variations in both major and trace element

compositions, and have compositions roughly intermediate to the other groups (Figure 2-8, 9a-d). Based on the REE concentrations and patterns, they can be subdivided into three groups: amphibolite groups I to III (Figure 2-8, 9a b).

Amphibolite group I is characterized by flat to very slightly LREE-depleted REE patterns (Figure 2-9a). They are compositionally uniform, and are intermediate among the amphibolites in terms of major elements (Figure 2-8). They show no obvious trace element anomalies with the exception of slightly negative Nb and Ta anomalies of $(Nb/Nb^*)_{PM} = 0.63\text{-}0.99$ and $(Ta/Ta^*)_{PM} = 0.59–1.1$ (Figure 2-9ab).

Amphibolite group II displays slightly to strongly LREE-enriched patterns and negative to positive Ti, Zr, Nb, Ta, Hf and Eu anomalies. They, with the exception of the AC228 and AC480, show negative Nb and Ta anomalies, with $(Nb/Nb^*)_{PM} = 0.18\text{-}0.63$ and $(Ta/Ta^*)_{PM} = 0.11\text{-}0.77$. They display negative correlations of Al_2O_3 and Na_2O against MgO content.

Amphibolite group III is defined by lower trace element concentrations than the other mafic rocks, and show large positive Eu anomalies, with $(Eu/Eu^*)_{CN} = 1.2\text{-}2.1$. They are further classified into two subgroups based on MgO contents. The low-MgO subgroup has relatively higher TiO_2 and FeO, and lower SiO_2 contents than that of the high-MgO subgroup at a given MgO. The low-MgO subgroup is characterized by strong positive Eu and Ti anomalies, whereas the high-MgO subgroup shows moderately positive Eu and negative Ti anomalies.

The hornblendites are clearly distinguished from other two groups by their high MgO contents (10-19 wt.%). They are also characterized by low Al_2O_3, Na_2O and K_2O contents which decrease with increasing MgO. The hornblendite and amphibolite groups I and II form a single array on the MgO vs Al_2O_3 diagram (Figure 2-8, 10). Hornblendites have relatively high REE contents, with convex-shaped LREE patterns

and negative Eu anomalies. In addition, they are depleted in HFSEs such as Ti, Zr, and Hf (Figure 2-9f). Because Th contents are highly variable possibly due to secondary alteration, Nb and Ta anomalies are also variable (Figure 2-9f).

The garnet-amphibolites have lower MgO contents than the other two groups (Figure 2-8). They have much lower SiO_2, Na_2O and K_2O contents, and higher TiO_2, FeO and P_2O_5 contents at a given MgO content (Figure 2-8). Except for AY121, the garnet-amphibolites have quite low SiO_2 content from 43 to 49 wt.%, and plot within the compositional range of modern evolved OIB magmas. The REE patterns of garnet-amphibolites are relatively uniform, and display slightly HREE-depleted patterns with variable LREE enrichment (Figure 2-9h). They display negative Zr and Hf anomalies, except for AC543, which lacks Zr and Hf anomalies, and AY121, which has positive Zr and Hf and negative Ti anomalies.

5. Discussion

Unlike other well-known Eoarchean terranes, there is no clear geological evidence for the primary lithofacies type and emplacement style of the mafic rocks distributed over the Acasta Gneiss Complex. Although the absence of pillowed structures and associated sediments, such as banded iron formation and chert may suggest a sub-surface origin as intrusive protoliths, we cannot rule out the possibility that such evidence is simply masked by the strong effects of deformation and metamorphic recyrstallization associated with younger felsic intrusions ranging from 4.03 to 3.40 Gyr. Thus, in order to decipher their origin and tectonic setting, we must rely on the petrological and geochemical signatures presented in this study.

5-1. Metamorphic grade estimated from the mafic rocks

Metamorphic temperature of the Acasta rocks was roughly estimated to be between 400 and 650 ˚C based on mineral assemblage (Bowring et al., 1990). We examined, in a more quantitative manner, the metamorphic grade based on both mineral assemblage and bulk compositions because it is still ambiguous whether the difference in the mineral assemblages is controlled by only metamorphic grade. In order to investigate original mineral assemblages and compositions, the secondary minerals, for example plagioclase pseudomorphs replaced by saussurite, actinolitic rims of hornblende and titanite replacing ilmenite, were avoided (Table 2- 1).

Figure 11a shows an A'FM diagram of basaltic system, projected from quartz, plagioclase and H_2O, and possible compositional variations of chlorite, amphibole and garnet under the amphibolite facies condition (Harte & Graham, 1975; Spear, 1993). A triangle of coexisting chlorite, hornblende and garnet is present from the greenschist to amphibolite facies and the chlorite and hornblende coexisting with the garnet become more magnesian with increasing metamorphic temperature. As a result, the garnet occurs only in a mafic rock with a quite low-$Mg^{\#}$ value under the greenschist facies to lower amphibolite facies conditions, but the garnet becomes common even in a magnesian mafic rock under the medium to higher amphibolite facies conditions.

Representative mineral and whole-rock compositions of the mafic rocks plot on the A'FM diagram along with typical compositional fields of hornblende, chlorite and garnet under the amphibolite facies condition (Figure 2-11a). The chlorite and hornblende in a garnet amphibolite without clinopyroxene and cummingtonite have the lowest Mg# value, and the whole-rock composition plots within the triangle of the chlorite, amphibole and garnet (Figure 2-11a). The chlorite and hornblende in the hornblendite without clinopyroxene have the highest Mg# value, and the whole-rock composition has lower Al_2O_3 content, and plots on the compositional variation of the

hornblende (Figure 2-11a). On the other hand, the garnet-free amphibolites with chlorite and hornblende are more magnesian than the garnet-amphibolite. The good correlation of their mineral assemblages and compositions with whole-rock compositions can be well explained by compositional control rather than difference in metamorphic temperature.

Clinopyroxene appears in the high Ca field of the ACF diagram (Figure 2-11b), and a tie line between garnet and hornblende breaks down into another tie line between plagioclase and cummingtonite under the condition. In addition, the amphibole becomes more aluminous with increasing metamorphic temperature. The hornblende and garnet assemblage disappears and is replaced by the parageneses Pl + Hbl + Cum or Pl + Grt + Cum at higher metamorphic grade. On the other hand, a metabasite with high CaO contents contains clinopyroxene and hornblende with/without plagioclase, depending on the Al_2O_3 content (Figure 2-11b). The garnet-amphibolites all contain garnet, hornblende, plagioclase and cummingtonite (Figure 2-11b). Regardless of the whole-rock compositions, the coexistence of the four minerals indicates the upper amphibolite facies metamorphic condition. Some amphibolites contain clinopyroxene, hornblende and plagioclase whereas a hornblendite contains only clinopyroxene and hornblende, consistent with lower Al_2O_3 contents of the hornblendite (Figure 2-11b).

The mineral assemblages and compositions of the mafic rocks indicate that they underwent medium to upper amphibolite facies metamorphism. The difference of mineral assemblages is due to variation of the whole-rock compositions. Higher FeO contents lead to expansion of a stability field of garnet whereas higher CaO contents result in presence of clinopyroxene. In addition, a good correlation of the mineral assemblages and compositions with whole-rock compositions do not support significant elemental mobility during/after the main metamorphic event.

5-2. Processes governing whole-rock variations in Acasta mafic rocks

5-2-1.Garnet-amphibolite

The garnet-amphibolite is clearly different from the other groups in several respects. Firstly, their occurrences are limited to the northeastern part of the AGC. Secondly, they possess higher TiO_2, FeO, MnO and P_2O_5 contents than the other samples (Figure 2-8). The high FeO content in the garnet-amphibolitse is consistent with the presence of garnet because garnet tends to appear in metabasalts with sufficiently Fe-rich compositions (Spear, 1981). Thirdly, they show characteristic REE patterns with terms of strong depletion in HREEs. If the garnet-amphibolites preserve their original magmatic composition, in particular for the MREEs and HREEs, their depletion in HREEs suggests partial melting of a mantle source with residual garnet (Nicholls and Harris, 1980), possibly due to early differentiation of the mantle (Blichert-Toft & Arndt 1999). However, further studies are required for constraining the origin of the garnet-amphibolites in the AGC.

5-2-2. Amphibolite group III

Amphibolite group III, which has low REE contents and positive Eu anomalies, is probably equivalent to the "metagabbro", "leucogabbro" and "hornblende-plagioclase schist" described by previous studies (e.g. Stern and Bleeker, 1998; Iizuka et al., 2007; Mojzsis et al., 2014). Mojzsis et al. (2014) reported a 3.86 Ga discordant age and 3.77 Ga concordant age from metamorphic zircon in the hornblende-plagioclase schist, indicating the protolith age is older than ca. 3.86 Ga. The similarity of their REE patterns to partition coefficients between a basaltic melt and plagioclase (Bédard, 2006), as well as to a gabbro or an anorthosite (e.g. Godard et al., 2009) indicates that the protoliths were formed through accumulation of

plagioclase during crystal fractionation (Mojzsis et al., 2014). Furthermore, their high TiO_2 and FeO contents suggest the accumulation of titanomagnetite accompanied with the plagioclase crystallization from a relatively evolved basaltic magma. Thus, amphibolite group III seems to originate from crystal cumulates derived from an evolved basaltic magma, and their parental magma composition is difficult to estimate.

5-2-2. Amphibolite groups I, II and hornblendites

Although the Acasta mafic rocks underwent variable deformation and severe metamorphism, their chemical compositions are roughly similar to modern MORB and OIB (Figure 2-8). In particular, the amphibolite groups I and II plot well within the compositional ranges of MORB and OIB, implying preservation of their original magmatic compositions. In that case, the compositional variations of the whole rocks may be the result of fractional crystallization of a basaltic magma. Amphibolite group II shows a large variation in MgO content, broadly correlated with their Al_2O_3 and Na_2O contents, whereas amphibolite group I has intermediate compositions within the range of amphibolite group II in terms of the major element compositions. Because Al behaves as an incompatible element and its abundances in magma increase with fractionation of olivine, negative correlation between Al_2O_3 and MgO contents is expected for magmatic differentiation. However, as illustrated in Figure 10, the array is much too steep to be explained by olivine fractionation, when compared with an olivine control line. The olivine control line is calculated assuming that the Fe^{2+}-Mg exchange coefficient between olivine and basaltic liquid is K=0.33 (Toplis, 2005) and the most magnesian sample (AC283) has a primary magma composition. This discrepancy indicates that fractional crystallization of a basaltic magma does not play a major role in generating whole-rock compositional variations.

Previous studies show that the Acasta Gneiss Complex have been subjected to numerous magmatic and metamorphic events, including the intrusion of granitic and syenitic sheets and that later thermal events caused pre-existing rocks to be metamorphosed and partially melted (e.g. Bleeker and Stern, 1997; Bowring et al., 1989; Bowring and Housh, 1995; Iizuka et al., 2007a; Bowring et al., 1990; Moorbath et al., 1997). Recently, it has been suggested that a migmatization event occurred at 3.92 Ga to form some groups of the Acasta gneisses (Mojzsis et al., 2014). Furthermore, the presence of numerous pegmatite dikes and quartz veins within the mafic rocks indicate that felsic magma and fluid percolated into the mafic rocks (Figure 2-2a,b). These lines of evidence suggest that *in-situ* anatexis formed the hornblende-rich restites and quartz-rich leucosomes (Iizuka et al., 2007b).

Melting experiments of metabasalts show that the plagioclase stability field expands and the amphibole field shrinks through dehydration melting (e.g. Rapp and Watson, 1995; Winther and Newton, 1991; Zamora, 2000). On the other hand, under water-saturated conditions, the plagioclase-out boundary shifts to a low temperature and pressure, whereas the amphibole stability field expands to higher temperature between about 5 and 20 kbar (e.g. Beard and Lofgren, 1991; Pawley and Holloway, 1993). As a result, a felsic melt may coexist with only amphibole at over 7 kbar and *ca.* 800 °C (Beard and Lofgren, 1991). Partial melting of a hydrated mafic rock produces a melt with high Al_2O_3 and low MgO contents, and its complementary residue has low Al_2O_3 and high MgO contents under water-saturated conditions (Beard and Lofgren, 1991). At the AGC, percolation of hydrous melts or fluids released from the surrounding felsic rocks could trigger the melting of mafic rocks in hydrous condition.

Figure 10 shows the composition of the melt, residue and starting material produced in a melting experiment on the MgO vs. Al_2O_3 diagram (Beard and Lofgren,

1990). Mixing between the melt, starting composition and residues is expected to form an array along the solid line shown in Figure 10. The amphibolite group I, amphibolite groups II, and hornblendites have compositional variations that lie along the line, consistent with the idea that they were generated by *in-situ* partial melting of hydrated mafic rocks. The hornblendites and high-Mg amphibolites may represent residues of melting, whereas the composition of low-Mg amphibolites may be explained by assimilation of the felsic melt by the precursor amphibolites.

Assuming that the felsic melt was in equilibrium with the hornblendite residue, the trace element compositions of this felsic melt were roughly estimated from the coexisting hornblendite compositions and partition coefficients between amphibole and silicate melts (Tiepolo et al., 2007). Figure 2-12 shows a comparison of the trace element patterns for amphibolite group II and hornblendites with the calculated melts. The calculated melt patterns share some of the features of the amphibolite group II patterns including enrichment of Th and LREEs, and negative anomalies of Nb, Ta, Zr, Hf and Ti (Figure 2-12). Variations in La content, $(La/Yb)_{CH}$ ratio and Ti anomaly as a function of Al_2O_3 content in hornblendite, amphibolite group I and II are shown in Figure 2-13, along with mixing lines between average compositions of hornblendites, amphibolite group I and the calculated melt. The Al_2O_3 content of the calculated melt is taken from a metabasalt melting experiment at 900 ˚C and 6.9 kb (Beard and Lofgren, 1991). All three diagrams demonstrate dispersion of the data points of amphibolite group II, but most of them are restricted within the field defined by the two mixing lines. The Al-rich samples among amphibolite group II tend to follow a trend along the mixing line between the calculated melt and amphibolite group I. This is consistent with the idea that they represent metasomatized amphibolites strongly affected by infiltration of felsic melts into the precursor. On the other hand, the

Mg-rich and Al-poor samples among amphibolite group II show features intermediate to amphibolite group I and the hornblendites, suggesting that their compositions are dominated by residue after the partial melting of amphibolite group I.

Based on the above discussions, we suggest that the mineral assemblages and compositions of the Acasta mafic rocks reflect the wide range of whole-rock compositions, that were acquired as a result of partial melting. The question that remains is when the anatexis occurred. At the AGC, the oldest protoliths were emplaced at ca. 4.03-3.94 Ga and were followed by two or three episodes of granitic intrusion at 3.74-3.72 Ga, 3.66 Ga and 3.6-3.58 Ga (Bowring et al., 1989; Bowring and Housh, 1995; Iizuka et al., 2006, 2007). The ca. 3.6 Ga magmatic activity may be the most intensive and is commonly recorded as zircon overgrowths in older felsic gneiss units (Bowring et al., 1990; Bowring and Williams, 1999). We therefore suggest that most of Acasta mafic rocks studied here belong to the oldest age group, and were recrystallized, hydrated and in some cases melted at around 3.6 Ga, together with the 4.03-3.94 Ga felsic rocks. Indeed, a 3.6 Ga pegmatite intruding the mafic rocks was identified as a fluid or hydrous melt released from granitoids (Iizuka et al., 2007). However, metamorphic zircons extracted from Acasta mafic rocks yield ages up to 3.85 Ga (Mojzsis et al., 2014), implying that pre-3.6 Ga events may have also affected the mafic rocks.

Another metamorphic event at ca. 3.4 Ga is also suggested by zircon overgrowths on 4.0 Ga cores (Stern and Bleeker, 1998; Reimink et al., 2014) and by whole-rock ^{147}Sm-^{143}Nd isotope systematics of various rocks in the AGC (e.g. Moorbath et al., 1997). This event would have influenced parts of the older units and reset Sm-Nd systematics over the AGC. Subsequently, younger granitic sheets intruded at 2.9 and 2.6 Ga (Bleeker et al., 1997), and Proterozoic thermal events related to the

Wopmay orogeny are also inferred from the $^{40}Ar/^{39}Ar$ analysis of hornblende and biotite and the U-Pb analysis of apatite (Hodges and Bowring, 1995; Sano et al., 1999). Events occurred after 2.9 Ga, therefore, would not have had a great impact on the whole-rock geochemistry of the Acasta mafic rocks.

To summarize, recrystallization and partial melting, which caused the intensive modification of the whole rock geochemistry of Acasta mafic rocks, probably occurred at pre-3.6 Ga and possibly at 3.4 Ga. Although the formation age of Acasta mafic rocks remains undated, they could have formed at, or older than, 4.0 Ga.

5-3. Primary signatures preserved in the least modified amphibolites

The enrichment of LREEs in the amphibolite group II can be explained by addition of LREE-enriched felsic magma or fluid to the mafic rocks with flat-REE patterns, as mentioned above. In general, magmatic processes, especially low-pressure fractional crystallization of basaltic magma, do not change the ratios of the incompatible element contents to Zr contents, one of the most immobile elements. Therefore, scatter on Zr variation diagrams is due to secondary movement of incompatible elements during post-magmatic events such as secondary alteration, infiltration of fluids, metamorphic dehydration melting and migmatization (e.g. Keppler, 1996; Kogiso et al., 1997; Polat and Hofmann, 2003; Tatsumi et al., 1986). Figure 2-14 illustrates the variation of LILEs, HFSEs and REEs against Zr concentrations. The solid lines display liquid lines of descent calculated from the sample with the lowest Zr concentration (AC384) among amphibolite group I, assuming they are perfectly incompatible in crystallizing phases. Strontium and Barium contents are highly scattered for all of the groups, indicating that the LILEs are strongly influenced by post-magmatic modification (Figure 2-14ab).

Good correlations of HFSE and REE contents with Zr contents for amphibolite group I indicate that primary magmatic compositions are largely preserved, except for the LILEs. Moreover, the group I samples have flat incompatible-element patterns. These flat incompatible-element patterns could not be produced by secondary alteration and partial melting of metamorphosed basalts because incompatibilities of some elements during magmatic processes are not necessarily correlated with their solubility in metamorphic fluids during metamorphism. In addition, amphibolite group I has constant major element compositions, similar to modern MORBs and OIBs, suggesting their major element compositions are also preserved. We therefore suggest that some of the least-modified samples (amphibolite group I) remain immune from remelting or contamination by partial melts, and retain primary signatures in terms of immobile elements.

5-4. Origin of the Acasta mafic rocks and implications for the Hadean mantle evolution

Given that the mafic rocks occur as enclaves within 3.6 to 4.0 Ga felsic gneisses, they appear to have originated earlier than the surrounding felsic rocks. Furthermore, the least-modified amphibolite group I has almost flat REE and PM-normalized incompatible element patterns, indicating that the precursor was a basaltic magma generated by partial melting of a primitive mantle-like source material. However, slight depletions of Nb and Ta commonly observed in amphibolite group I requires some explanation (Figure 2-9b). Considering modern basalt geochemistry, subduction-related magmatism can be inferred to explain the origin of Nb-Ta depletions. However, alternative explanations such as the influence of early differentiation has been envisaged for the ancient mantle in previous studies (Wade and

Wood, 2001). Using the immobile element characteristics of amphibolite group I, these two different scenarios for the origin of the Acasta mafic rocks will be discussed below.

5-4-1. Subduction-related scenario

Immobile elements such as the HFSEs have been widely used to identify different magma types, which, in turn, provides information on tectonic setting. In particular, the Th/Nb ratio is regarded as one of the most useful proxies for distinguishing subduction-related and non-subduction related magmas (e.g. Condie, 2005; Furnes et al., 2014; Pearce, 1983; Pearce, 2008). Thorium and niobium have similar incompatibilities during magmatic processes, but Nb is more fluid-immobile than Th, with the result that Nb is preferentially retained in subducting slabs (Tatsumi et al., 1986). Laboratory experiments simulating dehydration melting of amphibolites revealed that fluids or melts released from amphibolites tend to show variable Nb-depletion relative to Th and the REEs (Keppler, 1996; Kogiso et al., 1997; Rapp et al., 1999), due to residual Ti-rich phases such as Ti-amphiboles, rutile and titanite (Schmidt et al., 2004; Thorpe et al., 1992; Tiepolo et al., 2001; Tiepolo et al., 2002). Based on this consideration, Pearce (2008) proposed a Th/Yb versus Nb/Yb discrimination diagram, and illustrated that lavas derived from mantle influenced by subduction-related fluid and melts are displaced from a modern MORB and OIB array to higher Th/Yb and lower Nb/Yb ratios.

As shown in Figure 15a, the amphibolite group I is displaced from the MORB-OIB array to slightly higher Th/Yb and lower Nb/Yb, similar to many other Eoarchean mafic rocks (e.g. Polat et al., 2002; O'Neil et al., 2011), implying they form through subduction-related magmatism. However, there are two major uncertainties in applying this discrimination criteria to Eoarchan rocks. The first is that the Eoarchean

MORB-OIB array would be shifted to higher Th/Yb and lower Nb/Yb than that of today (e.g. Hofmann et al., 1986; Collerson and Kamber, 1999) if the continental crust contains a significant proportion of the bulk silicate Earth's Th and Nb budget, and grew with time progressively from the Archean to the present (e.g. Jochum et al., 1991). Secular changes of the MORB-OIB array through geologic time partially account for the displacement of the amphibolite group I to higher Th/Yb and lower Nb/Yb ratios.

The second is that Th concentration and Th/Yb ratio in Eoarchean rocks can be modified by secondary alteration processes because Th is more easily mobilized by aqueous fluids and melts compared with other HFSEs such as Nb, Zr and Hf (e.g. Keppler, 1996; Johnson and Plank, 1999). Since La has a similar incompatibility to Th and Nb during mantle melting but is thought to be less influenced by alteration than Th, we applied a La/Yb versus Nb/Yb diagram to the Eoarchean mafic rocks as an alternative (Figure 2-15b). On this projection, amphibolite group I and other Eoarchean mafic rocks plot slightly closer to the MORB-OIB array than those on the Th/Yb vs. Nb/Yb diagram. However, some samples are still displaced from the MORB-OIB array and primitive mantle towards the Nb-poor side, suggesting that the effect of secondary alteration on Th and La may be negligible, and Eoarchean mafic rocks, including the Acasta amphibolites were all derived from source regions which had experienced Th/Nb and La/Nb fractionation.

If these rocks can be recognized as subduction-related basalts, the present study of Acasta mafic enclaves within ~ 4.0 Ga felsic gneisses may provide evidence for the operation of plate tectonics before 4.0 Ga, *ca.* 200 Ma older than previously suggested (Furnes et al., 2014; O'Neil et al., 2011; Polat et al., 2002). Previous works propose that plate tectonics in the Early Archean was different from modern plate tectonics in terms of ~150 ˚C higher mantle temperatures (e.g. Herzberg et al., 2010; Komiya et al.,

2002b; Komiya, 2004; Nisbet et al., 1993; Ohta et al., 1996) and higher subduction geotherms (e.g. Grambling, 1981; Hayashi et al., 2000; Maruyama et al., 1996). At higher geothermal gradients, the subducting hydrated basaltic crust could melt, leading to the formation of TTG magmas (Barker and Arth, 1976; Martin, 1986; Rollinson, 1997; Smithies et al., 2003), and preventing hydration of mantle wedge and the consequent formation of arc basalts. Thus, the presence of arc-like basalts before ~4.0 Ga, presumably formed from a mantle metasomatized by slab-derived fluid is highly suggestive of intermittent subduction of cold slabs even in the early Archean.

5-4-2. Nb-Ta deficit mantle scenario

Negative Nb anomalies created at subduction zone settings is commonly accompanied with enrichment of highly incompatible elements and, in most cases, LREEs (Crawford et al., 1986; Hochstaedter et al., 1996; Johnson et al., 1985; Kamei et al., 2004; Mann, 1983; Pearce, 1983; Pearce and Peate, 1995; Shibata and Nakamura, 1997). The lack of conspicuous enrichment in highly incompatible elements and primitive mantle-like patterns except for Nb in amphibolite group I, allows us to envision an alternative view of the mantle evolution, namely mantle differentiation in the early Earth (e.g. Bennett et al., 2007; Boyet and Carlson, 2005). The primitive mantle composition was estimated from compositions of chondrite, based on assumption that Nb, Ta and REEs are highly refractory and perfectly lithophile elements (Sun and McDonough 1989). However, recent high-pressure melting experiments show that Nb and Ta are moderately siderophile under high-pressure conditions, over 20 GPa, implying that they were partitioned into the core during core-mantle differentiation (Cartier et al., 2014; Wade and Wood, 2001).

In the deep magma ocean model of core formation, liquid metal descends slowly in the magma ocean and is accumulated at the base of it. The metal layer last

equilibrates with silicate melt at the base of the magma ocean, leaving a siderophile element-depleted silicate mantle above the layer. Based on experiments which determine the partition coefficients for moderately siderophile elements, such as Ni and Co, primitive upper mantle composition is controlled by metal-silicate equilibrium at 27–40 GPa and 3000–3600 K (e.g. Wood et al., 2006; Righter, 2011). Under these conditions, Nb and Ta would behave as weakly siderophile elements during the final metal-silicate equilibrium, resulting in Nb and Ta-deficient primitive upper mantle. If such mantle regions survived replenishment by a chondiritic late veneer, or less depleted materials presumably stored in the lower mantle until the end of Hadean, shallow melting of primitive upper mantle with Nb-Ta depletion could generate the precursor to the Acasta mafic rocks in a non-subduction setting.

6. Conclusions

Mafic rocks are distributed throughout the Acasta Gneiss Complex as enclaves, bands and blocks. Based on their petrography, the mafic rocks are classified into three groups: amphibolite, hornblendite and garnet-amphibolite. The hornblendites dominantly contain actinolitic amphibole, and have high MgO and low Al_2O_3 contents. The garnet-amphibolites contain garnet, and have relatively high FeO and Al_2O_3 contents. The amphibolites have intermediate whole-rock compositions. Differences in mineral assemblages are due to their whole-rock compositions, and their mineral parageneses and mineral compositions indicate that they underwent amphibolite to upper amphibolite facies metamorphism.

The amphibolites are subdivided into three types based on the REE patterns: amphibolite groups I to III, respectively. Amphibolite group I is characterized by flat to slightly LREE-depleted patterns whereas group II show slightly to strongly

LREE-enriched patterns. Group III is characterized by low REE contents and large positive Eu anomalies, suggesting a plagioclase-enriched cumulate precursor. Good correlations between Zr contents and other incompatible elements, except Ba and Sr, for amphibolite group I suggest that they still preserve their original incompatible element compositions. By contrast, the other mafic rocks are highly scattered in most incompatible elements except for Hf, suggesting later elemental mobility. Amphibolite groups I and II and the hornblendites apparently show a strong negative correlation between MgO and Al_2O_3 contents, but the steep slope cannot be explained by simple fractional crystallization of a basaltic magma. Infiltration or extraction of partial melts with felsic compositions formed from hydrated amphibolite group I may accounts for this correlation between MgO and Al_2O_3 contents.

The amphibolite group I have primitive mantle-like incompatible element compositions, but show slightly negative Nb and Ta anomalies, similar to other early Archean mafic rocks. We consider two scenarios for the origin of the negative Nb and Ta anomalies observed in amphibolite group I. One is that they were formed at the subduction setting and the negative anomalies represent the signature of a subduction-related magma. This scenario implies the operation of plate tectonics and formation of mantle wedge metasomatized by slab-derived fluids back to ca. 4.0 Ga. Moreover, the formation of a hydrated mantle wedge implies intermittent subduction of cold slabs even in the early Archean. Although the subduction-related scenario is simple, the almost chondritic relative abundances of incompatible elements in amphibolite group I allow us to consider the alternative scenario that the source of the Acasta mafic rocks is Nb and Ta-deficient primitive mantle. Since it has been reported that the Nb and Ta are moderately siderophile under high pressure conditions, primitive upper mantle after the core formation could be depleted in Nb and Ta. Further studies

are clearly required to decide which scenario is most plausible to explain geochemical features of the Acasta mafic rocks and the evolution of Hadean mantle.

References

Amelin, Y., Lee, D.-C., Halliday, A.N., Pidgeon, R.T., 1999. Nature of the Earth's earliest crust from hafnium isotopes in single detrital zircons. Nature 399, 252-255.

Amelin, Y., Lee, D.C., Halliday, A.N., 2000. Early–middle Archaean crustal evolution deduced from Lu–Hf and U–Pb isotopic studies of single zircon grains. Geochimica et Cosmochimica Acta 64, 4205–4225.

Barker, F., Arth, J.G., 1976. Generation of trondhjemitic liquids and Archean bimodal trondhjemite-basalt suites. Geology 4, 596-600.

Beard, J.S., Lofgren, G.E., 1991. Dehydration melting and water-saturated melting of basaltic and andesitic greenstones and amphibolites at 1, 3, and 6. 9 kb. Journal of Petrology 32, 365-401.

Bédard, J.H., 2006. Trace element partitioning in plagioclase feldspar. Geochimica et Cosmochimica Acta 70, 3717-3742.

Bennett, V.C., Brandon, A.D., Nutman, A.P., 2007. Coupled ^{142}Nd-^{143}Nd isotopic evidence for Hadean mantle dynamics. Science 318, 1907-1910.

Bleeker, W., Stern, R.A., 1997. The Acasta gneisses: an imperfect sample of Earth's oldest crust. In: Cook, F., Erdmer, P. (Eds.), Slave-Northern Cordillera lithospheric evolution (SNORCLE) transect and cordilleran tectonics workshop meeting, Lithosphere Report, pp. 32-35.

Blichert-Toft, J., Arndt, N.T., 1999. Hf isotope compositions of komatiites. Earth and Planetary Science Letters 171, 439-451.

Bowring, S.A., Williams, I.S., Compston, W., 1989. 3.96 Ga gneisses from the Slave province, Northwest Territories. Geology 17, 760-764.

Bowring, S.A., Housh, T.B., Isachsen, C.E., 1990. The Acasta gneisses: Remnant of Earth's early crust. In: Newsom, H.E., Jones, J.H. (Eds.), Origin of the Earth. Oxford University Press, New York, pp. 319-343.

Bowring, S.A., Housh, T., 1995. The Earth's early evolution. Science 269, 1535-1540.

Bowring, S.A., Williams, I.S., 1999. Priscoan (4.00-4.03 Ga) orthogneisses from northwestern Canada. Contributions to Mineralogy and Petrology 134, 3-16.

Boyet, M., Carlson, R.W., 2005. ^{142}Nd evidence for early (>4.53 Ga) global differentiation of the silicate Earth. Science 309, 576-581.

Caro, G., Bourdon, B., Wood, B.J., Corgne, A., 2005. Trace-element fractionation in Hadean mantle generated by melt segregation from a magma ocean. Nature 436, 246-249.

Caro, G., 2011. Early Silicate Earth Differentiation. Annual Review of Earth and Planetary Sciences 39, 31-58.

Cartier, C., Hammouda, T., Boyet, M., Bouhifd, M.A., Devidal, J.-L., 2014. Redox control of the fractionation of niobium and tantalum during planetary accretion and core formation. Nature Geoscience 7, 573-576.

Cates, N.L., Mojzsis, S.J., 2007. Pre-3750 Ma supracrustal rocks from the Nuvvuagittuq supracrustal belt, northern Québec. Earth and Planetary Science Letters 255, 9-21.

Chambers, J.E., 2004. Planetary accretion in the inner Solar System. Earth and Planetary Science Letters 223, 241–252

Collerson, K.D. , and Kamber, B.S ., 1999, Evolution of the continents and the atmosphere inferred from Th-U-Nb systematics of the depleted mantle. Science 283 1519-1522

Condie, K.C., 2005. High field strength element ratios in Archean basalts: a window to

evolving sources of mantle plumes. Lithos 79, 491-504.

Crawford, A.J., Beccaluva, L., Serri, G., Dostal, J., 1986. Petrology, geochemistry and tectonic implications of volcanics dredged from the intersection of the Yap and Mariana trenches. Earth and Planetary Science Letters 80, 265-280.

Furnes, H., Rosing, M., Dilek, Y., de Wit, M., 2009. Isua supracrustal belt (Greenland)—a vestige of a 3.8 Ga suprasubduction zone ophiolite, and the implications for Archean geology. Lithos 113, 115–132.

Furnes, H., de Wit, M., Dilek, Y., 2014. Four billion years of ophiolites reveal secular trends in oceanic crust formation. Geoscience Frontiers 5, 571-603.

Godard, M., Awaji, S., Hansen, H., Hellebrand, E., Brunelli, D., Johnson, K., Yamasaki, T., Maeda, J., Abratis, M., Christie, D., Kato, Y., Mariet, C., Rosner, M., 2009. Geochemistry of a long in-situ section of intrusive slow-spread oceanic lithosphere: results from IODP site U1309 (Atlantis Massif, 30°N mid-Atlantic-ridge). Earth and Planetary Science Letters 279, 110–122.

Goto, A., Tatsumi, Y., 1994. Quantitative analysis of rock samples by an X-ray fluorescence spectrometer (I). The Rigaku Journal 11, 40-59.

Grambling, J.A., 1981. Pressures and temperatures in Precambrian metamorphic rocks. Earth and Planetary Science Letters 53, 63-68.

Guitreau, M., Blichert-Toft, J., Mojzsis, S.J., Roth, A.S.G., Bourdon, B., Cates, N.L., Bleeker, W., 2014. Lu–Hf isotope systematics of the Hadean–Eoarchean Acasta Gneiss Complex (Northwest Territories, Canada). Geochimica et Cosmochimica Acta 135, 251-269.

Harte, B., Graham, C.M., 1975. The graphical analysis of greenschist to amphibole facies mineral assemblages in metabasites. Journal of Petrology 16, 347-370.

Hayashi, M., Komiya, T., Nakamura, Y., Maruyama, S., 2000. Archean regional metamorphism of the Isua supracrustal belt southern West Greenland: Implications for a driving force for Archean plate tectonics. International Geology Review 42, 1055-1115.

Herzberg, C., Condie, K., Korenaga, J., 2010. Thermal history of the Earth and its petrological expression. Earth and Planetary Science Letters 292, 79-88.

Hochstaedter, A.G., Kepezhinskas, P., Defant, D., Drummond, M., Koloskov, A., 1996. Insights into the volcanic arc mantle wedge from magnesian lavas from the Kamchatka arc. Journal of Geophysical Research 101, 697-712, doi:10.1029/95JB02404.

Hodges, K.V., Bowring, S.A., Coleman, D.S., Hoakins, D.P., Davidek, K.L., 1995. Multi-stage thermal history of the 4.0 Ga Acasta Gneisses. In AGU Fall Meeting. EOS Transactions. p. 76. F708.

Hofmann, A.W., Jochum, K.P., Seufert, M., White, W.M., 1986. Nb and Pb in oceanic basalts: new constraints on mantle evolution. Earth and Planetary Science Letters 79, 33-45.

Iizuka, T., Horie, K., Komiya, T., Maruyama, S., Hirata, T., Hidaka, H., Windley, B.F., 2006. 4.2 Ga zircon xenocryst in an Acasta Gneiss from northwestern Canada: Evidence for early continental crust. Geology 34, 245-248.

Iizuka, T., Komiya, T., Maruyama, S., 2007a. The Early Archean Acasta Gneiss Complex: Geological, Geochronological and Isotopic Studies and Implications for Early Crustal Evolution. In: van Kranendonk, M.J., Smithies, R.H., Bennett, V., C. (Eds.), Earth's Oldest Rocks. Developments in Precambrian Geology vol. 15. Elsevier, Amsterdam, pp. 127-147.

Iizuka, T., Komiya, T., Ueno, Y., Katayama, I., Uehara, Y., Maruyama, S., Hirata, T., Johnson, S.P., Dunkley, D.J., 2007b. Geology and zircon geochronology of the Acasta Gneiss Complex, northwestern Canada: New constraints on its tectonothermal history. Precambrian Research 153, 179-208.

Iizuka, T., Komiya, T., Johnson, S.P., Kon, Y., Maruyama, S., Hirata, T., 2009. Reworking of Hadean crust in the Acasta gneisses, northwestern Canada: Evidence from in-situ Lu-Hf isotope analysis of zircon. Chemical Geology 259, 230-239.

Jenner, F.E., Bennett, V.C., Nutman, A.P., Friend, C.R.L., Norman, M.D., Yaxley, G., 2009. Evidence for subduction at 3.8 Ga: geochemistry of arc-like metabasalts from the southern edge of the Isua Supracrustal Belt. Chemical Geology 261, 83–98.

Jenner F. E. and O'Neill H. St. C., 2012. Analysis of 60 elements in 616 ocean floor basaltic glasses. Geochemistry Geophysics Geosystems 13, Q02005, doi:10.1029/2011GC004009.

Jochum, K.P., Arndt, N.T., Hofmann, A.W., 1991. Nb–Th–La in komatiites and basalts; constraints on komatiite petrogenesis and mantle evolution. Earth and Planetary Science Letters 107, 272–289.

Johnson, r.w., Jaques, a.l., Hickey, r.l., Mckee, c.o., Chappell, b.w., 1985. Manam Island, Papua New Guinea: Petrology and Geochemistry of a Low-TiO_2 Basaltic Island-Arc Volcano. Journal of Petrology 26, 283-323.

Johnson, M.C., Plank, T., 1999. Dehydration and melting experiments constrain the fate of subducted sediments. Geochemistry Geophysics Geosystems 1, GC000014.

Kamei, A., Owada, M., Nagao, T., Shiraki, K., 2004. High-Mg diorites derived from

sanukitic HMA magmas, Kyushu Island, southwest Japan arc: evidence from clinopyroxene and whole rock compositions. Lithos 75, 359-371.

Keppler, H., 1996. Constraints from partitioning experiments on the composition of subduction-zone fluids. Nature 380, 237-240.

Kleine, T., Münker, C., Mezger, K., Palme, H., 2002. Rapid accretion and early core formation on asteroids and the terrestrial planets from Hf-W chronometry. Nature 418, 952-955.

Kogiso, T., Tatsumi, Y., Nakano, S., 1997. Trace element transport during dehydration processes in the subducted oceanic crust: 1. Experiments and implications for the origin of ocean island basalts. Earth and Planetary Science Letters 148, 193-205.

Komiya, T., S. Maruyama, S., Nohda, T. Masuda, M., Hayashi, and S. Okamoto, 1999, Plate tectonics at 3.8 – 3.7 Ga; Field evidence from the Isua accretionary complex, southern West Greenland: Journal of Geology 107, 515-554.

Komiya, T., Hayashi, M., Maruyama, S., Yurimoto, H., 2002a. Intermediate-P/T type Archean metamorphism of the Isua supracrustal belt: Implications for secular change of geothermal gradients at subduction zones and for Archean plate tectonics. American Journal of Science 302, 804-826.

Komiya, T., Maruyama, S., Hirata, T., Yurimoto, H., 2002b. Petrology and geochemistry of MORB and OIB in the mid-Archean North Pole region, Pilbara craton, Western Australia: Implications for the composition and temperature of the upper mantle at 3.5 Ga. International Geology Review 44, 988-1016.

Komiya, T., 2004. Material circulation model including chemical differentiation within the mantle and secular variation of temperature and composition of the mantle.

Physics of the Earth and Planetary Interiors 146, 333-367.

Komiya, T., Maruyama, S., Hirata, T., Yurimoto, H., Nohda, S., 2004. Geochemistry of the oldest MORB and OIB in the Isua Supracrustal Belt, southern West Greenland: Implications for the composition and temperature of early Archean upper mantle. The Island Arc 13, 47-72.

Komiya, T., Yamamoto, S., Aoki, S., Sawaki, Y., Ishikawa, A., Tashiro, T., Koshida, K., Shimojo, M., Aoki, K., 2015. Geology of the Eoarchean, >3.95 Ga, Nulliak supracrustal rocks in the Saglek Block, northern Labrador, Canada: The oldest geological evidence for plate tectonics. Tectonophysics in press.

Labrosse, S., Hernlund, J.W., Coltice, N., 2007. A crystallizing dense magma ocean at the base of the Earth's mantle. Nature 450, 866-869.

Leake, B.E., Woolley, A.R., Arps, C.E.S., Birch, W.D., Gilbert, M.C., Grice, J.D., Hawthorne, F.C., Kato, A., Kisch, H.J., Krivovichev, V.G., Linthout, K., Laird, J., Mandarino, J.A., Maresch, W.V., Nickel, E.H., Rock, N.M.S., Schumacher, J.C., Smith, D.C., Stephenson, N.C.N., Ungaretti, L., Whittaker, E.J.W., Guo, Y., 1997. Nomenclature of amphiboles: Report of the subcommittee an amphiboles of the International Mineralogical Association, Commission on New Minerals and Mineral Names. American Mineralogist 82, 1019-1037.

Mann, A., 1983. Trace element geochemistry of high alumina basalt - Andesite - Dacite - Rhyodacite lavas of the Main Volcanic Series of Santorini Volcano, Greece. Contributions to Mineralogy and Petrology 84, 43-57.

Martin, H., 1986. Effect of steeper Archean geothermal gradient on geochemistry of subduction-zone magmas. Geology 14, 753-756.

Maruyama, S., Liou, J.G., Terabayashi, M., 1996. Blueschists and eclogites of the world and their exhumation. International Geology Review 38, 485-594.

Miyashiro, A., 1953. Calcium-poor garnet in relation to metamorphism. Geochemica et Cosmochemica Acta 4, 179–208.

Mojzsis, S.J., Cates, N.L., Caro, G., Trail, D., Abramov, O., Guitreau, M., Blichert-Toft, J., Hopkins, M.D., Bleeker, W., 2014. Component geochronology in the polyphase ca. 3920 Ma Acasta Gneiss. Geochimica et Cosmochimica Acta 133, 68-96.

Moorbath, S., Whitehouse, M.J., Kamber, B.S., 1997. Extreme Nd-isotope heterogeneity in the early Archaean - fact or fiction ? Case histories from northern Canada and West Greenland. Chemcal Geolgy. 135, 213-231.

Nicholls, I.A., Harris, K.L., 1980. Experimental rare Earth element partition coefficients for garnet, clinopyroxene and amphibole coexisting with andesitic and basaltic liquids. Geochimica et Cosmochimica Acta 44, 287–308.

Nisbet, E.G., Cheadle, M.J., Arndt, N.T., Bickle, M.J., 1993. Constraining the potential temperature of the Archean mantle: A review of the evidence from komatiites. Lithos 30, 291-307.

Nutman, A.P., McGregor, V.R., Friend, C.R.L., Bennett, V.C., Kinny, P.D., 1996. The Itsaq Gneiss Complex of southern West Greenland; the world's most extensive record of early crustal evolution (3900-3600 Ma). Precambrian Research 78, 1-39.

O'Neil, J., Francis, D., Carlson, R.W., 2011. Implications of the Nuvvuagittuq Greenstone Belt for the Formation of Earth's Early Crust. Journal of Petrology 52, 985-1009.

Ohta, H., Maruyama, S., Takahashi, E., Watanabe, Y., Kato, Y., 1996. Field occurrence, geochemistry and petrogenesis of the Archean Mid-Oceanic Ridge Basalts (AMORBs) of the Cleaverville area, Pilbara Craton, Western Australia. Lithos

37, 199-221.

Pawley, A.R., Holloway, J.R., 1993. Water sources for subduction zone volcanism—new experimental constraints. Sciences 260, 664–667.

Pearce, J.A., 1983. Role of the sub-continental lithosphere in magma genesis at active continental margins. In: Norry, M.J., Hawkesworth, C.J. (Eds.), Continental basalts and mantle xenoliths. Shiva Nantwich, pp. 230-249.

Pearce, J.A., Peate, D.W., 1995. Tectonic Implications of the Composition of Volcanic ARC Magmas. Annual Review of Earth and Planetary Sciences 23, 251-285.

Pearce, J.A., 2008. Geochemical fingerprinting of oceanic basalts with applications to ophiolite classification and the search for Archean oceanic crust. Lithos 100, 14-48.

Polat, A., Hofmann, A.W., Rosing, M., 2002. Boninite-like volcanic rocks in the 3.7-3.8 Ga Isua greenstone belt, West Greenland: geochemical evidence for intra-oceanic subduction zone processes in the early Earth. Chemical Geology 184, 231-254.

Polat, A., Hofmann, A.W., 2003. Alteration and geochemical patterns in the 3.7-3.8 Ga Isua greenstone belt, West Greenland. Precambrian Research 126, 197-218.

Polat, A., Hofmann, A.W., Münker, C., Regelous, M., Appel, P.W.U., 2003. Contrasting geochemical patterns in the 3.7–3.8 Ga pillow basalt cores and rims, Isua greenstone belt, Southwest Greenland: implications for postmagmatic alteration processes. Geochimica et Cosmochimica Acta 67, 441-457.

Polat, A., Appel, P.W.U., Fryer, B.J., 2011. An overview of the geochemistry of Eoarchean to Mesoarchean ultramafic to mafic volcanic rocks, SW Greenland: Implications for mantle depletion and petrogenetic processes at subduction zones in the early Earth. Gondwana Research 20, 255–283.

Polat, A., Fryer, B., Samson, I.M., Weisener, C., Appel, P.W.U., Frei, R., Windley, B.F., 2012. Geochemistry of ultramafic rocks and hornblendite veins in the Fiskenæs-set layered anorthosite complex, SW Greenland: Evidence for hydrous uppermantle in the Archean. Precambrian Research 214-215, 124–153.

Rapp, R.P., Watson, E.B., 1995. Dehydration melting of metabasalt at 8–32kbar–implications for continental growth and crust–mantle recycling. Journal of Petrology 36, 891–931.

Rapp, R.P., Shimizu, N., Norman, M.D., Applegate, G.S., 1999. Reaction between slab-derived melts and peridotite in the mantle wedge: experimental constraints at 3.8 GPa. Chemical Geology. 160, 335-356.

Reimink, J.R., Chacko, T., Stern, R.A., Heaman, L.M., 2014. Earth's earliest evolved crust generated in an Iceland-like setting. Nature Geoscience 7, 529-533.

Righter, K., 2011. Prediction of metal-silicate partition coefficients for siderophile elements: an update and assessment of PT conditions for metal-silicate equilibrium during accretion of the Earth. Earth and Planetary Science Letters. 304, 158–167.

Rizo, H., Boyet, M., Blichert-Toft, J., Rosing, M.T., 2013. Early mantle dynamics inferred from ^{142}Nd variations in Archean rocks from southwest Greenland. Earth and Planetary Science Letters 377-378, 324-335.

Rollinson, H., 1997. Eclogite xenoliths in west African kimberlites as residues from Archaean granitoid crust formation. Nature 389, 173-176.

Roth, A.S.G., Bourdon, B., Mojzsis, S.J., Rudge, J.F., Guitreau, M., Blichert-Toft, J., 2014. Combined ^{147,146}Sm-^{143,142}Nd constraints on the longevity and residence time of early terrestrial crust. Geochemistry, Geophysics, Geosystems-G3 15, 2329-2345.

Rubibie D.C., Frost D.J., Mann U., Asahara Y., Nimmo F., Tsuno K., Kegler P., Holzheid A. and Palme H., 2011. Heterogeneous accretion, composition and core-mantle differentiation of the Earth. Earth and Planetary Science Letters 301, 342.

Sano, Y., Takeda, K., Hidaka, H., Yokoyama, K., Nutman, A.P., 1999. Palaeoproterozoic thermal events recorded in the ~ 4.0 Ga Acasta gneiss, Canada: Evidence from SHRIMP U-Pb dating of apatite and zircon. Geochimica et Cosmochimica Acta 63, 899-905.

Schmidt, M.W., Dardon, A., Chazot, G., Vannucci, R., 2004. The dependence of Nb and Ta rutile–melt partitioning on melt composition and Nb/Ta fractionation during subduction processes. Earth and Planetary Science Letters 226, 415-432.

Shibata, T., Nakamura, E., 1997. Across-arc variations of isotope and trace element compositions from Quaternary basaltic volcanic rocks in northeastern Japan: Implications for interaction between subducted oceanic slab and mantle Wedge. Journal of Geophysical Research 102, 8051-8064.

Shimizu, N., 1995. Chromatographic chemical modifications during migration of MORB melts. In AGU Fall Meeting. EOS Transactions. p. 75. S266-267.

Smithies, R.H., Champion, D.C., Cassidy, K.F., 2003. Formation of Earth's early Archaean continental crust. Precambrian Research 127, 89-101.

Sun, S.S., McDonough, W.F., 1989. Chemical and isotopic systematics of oceanic basalts: implications for mantle composition and processes. In Magmatism in the Ocean Basins, Geological Society of London Special Publication 42, 313–345.

Song, B., Nutman, A.P., Liu, D., Wu, J., 1996. 3800 to 2500 Ma crustal evolution in the

Anshan area of Liaoning Province, northeastern China. Precambrian Research 78, 79-94.

Spear, F.S., 1981 Amphibole-plagioclase equilibria: an empirical model for the relation albite+tremolite = edenite + 4 quartz. Contributions to Mineralogical Petrology 77, 355-364.

Spear F S., 1988. Thermodynamic projection and extrapolation of highvariance mineral assemblages. Contributions to Mineralogy and Petrology 98 346–351

Spear, F.S., 1993. Metamorphic phase equilibria and pressure-temperature-time paths. Mineralogical Society of America, Washington, D. C., 799 pp.

Stern, R.A., Bleeker, W., 1998. Age of the world's oldest rocks refined using Canada's SHRIMP: The Acasta gneiss complex, Northwest Territories, Canada. Geoscience Canada 25, 27-31.

Stevenson, D.J., 1987. Origin of the Moon — the collision hypothesis. Annual Review of Earth and Planetary Sciences 15, 271–315.

Tatsumi, Y., Hamilton, D.L., Nesbitt, R.W., 1986. Chemical characteristics of fluid phase released from a subducted lithosphere and origin of arc magmas: Evidence from high-pressure experiments and natural rocks. Journal of Volcanology and Geothermal Research 29, 293-309.

Thorpe, R.I., Cumming, G.L., Mortensen, J.K., 1992. A significant Pb isotope boundary in the Slave Province and its probable relation to ancient basement in the western Slave Province. In: Richardson, D.G., Irving, M. (Eds.), Project Summaries, Canada-Northwest Territories Mineral Development Subsidiary Agreement 1987–1991. Open File 2484. Geological Survey of Canada, pp. 179-184.

Tiepolo, M., Bottazzi, P., Foley, S.F., Oberti, R., Vannucci, R., Zanetti, A., 2001.

Fractionation of Nb and Ta from Zr and Hf at mantle depths: the role of titanian pargasite and kaersutite. Journal of Petrology 42, 221-232.

Tiepolo, M., Oberti, R., Vannucci, R., 2002. Trace-element incorporation in titanite: constraints from experimentally determined solid/liquid partition coefficients. Chemical Geology 191, 105-119.

Tiepolo, M., Oberti, R., Zanetti, A., Vannucci, R., Foley, S.F., 2007. Trace-element partitioning between amphibole and silicate Melt. Reviews in Mineralogy and Geochemistry 67, 417-452.

Toplis, M.J., 2005. The thermodynamics of iron and magnesium partitioning between olivine and liquid: criteria for assessing and predicting equilibrium in natural and experimental systems. Contributions to Mineralogy and Petrology 149, 22–39.

Wade, J., Wood, B.J., 2001. The Earth's 'missing' niobium may be in the core. Nature 409, 75-78.

Williams, I. S., Black, L, P,. Compston, W., 1986. Four zircon ages from one rock: the evolution of a 3930 Ma-old granulite from Mount Sones, Antarctica, Terra Cognita 6, 153.

Winther, K.T., Newton, R.C., 1991. Experimental melting of hydrous low-K tholeiite:evidence on the origin of Archean cratons. Bulletin of the Geological Society of Denmark 39, 213–228.

Wood B.J., Walter M.J., Wade J. 2006. Accretion of the Earth and segregation of its core. Nature 441, 825-833

Figure captions

Figure 2-1. Geological map of the Acasta Gneiss Complex (AGC), revised after Iizuka et al. (2007), sample localities are also shown. Mafic to intermediate rocks occur as blocks, pods and layers all over the AGC. They are intruded by, or occur as enclaves within, the felsic gneisses. The numbers beside open star symbols show magmatic ages of the felsic and layered gneisses (Bowring et al., 1989b; Bowring and Housh, 1995; Bleeker and Stern, 1997; Stern and Bleeker, 1998; Bowring and Williams, 1999; Iizuka et al., 2006, 2007; Mojzsis et al., 2014; Reimink et al., 2014).

Figure 2-2. Photographs of representative outcrops of the mafic to intermediate rocks in the eastern (a-f) and western areas (g and h). (a) Discontinuous and elongated mafic rocks surrounded by felsic gneisses (N65˚14'21",W115˚57'46"). (b) Mafic rock blocks cut by granitic gneisses. The gneissic structures of mafic rocks are truncated by the felsic intrusions. White pegmatites occur along their boundary with the felsic intrusions and are intruded into the mafic rock. (c) Massive mafic enclaves in the granitic gneisses, strongly deformed, are mixed with the ambient felsic gneisses (N65˚17'43",W115˚51'43"). (d) Massive mafic enclaves in granitic gneiss (N65˚15'51",W115˚58'05"). (e) A gabbroic rock, cut by a metamorphosed basaltic dike (N65˚14'47",W115˚57'05"). (f) Mafic rock, partially melted to form migmatite. (g and h) Rhythmical layering of leucocratic and melanocratic layers (N65˚17'67",W115˚59'22"). Photos of (a), (b) and (f) are from the same location.

Figure 2-3. Localities of the mafic rocks studied. Yellow circle; clinopyroxene-free amphibolite, large yellow double circle; clinopyroxene-bearing amphibolite, green triangle; clinopyroxene-free hornblendite, green double triangle; clinopyroxene-bearing hornblendite, pink square; cummingtonite-free garnet-amphibolite, and large pink double square; cummingtonite-bearing garnet-amphibolite.

Figure 2-4. Comparisons of trace element compositions, analyzed by acid digestion (vertical axes) and bead digestion methods (lateral axes). Error bars are 2SD of 100 data for each sample analysis.

Figure 2-5. Photomicrographs of representative textures of (a-d) amphibolites, (e, f) hornblendite and (g, h) garnet-amphibolites. (a) A fine-grained amphibolite with thin hornblende laths and irregular forms of plagioclases (AC177). (b) A medium-grained amphibolite with hornblende, clinopyroxene and plagioclase (AC477). Clinopyroxenes occur as discrete grains or cores within hornblendes. (c) A medium-grained amphibolite with hornblende and plagioclase (AY61). (d) A fine-grained amphibolite, which contains significant amounts of fine-grained biotite (AC430). (e) A coarse-grained hornblendite, comprising large, euhedral to subhedral hornblende grains with tiny quartz, biotite and chlorite inclusions (AY259). (f) A hornblendite with granoblastic texture, containing clinopyroxene grains (AC148). The upper light panel shows a backscattered electron image of the clinopyroxene with amphibole and calcite inclusions. (g) A garnet-amphibolite with large, roundish and irregularly fractured garnets and relatively large amounts of apatite and ilmenite (AY105). (h) A

garnet-amphibolite with cummingtonite (AY104). The cummingtonite grains occur along the rim of the hornblende, accompanied with pinkish garnet, plagioclase, apatite and ilmenite. Hbl: hornblende, Cpx: clinopyroxene, Pl: plagioclase, Bt: biotite, Chl: chlorite, Qtz: quartz, Cal: calcite, Grt: garnet, Ap: apatite, Ilm: ilmenite and Cum: cummingtonite.

Figure 2-6. Photomicrographs of hornblendites and amphibolites, illustrating retrograde characteristics (c-h). (a) Calcite-filling boundaries among amphibole grains in a hornblendite of AC148. (b) A hornblendite (AC283) containing numerous small ilmenite grains. (c) Biotite-replacing chlorite in an amphibolite (AY34). (d) A hornblende is partially replaced by chlorites (AY61). (e) An ilmenite grain rimmed by secondary titanites (AY61). (f) Titanite veins crosscutting hornblende and plagioclase (AY61). (g) Numerous small ilmenite grains exsolved from a large amphibole grain (AY110). (h) Plagioclases break down into fine-grained epidote and albite grains (AC415). Hbl; hornblende, Cal; calcite, Ttn; titanite, Chl; chlorite, Bt; biotite, Pl; plagioclase, Ilm; ilmenite.

Figure 2-7. Mg# vs. Si per formula unit diagram for average compositions of Ca-amphiboles in each mafic rock. Core compositions are selected for some amphiboles with different compositions in their rims and cores. The Si contents are calculated on the basis of 23 oxygens. (b) Compositions of clinopyroxenes from AC279, AC477 and AC148 on a Wo-En-Fs diagram. (c) Ternary plots of molar Mn, Mg and Fe contents of garnets in garnet-amphibolites. The dark gray, pale gray and black areas show compositional fields of garnets under greenschist, amphibolite and granulite facies conditions, respectively (Miyashiro, 1953).

Figure 2-8. MgO vs. major element diagrams for amphibolite groups I to III, hornblendite and garnet-amphibolite, compared with modern MORB and OIB.

Figure 2-9. Chondrite-normalized REE patterns and primitive mantle-normalized trace element diagrams for the amphibolite groups I and II (a, c), amphibolite group III (c, d), hornblendites (e, f) and garnet-amphibolites (g, h). Chondrite and primitive mantle values are from Sun & McDonough (1989).

Figure 2-10. Compositional variations of amphibolite groups I and II, hornblendites and felsic rocks on MgO vs. Al_2O_3 diagrams. Open and gray diamonds show whole-rock compositions of 3.6-4.0 Ga felsic gneisses (Mojzsis et al., 2014; Reimink et al., 2014). A dotted arrow shows an olivine fractionation trend from the highest MgO sample; the compositional variation of amphibolite groups I and II clearly deviate from this trend, especially for relatively low MgO samples. An aluminous partial melt and a residue with high MgO and low Al_2O_3 contents, generated by melting a metabasalt under water-saturated condition (Beard and Lofgren, 1991), are also shown.

Figure 2-11. Representative whole-rock and mineral compositions of mafic rocks projected onto AFM (a) and ACF (b) diagrams. The mineral parageneses on the AFM and ACF diagrams based on amphibolite and upper amphibolite faces conditions, respectively (Spear, 1988). Samples without clinopyroxene and cummingtonite are plotted on the AFM diagram whereas clinopyroxene or cummingtonite-bearing samples are plotted on the ACF diagram. Large symbols

indicate whole-rock compositions, small symbols display average mineral compositions. Triangle: hornblendite; circle: amphibolite; square: garnet-amphibolite.

Figure 2-12. Comparison of the high Al_2O_3 samples from amphibolite group II, with over 15 wt.% Al_2O_3, and hornblendites with calculated melts. The calculation method for the melt is described in text.

Figure 2-13. Al_2O_3 content vs. La content, $(La/Yb)_N$ ratio and Ti anomaly diagrams for amphibolite group I (solid circles), amphibolite group II (open circles), hornblendites (triangles) and the average calculated melt (a diamond). Solid and dotted lines show mixing trends between the average calculated melt and amphibolite group I, and between average calculated melt and hornblendite, respectively.

Figure 2-14. Zirconium vs. incompatible element diagrams for amphibolite groups I to III, hornblendites, and garnet-amphibolites. Lines were drawn between the origin and AC384, the sample with the lowest Zr content among amphibolite group I; mean fractionation trends assume that they are highly incompatible elements. Good correlations of the REE, Th, Ti, and Nb with Zr for amphibolite group I indicate that they still preserve their original compositions.

Figure 2-15. (a) Nb/Yb vs. Th/Yb (after Pearce, 2008) and (b) Nb/Yb vs. La/Yb diagrams for amphibolite group I, early Archean metabasalts and modern MORBs and OIBs. Amphibolite group I plotted above the MORB-OIB array,

indicating that they underwent a Nb-Th decoupling process. However, amphibolite group I plot almost on the primitive mantle on the Nb/Yb vs. La/Yb diagram. Literature data taken from Polat et al. (2002) and Furnes et al. (2009) for Isua boninitic metabasalt, Polat et al. (2003) and Polat and Hofmann. (2003) for undifferentiated amphibolite, O'Neil et al. (2011) for Nuvvuagittuq faux-amphibolite, Jenner and O'Neil (2012) for present MORB and Chen et al. (1990) and Xu et al. (2005) for Hawaii basalt.

Table 1. Major element compositions of constituent minerals from representative samples of Acasta mafic rocks

	Amphibolite (no cpx)						**Amphibolite (with cpx)**			**Garnet-amphibolite (no cum)**				**Garnet-amphibolite (with cum)**				**Hornblendite (no cpx)**		**Hornblendite (with cpx)**	
sample	AY61 hbl	AY61 pl	AY61 chl	AC463 hbl	AC463 pl	AC463 Chl	AC279 hbl	AC279 pl	AC279 cpx	AY105 hbl	AY105 pl	AY105 chl	AY105 grt	AY104 hbl	AY104 pl	AY104 cum	AY104 grt	AY259 hbl	AY259 chl	AC148 hbl	AC148 cpx
The number of analysis	10	8	6	11	7	7	19	20	4	4	3	4	10	5	10	6	7	13	3	13	2
SiO_2	42.55	60.89	25.60	44.77	59.55	26.24	43.81	60.43	52.73	41.55	62.04	26.59	37.83	41.39	60.97	53.53	37.98	51.69	26.37	52.94	54.42
TiO_2	0.79	0.01	0.04	0.79	0.00	0.04	0.92	0.01	0.02	0.85	0.00	0.04	0.03	0.49	0.01	0.06	0.02	0.26	0.04	0.26	0.00
Al_2O_3	12.54	24.68	19.47	10.41	25.47	19.86	10.60	25.40	0.84	12.83	24.04	16.11	21.24	15.01	24.63	0.43	21.43	3.88	19.52	3.71	0.33
Cr_2O_3	0.01	0.02	0.01	0.13	0.00	0.16	0.12	0.03	0.02	0.00	0.00	0.00	0.01	0.02	0.02	0.00	0.01	0.27	0.58	0.28	0.10
FeO^T	19.94	0.06	29.35	16.47	0.03	25.46	19.18	0.10	10.44	22.64	0.05	32.12	29.17	21.14	0.04	27.62	30.71	12.84	23.50	8.64	4.60
Fe_2O_3	4.24	-	-	2.00	-	-	4.08	-	-	6.91	-	-	-	9.96	-	-	-	1.41	-	1.40	-
FeO	15.70	-	-	14.47	-	-	15.10	-	-	15.72	-	-	-	11.18	-	-	-	11.43	-	7.24	-
MnO	0.20	0.01	0.20	0.18	0.01	0.19	0.31	0.01	0.17	0.23	0.01	0.09	4.53	0.24	0.01	0.57	1.97	0.06	0.00	0.01	0.00
MgO	7.55	0.00	12.33	9.98	0.00	14.19	8.57	0.01	11.22	5.86	0.00	10.51	1.69	6.73	0.01	14.23	2.46	14.27	15.63	17.34	15.41
CaO	11.82	6.54	0.01	12.32	7.63	0.06	11.86	6.70	23.62	10.75	5.58	0.07	5.90	10.37	6.01	0.46	5.42	12.05	0.04	12.47	24.28
Na_2O	1.23	7.77	0.07	0.97	7.39	0.03	1.07	7.13	0.35	1.39	7.90	0.11	0.02	1.36	7.40	0.08	0.02	0.43	0.03	0.42	0.21
K_2O	0.97	0.11	0.04	1.01	0.09	0.03	1.03	0.25	0.01	0.74	0.08	0.03	0.01	0.36	0.17	0.01	0.00	0.30	0.00	0.29	0.00
Si in formura	6.43			6.74			6.62			6.34				6.16				7.59		7.60	
$Mg/(Mg+Fe^{2+})$	0.46			0.55			0.50			0.40				0.52				0.69		0.81	
$Mg/(Mg+Fe^T)$			0.43			0.50			0.66			0.37				0.48			0.54		0.86
An content		0.32			0.36			0.34			0.28				0.31						
Almandine													65.80				69.75				
Grossular													17.04				15.77				
Pyrope													6.81				9.95				
Spessartine													10.34				4.54				

FeO^T;total Fe, assumed to be FeO.

Fe_2O_3 were calculated assuming stoichiometry

Amphiboles calculated on the basis of 23 oxygens

An = Ca/(Ca + Na)

Almandine; $Fe^T/(Fe^T + Ca + Mg + Mn)$, Grossular; $Ca/(Ca + Fe^T + Mg + Mn)$, Pyrope; $Mg/(Mg + Ca + Fe^T + Mn)$, Spessartine; $Mn/(Mn + Ca + Fe^T + Mg)$

Table 2. Results of the major elements of JB-3 and their recommended values

Elements (ppm)	Measured (n=4)	RSD (%)	avg/PV	Preferred value
SiO_2	50.9	0.33	1.00	51.0
TiO_2	1.44	1.04	1.00	1.44
Al_2O_3	17.1	0.98	0.99	17.2
Fe_2O_3	11.9	1.68	1.01	11.8
MnO	0.176	1.01	1.00	0.177
MgO	5.09	3.18	0.98	5.19
CaO	9.79	0.49	1.00	9.79
Na_2O	2.82	5.24	1.03	2.73
K_2O	0.777	1.56	1.00	0.780
P_2O_5	0.292	15.01	0.99	0.294

Preferred value :

N. Imai et al. (1995) Geostandards Newsletter, 19, 135-213.

Table 3. Results of a basaltic reference material W-2 (USGS) analyses of two decomposition methods.

Elements(ppm)	Glass bead digestion			$HF-HClO_4$ digestion			Preferred value
	Measured (n=6)	RSD (%)	avg/PV	Measured (n=4)	RSD (%)	avg/PV	
V	276	4.0	1.03	265	7.9	0.99	268
Cr	87.7	10.5	0.94	84.2	9.4	0.90	93
Co	43.7	5.1	0.97	43.8	5.3	0.97	45
Ni	71.2	6.7	0.99	74.7	5.3	1.04	72
Cu	104	2.6	0.99	117	6.8	1.12	105
Zn	81.4	8.3	1.06	80.9	6.2	1.05	77
Rb	19.3	2.5	0.92	19.3	6.0	0.92	21
Sr	198	3.1	1.01	195	7.9	1.00	196
Y	19.3	3.9	0.88	19.2	8.0	0.87	22
Zr	87.6	5.3	0.95	85.1	7.2	0.92	92
Nb	7.51	5.5	1.00	7.64	4.1	1.02	7.5
Cs	0.868	1.9	0.94	0.873	6.9	0.95	0.92
Ba	171	1.5	0.99	171	5.8	1.00	172
La	10.2	1.2	0.95	10.1	5.9	0.94	10.8
Ce	22.9	2.1	0.98	22.6	6.8	0.97	23.4
Pr	2.94	2.4	0.98	2.90	6.4	0.97	3
Nd	13.3	2.5	1.02	13.1	6.5	1.01	13
Sm	3.27	2.7	0.99	3.22	6.8	0.97	3.3
Eu	1.10	3.3	1.02	1.08	7.7	1.00	1.08
Gd	3.86	3.7	1.05	3.84	5.3	1.05	3.66
Tb	0.626	3.7	1.01	0.617	5.9	1.00	0.62
Dy	3.99	2.3	1.05	3.92	6.0	1.03	3.79
Ho	0.810	3.8	1.03	0.794	6.5	1.01	0.79
Er	2.29	3.8	1.03	2.24	6.8	1.01	2.22
Tm	0.323	3.4	0.98	0.314	7.4	0.95	0.33
Yb	2.10	2.9	1.03	2.04	7.5	0.99	2.05
Lu	0.311	3.4	1.00	0.304	7.4	0.98	0.31
Hf	2.48	4.9	1.01	2.38	4.1	0.97	2.45
Ta	0.471	16.8	1.00	0.450	16.8	0.96	0.47
Pb	8.05	4.3	1.05	7.59	4.4	0.99	7.7
Th	2.18	5.0	1.00	2.14	11.4	0.98	2.17
U	0.517	4.8	1.01	0.497	10.8	0.98	0.51
$(Nb/Nb^*)_{PN}$	0.520	7.6	1.02	0.538	5.9	1.05	0.51
$(Ta/Ta^*)_{PN}$	0.568	18.0	1.02	0.550	8.0	0.99	0.56
$(Eu/Eu^*)_{CN}$	0.948	2.1	1.00	0.942	1.7	1.00	0.95
$(Zr/Zr^*)_{PN}$	0.910	6.3	0.94	0.899	3.1	0.93	0.96
$(Hf/Hf^*)_{PN}$	0.933	4.1	1.00	0.911	8.4	0.98	0.93
Nb/Yb	3.57	7.2	0.98	3.75	3.6	1.03	3.66
La/Yb	4.87	2.3	0.92	4.98	2.3	0.95	5.27
Th/Yb	1.04	3.3	0.98	1.05	4.6	0.99	1.06

Preferred value : http://georem.mpch-mainz.gwdg.de/sample_query_pref.asp

$(Nb/Nb^*)_{PM} = 2\times Nb_{PM}/(Th_{PM}+La_{PM})$, $(Ta/Ta^*)_{PM} = 2\times Ta_{PM}/(Th_{PM}+La_{PM})$,

$(Eu/Eu^*)_{CN} = 2\times Eu_{CN}/(Sm_{CN}+Gd_{CN})$, $(Zr/Zr^*)_{PM} = 2\times Zr_{PM}/(Sm_{PM}+Nd_{PM})$,

$(Hf/Hf^*)_{PM} = 2\times Hf_{PM}/(Sm_{PM}+Nd_{PM})$

Table 4. Trace element data measured by HF-$HClO_4$ digestion method.

	Hornblendite					Garnet-amphibolite					Amphibolite group I								
Sample	AC354	AC148	AY259	AC283	AC290	AC543	AY121	AY100	AY104	AY105	AC177	AC179	AC181	AC234	AC489	AC384	AY9	AY118	AY110
V	101	154	120	107	167	134	2.16	4.14	3.53	4.58	324	282	226	339	337	226	376	279	250
Cr	1935	1547	1165	1301	699	4.30	4.22	4.39	3.66	3.50	142	171	171	160	152	242	134	343	289
Co	45.8	48.1	46.4	93.0	56.3	60.9	17.3	21.0	60.6	49.6	50.1	40.0	47.8	51.2	46.8	45.2	49.8	53.9	49.1
Ni	518	318	563	1263	270	3.09	1.34	1.97	1.80	2.39	81.6	69.3	83.1	82.4	101	135	82.7	189	184
Cu	0.944	1.57	15.0	83.5	24.0	232	28.6	39.8	5.33	16.1	130	55.7	35.5	123	38.4	31.0	10.9	101	63.3
Zn	160	115	178	96.1	108	148	61.4	78.0	140	116	107	92.5	115	112	105	106	114	138	103
Rb	11.9	1.52	3.81	1.35	7.92	9.38	3.73	4.64	5.06	10.6	12.4	12.3	6.70	22.9	13.2	17.8	5.28	12.4	7.24
Sr	19.9	19.2	10.2	9.94	96.0	223	308	135	113	160	109	122	150	132	124	125	311	142	165
Y	22.2	20.4	36.0	9.48	25.7	29.2	32.2	31.0	25.3	28.1	23.5	20.9	20.8	21.6	24.2	16.3	23.6	28.8	23.1
Zr	7.98	20.7	26.1	16.3	58.8	101	188	40.7	13.9	19.6	21.9	21.6	18.8	25.4	24.9	28.3	30.6	111	68.9
Nb	2.65	2.84	4.90	3.56	15.7	12.5	8.50	11.4	7.38	8.18	3.30	2.95	2.78	2.85	4.17	2.07	3.59	6.91	5.59
Cs	0.227	0.010	0.075	0.128	0.062	0.181	0.124	0.141	0.144	0.362	0.129	0.099	0.030	0.187	0.185	0.078	0.078	0.177	0.179
Ba	20.6	4.72	23.2	8.78	80.8	200	121	63.2	50.6	133	42.9	48.4	54.2	111	58.8	47.6	165	82.4	92.0
La	10.8	8.86	5.73	4.12	21.1	24.5	11.5	7.43	16.1	17.4	4.60	3.20	3.64	3.96	4.57	3.01	4.59	6.78	7.73
Ce	23.2	25.2	18.1	10.9	54.5	51.9	27.7	18.3	36.0	38.1	12.2	8.86	10.0	10.2	12.5	7.50	11.4	16.2	19.0
Pr	3.20	3.50	2.89	1.58	7.56	6.17	4.19	2.74	4.72	5.01	1.79	1.36	1.36	1.52	1.81	1.10	1.73	2.41	2.59
Nd	15.2	15.1	14.8	7.35	33.5	25.3	21.2	15.0	22.0	23.3	9.16	7.24	7.05	7.91	9.29	5.68	8.87	12.5	12.5
Sm	3.95	3.59	4.51	1.92	7.31	5.53	5.70	4.92	5.17	5.64	2.73	2.31	2.23	2.43	2.83	1.80	2.68	3.83	3.33
Eu	0.931	0.675	1.06	0.485	1.42	1.85	2.51	1.85	1.79	1.92	0.958	0.854	1.16	0.895	1.04	0.693	0.972	1.38	1.17
Gd	4.22	3.80	5.66	2.21	7.02	5.96	6.92	7.12	6.19	6.82	3.75	3.26	3.18	3.43	3.95	2.53	3.77	5.10	4.19
Tb	0.710	0.631	1.02	0.342	1.02	0.937	1.07	1.10	0.894	0.998	0.657	0.577	0.569	0.606	0.691	0.450	0.661	0.860	0.693
Dy	4.54	4.07	7.00	2.09	6.01	5.92	6.61	6.68	5.29	5.97	4.49	3.93	3.92	4.14	4.67	3.10	4.48	5.68	4.51
Ho	0.925	0.825	1.49	0.409	1.14	1.18	1.32	1.29	1.02	1.16	0.970	0.852	0.851	0.895	0.998	0.668	0.971	1.19	0.948
Er	2.71	2.40	4.49	1.12	3.12	3.39	3.63	3.41	2.70	3.04	2.86	2.49	2.51	2.63	2.91	1.98	2.85	3.44	2.75
Tm	0.407	0.357	0.703	0.156	0.420	0.480	0.492	0.440	0.339	0.382	0.421	0.369	0.369	0.392	0.426	0.291	0.425	0.503	0.396
Yb	2.73	2.35	4.80	1.01	2.64	3.16	3.26	2.76	2.10	2.33	2.81	2.47	2.46	2.60	2.81	1.95	2.81	3.34	2.62
Lu	0.398	0.345	0.734	0.148	0.375	0.466	0.490	0.400	0.300	0.332	0.432	0.379	0.371	0.402	0.431	0.301	0.432	0.515	0.399
Hf	0.350	0.688	0.892	0.638	1.81	2.91	5.38	1.34	0.696	0.784	0.913	0.825	0.772	0.906	0.974	1.01	1.05	3.05	2.00
Ta	0.103	0.198	0.289	0.362	0.806	0.617	0.618	0.725	0.495	0.515	0.181	0.157	0.149	0.153	0.229	0.125	0.168	0.387	0.325
Pb	5.48	3.50	1.82	0.615	5.78	15.4	5.77	2.85	1.96	3.18	1.67	1.38	2.17	2.77	3.24	8.85	4.51	2.01	2.00
Th	0.018	0.240	0.031	1.62	1.94	1.72	1.31	1.81	1.19	0.878	0.614	0.532	0.577	0.552	0.774	0.435	0.619	1.87	1.31
U	0.145	0.295	0.314	0.223	0.639	0.387	0.530	0.886	0.395	0.299	0.135	0.183	0.133	0.244	0.434	0.166	0.131	0.341	0.373

FeO^T;total Fe, assumed to be FeO.

Amphibolite group II																Depleted-amphibolite				
AY13	AY14	AC499	C389	AC480	AC462	AC279	AC463	AC415	AC477	AY112	AY65	AC228	AC368	AY16	AC440	AY61	AC538	AY33	AC273	AC416
291	391	124	240	222	185	217	170	217	254	17.9	101	170	137	240	99.1	175	100	587	136	125
319	233	62.8	571	185	963	380	477	470	364	3.89	350	67.9	63.5	11.6	94.1	3.62	4.41	6.17	134	487
50.5	51.9	40.0	49.9	38.3	50.5	49.8	52.2	50.3	45.4	20.1	32.4	29.6	28.3	43.2	22.6	68.3	60.8	56.4	39.3	38.4
189	166	17.4	147	61.9	189	98.9	144	123	130	2.92	71.7	25.1	29.6	57.9	61.9	2.16	2.84	13.5	130	187
110	85.7	9.41	59.3	15.7	28.7	9.64	2.67	13.2	40.2	10.2	3.45	32.1	9.66	52.2	3.53	3.84	6.07	14.7	2.43	10.1
105	101	101	70.3	147	139	120	120	107	107	108	103	137	116	101	80.6	128	135	92.8	83.8	72.8
11.5	7.03	12.4	8.35	25.7	9.56	7.13	16.3	7.21	15.0	10.0	65.2	29.5	26.2	11.6	7.13	23.1	19.1	23.2	33.6	35.8
113	161	213	137	152	105	126	91.3	120	183	193	447	270	369	430	384	174	214	155	218	282
25.6	22.4	17.2	16.1	27.3	41.1	22.4	24.0	13.8	13.2	49.0	11.6	33.5	29.5	17.4	17.8	5.92	9.51	5.33	7.78	6.17
65.6	53.5	51.9	55.3	77.4	54.4	48.5	64.6	28.9	25.7	72.4	38.7	73.0	63.4	28.5	60.1	10.4	19.9	10.5	18.5	18.8
4.85	5.57	5.97	4.97	8.81	15.9	5.98	6.69	3.20	2.45	11.2	4.83	22.2	13.4	8.13	9.05	1.44	3.02	1.44	4.91	1.73
0.646	0.288	0.200	0.166	0.195	0.172	0.088	0.333	0.163	0.111	0.298	1.61	0.727	0.329	0.642	0.161	1.11	0.512	1.00	1.26	0.550
99.1	102	285	49.1	398	247	130	307	109	188	210	833	529	379	290	272	395	267	214	386	464
7.23	7.51	9.97	11.8	12.5	21.6	11.7	8.02	7.17	8.96	16.6	36.4	28.5	39.4	28.5	19.4	2.69	4.74	2.86	5.43	5.81
16.8	17.4	23.0	24.7	29.8	50.0	25.3	20.7	15.9	16.8	44.0	66.6	67.8	88.5	61.8	39.5	5.42	9.72	5.60	10.7	10.1
2.44	2.44	2.93	2.98	4.19	6.51	3.28	2.93	2.04	1.87	6.53	7.18	9.08	11.2	7.53	4.81	0.703	1.20	0.683	1.25	1.18
12.0	11.7	12.6	12.8	18.6	28.3	14.9	13.6	9.06	7.39	32.6	26.1	38.7	46.7	30.9	19.5	3.15	5.27	3.01	5.10	5.03
3.36	3.18	2.92	3.01	4.34	7.02	3.63	3.69	2.23	1.62	8.61	3.94	7.82	8.51	5.45	4.07	0.831	1.36	0.776	1.24	1.17
1.14	1.11	0.988	1.01	1.19	1.27	1.15	1.13	0.721	0.646	3.08	1.20	2.42	1.98	1.86	1.08	0.613	0.811	0.489	0.521	0.466
4.36	4.02	3.33	3.46	4.97	8.03	4.33	4.40	2.67	2.05	10.4	3.32	7.87	7.51	4.63	3.87	1.09	1.71	0.993	1.49	1.37
0.747	0.679	0.525	0.541	0.817	1.32	0.696	0.731	0.436	0.354	1.64	0.409	1.16	1.04	0.619	0.574	0.182	0.288	0.166	0.242	0.206
4.97	4.43	3.32	3.36	5.30	8.55	4.49	4.66	2.82	2.43	10.3	2.33	7.03	6.17	3.62	3.46	1.21	1.90	1.10	1.54	1.29
1.06	0.936	0.679	0.667	1.12	1.74	0.917	0.953	0.583	0.535	2.06	0.459	1.40	1.19	0.701	0.684	0.250	0.393	0.227	0.313	0.259
3.06	2.70	1.94	1.86	3.29	4.85	2.62	2.75	1.67	1.61	5.72	1.34	3.92	3.41	2.02	2.01	0.709	1.12	0.643	0.903	0.719
0.446	0.392	0.277	0.255	0.487	0.676	0.369	0.398	0.242	0.242	0.776	0.185	0.541	0.456	0.265	0.298	0.098	0.158	0.092	0.132	0.100
2.95	2.59	1.84	1.66	3.24	4.15	2.38	2.62	1.60	1.64	5.04	1.26	3.49	2.96	1.80	2.04	0.650	1.06	0.612	0.889	0.654
0.448	0.395	0.281	0.240	0.484	0.571	0.352	0.389	0.242	0.255	0.760	0.185	0.517	0.426	0.267	0.311	0.097	0.161	0.091	0.130	0.096
2.09	1.64	1.48	1.66	2.16	1.88	1.58	1.78	0.962	0.837	2.13	0.996	1.95	1.89	1.02	1.75	0.401	0.705	0.404	0.585	0.595
0.279	0.312	0.315	0.318	0.454	0.860	0.342	0.400	0.176	0.182	0.694	0.160	1.06	0.643	0.448	0.842	0.091	0.217	0.095	0.277	0.102
1.85	4.28	4.18	2.29	6.69	2.74	2.40	1.73	1.31	9.04	5.29	4.50	7.53	7.92	6.13	6.28	4.26	5.44	3.54	3.59	2.37
1.52	1.33	1.22	3.23	0.575	3.33	0.808	1.56	0.528	0.780	3.61	1.54	1.14	2.43	0.673	8.14	0.399	0.892	0.475	1.02	0.970
0.323	0.513	0.204	0.567	0.539	0.211	2.06	0.358	0.285	0.854	0.926	1.07	0.504	0.753	0.429	0.623	0.336	0.200	0.466	0.000	0.216

Table 5. Major (wt %) and trace (ppm) element data for Acasta mafic rocks. The data of trace elements were measured by bead digestion method.

	Hornblendite					Garnet-amphibolite					
Sample	AC354	AC148	AY259	AC283	AC290	AC543	AY121	AY99	AY100	AY104	AY105
SiO_2	53.36	52.50	50.82	49.09	51.59	48.90	58.18	47.07	46.70	43.38	43.47
TiO_2	0.21	0.31	0.42	0.59	1.40	2.85	0.95	2.86	3.16	3.13	3.25
Al_2O_3	3.50	3.47	4.92	3.10	7.99	13.52	17.49	14.97	14.00	14.91	14.14
FeO^T	10.09	8.79	13.18	13.95	12.84	17.78	10.48	18.22	20.29	19.02	18.49
MnO	0.34	0.28	0.46	0.28	0.24	0.26	0.16	0.39	0.42	0.51	0.37
MgO	16.94	16.56	14.45	19.07	10.36	3.11	1.73	3.54	3.73	4.60	4.09
CaO	12.13	14.55	11.95	9.81	11.82	6.98	6.36	8.05	7.97	8.84	9.73
Na_2O	0.22	0.42	0.45	0.07	0.57	2.62	3.27	2.23	1.73	1.94	1.90
K2O	0.38	0.29	0.42	0.10	0.63	1.13	0.32	0.59	0.32	0.42	0.75
P_2O_5	0.01	0.03	0.02	0.01	0.14	0.13	1.32	1.16	1.32	1.37	1.67
V	133	193	157	151	215	150	48.2	52.8	48.4	22.3	23.7
Cr	2329	1879	1426	1750	780	2.97	3.71	3.41	4.97	2.80	2.86
Co	51.9	53.2	52.4	105	62.1	59.1	16.6	26.4	19.8	62.8	50.2
Ni	619	371	662	1519	297	5.06	3.14	4.88	4.28	1.67	4.46
Cu	2.08	3.18	17.0	90.6	26.2	251	34.0	102	41.4	5.10	16.3
Zn	171	121	189	102	110	149	60.9	77.7	79.8	141	115
Rb	12.6	1.76	4.54	1.65	8.41	9.43	3.78	11.5	4.75	5.44	11.4
Sr	22.8	20.7	11.6	11.2	100	212	297	173	130	116	166
Y	24.0	21.7	39.3	10.3	26.9	28.1	31.6	30.8	30.3	25.7	29.2
Zr	11.4	23.8	31.8	17.3	105	163	294	54.4	58.3	48.1	32.7
Nb	2.79	3.05	5.33	3.86	16.4	10.7	8.69	11.0	12.4	7.79	8.64
Cs	0.229	0.026	0.138	0.152	0.071	0.196	0.134	0.184	0.150	0.160	0.377
Ba	21.2	5.14	24.1	9.73	83.3	195	117	63.0	64.3	52.7	137
La	11.8	8.91	5.81	4.42	21.3	24.3	11.2	10.2	7.28	16.4	18.3
Ce	25.2	25.4	18.4	11.6	55.8	51.4	26.7	23.8	17.7	36.9	40.4
Pr	3.43	3.51	2.92	1.67	7.67	6.10	4.04	3.34	2.65	4.80	5.23
Nd	16.3	15.1	15.1	7.76	34.1	25.0	20.4	17.2	14.5	22.7	24.3
Sm	4.21	3.59	4.69	2.01	7.47	5.47	5.48	5.11	4.77	5.36	5.90
Eu	0.962	0.674	1.10	0.505	1.44	1.81	2.44	1.94	1.80	1.84	1.99
Gd	4.42	3.85	5.87	2.33	7.12	5.79	6.67	7.07	7.06	6.41	7.11
Tb	0.734	0.641	1.06	0.360	1.04	0.922	1.03	1.08	1.08	0.936	1.04
Dy	4.68	4.08	7.21	2.16	6.09	5.69	6.38	6.56	6.52	5.55	6.16
Ho	0.952	0.839	1.54	0.424	1.16	1.16	1.27	1.28	1.27	1.08	1.20
Er	2.79	2.42	4.65	1.15	3.13	3.31	3.50	3.36	3.36	2.78	3.15
Tm	0.412	0.359	0.724	0.163	0.423	0.470	0.469	0.429	0.432	0.357	0.394
Yb	2.82	2.38	5.00	1.06	2.70	3.12	3.14	2.70	2.73	2.21	2.42
Lu	0.408	0.352	0.763	0.151	0.384	0.462	0.474	0.387	0.393	0.311	0.349
Hf	0.415	0.738	0.991	0.636	2.818	4.41	8.24	1.60	1.72	1.38	1.04
Ta	0.101	0.197	0.297	0.363	0.770	0.630	0.670	0.954	0.952	0.519	0.538
Pb	5.55	3.71	2.06	0.678	4.80	14.7	5.52	3.37	2.87	2.24	4.28
Th	0.024	0.358	0.038	1.82	1.68	1.63	1.19	1.78	1.77	1.25	0.915
U	0.144	0.280	0.305	0.230	0.641	0.397	0.531	0.625	0.856	0.425	0.314
$(Nb/Nb^*)_{PN}$	0.449	0.497	1.68	0.389	0.906	0.552	0.805	0.862	1.11	0.567	0.648
$(Ta/Ta^*)_{PN}$	0.283	0.559	1.63	0.634	0.739	0.563	1.08	1.30	1.48	0.657	0.701
$(Eu/Eu^*)_{CN}$	0.677	0.551	0.641	0.711	0.593	0.975	1.23	0.986	0.950	0.961	0.939
$(Zr/Zr^*)_{PN}$	0.095	0.221	0.262	0.302	0.444	0.948	1.92	0.402	0.485	0.298	0.187
$(Hf/Hf^*)_{PN}$	0.125	0.249	0.296	0.401	0.434	0.928	1.94	0.429	0.520	0.310	0.216
Nb/Yb	0.990	1.28	1.07	3.64	6.09	3.44	2.77	4.07	4.55	3.53	3.57
La/Yb	4.18	3.74	1.16	4.17	7.91	7.79	3.56	3.78	2.67	7.43	7.57
Th/Yb	0.008	0.150	0.008	1.72	0.624	0.523	0.380	0.659	0.649	0.564	0.378

FeO^T;total Fe, assumed to be FeO.

$(Nb/Nb^*)_{PM} = 2\times Nb_{PM}/(Th_{PM}+La_{PM})$, $(Ta/Ta^*)_{PM} = 2\times Ta_{PM}/(Th_{PM}+La_{PM})$, $(Eu/Eu^*)_{CN} = 2\times Eu_{CN}/(Sm_{CN}+Gd_{CN})$

$(Zr/Zr^*)_{PM} = 2\times Zr_{PM}/(Sm_{PM}+Nd_{PM})$, $(Hf/Hf^*)_{PM} = 2\times Hf_{PM}/(Sm_{PM}+Nd_{PM})$

Amphibolite group I												
AC176	AC177	AC179	AC181	AC183	AC203	AC234	AC479	AC489	AC490	AC384	AY6	AY9
50.67	50.32	50.24	50.34	50.01	49.76	50.14	48.46	49.97	50.55	50.13	50.25	49.57
1.06	1.16	1.05	0.87	1.16	1.20	1.03	1.36	1.17	1.12	0.76	1.08	1.12
14.28	13.82	14.59	14.05	13.41	13.46	13.89	14.06	14.30	14.35	14.66	14.14	13.68
12.98	13.33	12.30	13.33	15.12	15.47	14.33	14.33	13.65	12.34	10.86	13.06	14.64
0.22	0.23	0.21	0.22	0.22	0.22	0.23	0.24	0.20	0.20	0.21	0.27	0.23
5.35	6.29	6.43	6.64	6.07	5.92	6.42	5.77	6.37	5.35	7.82	6.08	6.37
10.09	10.07	10.34	10.51	9.87	10.29	9.95	10.08	10.47	10.69	10.30	8.96	9.86
2.45	1.93	2.14	1.96	1.81	1.76	1.66	2.32	2.04	2.16	2.45	2.27	2.20
0.61	0.63	0.69	0.47	0.95	0.50	0.84	0.78	0.54	0.42	1.02	1.18	0.52
0.08	0.09	0.09	0.08	0.08	0.07	0.08	0.11	0.10	0.09	0.06	0.09	0.09
327	338	328	269	340	352	341	335	345	319	274	330	368
145	152	208	180	121	130	158	200	160	185	261	139	133
43.6	50.6	47.1	50.8	50.4	45.3	50.7	49.9	45.5	44.2	47.5	48.1	48.7
66.6	84.4	84.3	87.5	70.3	69.1	77.1	96.2	97.1	99.8	149	75.0	76.6
36.3	127	68.0	38.6	139	74.7	128	110	49.9	56.1	31.9	122.0	17.2
113	105	104	114	104	109	107	146	109	104	105	605	113
17.6	12.9	14.0	6.98	15.9	8.95	22.9	15.9	13.0	7.01	18.9	30.62	5.32
129	113	136	155	112	97	128	109	119	110	132	123	297
22.5	23.8	23.4	21.1	23.1	23.4	21.1	25.2	23.4	22.0	16.9	23.6	22.5
61.2	66.8	66.9	56.2	64.5	63.6	54.7	79.3	70.3	67.7	42.8	64.7	62.0
3.06	3.35	3.26	2.82	3.26	3.27	2.75	4.03	4.26	3.65	2.13	3.36	3.53
0.11	0.146	0.120	0.041	0.27	0.08	0.202	0.16	0.186	0.08	0.128	0.19	0.095
81.8	43.5	56.0	56.2	61.0	73.6	108	95.2	57.4	43.0	49.9	348.9	157
2.95	4.69	3.67	3.77	3.83	4.34	3.88	4.38	4.38	2.50	3.09	3.83	4.42
8.79	12.4	10.1	10.3	10.6	11.0	9.91	12.5	12.0	8.40	7.68	10.22	11.0
1.40	1.81	1.56	1.40	1.62	1.71	1.48	1.91	1.73	1.41	1.13	1.54	1.65
7.54	9.29	8.21	7.25	8.42	8.84	7.59	10.0	8.89	7.78	5.83	8.20	8.45
2.45	2.79	2.63	2.30	2.63	2.65	2.34	3.01	2.71	2.55	1.84	2.57	2.55
0.909	0.973	0.984	1.18	0.941	0.988	0.866	1.11	1.01	0.957	0.721	0.933	0.941
3.61	3.87	3.75	3.30	3.78	3.83	3.39	4.19	3.82	3.70	2.64	3.75	3.64
0.646	0.677	0.657	0.595	0.665	0.666	0.589	0.725	0.674	0.638	0.472	0.670	0.634
4.34	4.61	4.52	4.06	4.44	4.45	3.96	4.80	4.47	4.27	3.25	4.51	4.30
0.937	0.990	0.981	0.897	0.969	0.968	0.865	1.036	0.959	0.906	0.697	0.979	0.935
2.77	2.93	2.91	2.60	2.85	2.86	2.54	3.03	2.82	2.63	2.08	2.95	2.74
0.414	0.426	0.422	0.379	0.424	0.423	0.378	0.445	0.414	0.390	0.303	0.455	0.412
2.72	2.86	2.81	2.51	2.82	2.84	2.53	2.93	2.74	2.59	2.04	2.93	2.75
0.420	0.447	0.440	0.391	0.438	0.439	0.391	0.447	0.419	0.400	0.318	0.444	0.426
1.80	1.97	1.97	1.70	1.94	1.90	1.63	2.26	2.02	1.98	1.28	1.95	1.84
0.163	0.179	0.176	0.154	0.191	0.189	0.147	0.252	0.249	0.226	0.132	0.209	0.163
2.69	1.94	1.76	2.45	2.96	1.86	2.50	11.5	3.08	3.85	9.34	633.30	4.27
0.550	0.622	0.608	0.592	0.641	0.587	0.527	0.430	0.724	0.715	0.428	0.599	0.597
0.166	0.153	0.154	0.193	0.154	0.156	0.131	0.127	0.238	0.219	0.429	0.149	0.168
0.797	0.665	0.732	0.636	0.697	0.693	0.652	0.989	0.801	0.849	0.627	0.747	0.735
0.738	0.616	0.685	0.603	0.709	0.697	0.606	1.07	0.815	0.915	0.674	0.806	0.591
0.932	0.905	0.957	1.31	0.913	0.948	0.939	0.955	0.960	0.952	0.999	0.918	0.943
0.985	0.908	0.997	0.953	0.949	0.909	0.898	0.999	0.990	1.05	0.904	0.975	0.924
1.06	0.969	1.06	1.04	1.04	0.99	0.969	1.03	1.03	1.12	0.983	1.065	0.992
1.13	1.17	1.16	1.13	1.16	1.15	1.09	1.38	1.55	1.41	1.04	1.15	1.28
1.09	1.64	1.31	1.51	1.36	1.53	1.53	1.50	1.60	0.96	1.52	1.31	1.61
0.202	0.217	0.216	0.236	0.227	0.207	0.209	0.147	0.264	0.276	0.210	0.204	0.217

Amphibolite group II												
AY118	AY110	AY13	AY14	AC499	C389	AC480	AC462	AC279	AC463	AC415	AC477	AY112
49.83	49.84	49.96	48.35	52.00	54.96	50.42	50.87	51.02	49.49	50.51	51.16	53.02
1.55	1.34	1.49	1.94	0.60	0.89	0.89	0.87	1.02	0.95	0.77	0.55	1.67
13.42	14.39	13.70	14.53	15.51	10.29	14.25	11.87	11.69	11.43	11.48	13.65	14.94
14.28	13.08	12.84	13.29	9.76	10.06	10.49	13.45	13.36	13.32	12.51	11.08	15.88
0.22	0.19	0.21	0.21	0.19	0.15	0.27	0.23	0.24	0.24	0.23	0.23	0.30
7.70	7.50	7.70	7.12	6.36	9.82	7.54	7.67	7.23	9.09	9.23	7.55	2.07
9.55	9.69	9.73	10.12	9.42	10.36	10.01	10.28	10.74	10.44	10.57	10.66	7.56
1.81	2.16	1.90	2.10	3.15	1.45	2.46	1.56	2.03	1.55	1.55	2.46	2.96
0.59	0.51	0.64	0.57	1.19	0.51	1.63	1.06	0.94	1.12	0.75	1.07	0.78
0.15	0.13	0.13	0.12	0.06	0.08	0.10	0.10	0.10	0.11	0.07	0.04	0.56
274	254	308	415	140	239	246	216	239	214	243	258	57.7
329	281	350	255	63.2	543	201	1056	411	521	535	401	5.34
51.6	47.6	51.7	53.2	40.7	48.0	42.8	53.2	53.7	56.4	53.7	42.6	19.4
171	171	204	179	17.5	131	71.0	202	110	157	140	117	4.90
96.9	63.4	108	85.5	7.79	63.3	18.6	29.0	13.8	7.05	13.7	43.3	17.9
131	102	105	99.2	97.2	66.1	150	136	122	119	114	106	101
12.2	7.15	12.3	7.49	12.4	8.07	27.3	10.4	7.82	16.9	7.93	14.7	9.62
134	157	116	168	212	131	160	111	130	96.0	127	178	185
27.6	22.2	26.4	23.5	17.3	15.3	28.7	42.8	23.3	25.2	14.8	12.8	47.3
119	84.7	94.8	90.4	76.0	79.6	96.7	82.3	94.6	80.2	43.0	32.6	83.9
6.88	5.63	5.11	5.76	5.99	4.86	9.04	16.4	6.19	7.01	3.41	2.47	12.2
0.183	0.184	0.672	0.302	0.210	0.175	0.203	0.201	0.115	0.341	0.226	0.124	0.296
77.6	88.5	101	105	287	48.5	421	256	134	325	117	180	198
6.70	7.43	7.55	7.85	9.89	11.3	12.6	22.6	11.6	8.41	7.00	8.80	15.5
15.7	18.3	17.4	18.1	23.1	23.6	29.9	52.4	25.6	21.7	15.7	16.5	41.0
2.33	2.50	2.51	2.53	2.93	2.86	4.24	6.85	3.35	3.06	2.05	1.82	6.09
12.1	12.0	12.3	12.0	12.5	12.2	19.0	29.5	15.1	14.3	9.22	7.10	30.5
3.72	3.24	3.51	3.30	2.89	2.90	4.43	7.32	3.76	3.87	2.29	1.56	8.17
1.33	1.15	1.18	1.13	1.00	0.985	1.23	1.34	1.21	1.19	0.758	0.602	2.95
4.98	4.05	4.57	4.17	3.38	3.29	5.09	8.38	4.47	4.54	2.77	1.88	10.0
0.828	0.674	0.769	0.688	0.534	0.519	0.840	1.39	0.712	0.754	0.452	0.337	1.57
5.44	4.39	5.13	4.57	3.30	3.20	5.51	8.89	4.63	4.91	2.97	2.33	9.90
1.15	0.920	1.09	0.949	0.685	0.639	1.15	1.82	0.945	1.01	0.621	0.505	1.99
3.32	2.66	3.15	2.78	1.96	1.77	3.41	5.06	2.67	2.89	1.77	1.53	5.51
0.487	0.382	0.463	0.407	0.281	0.243	0.495	0.695	0.373	0.415	0.255	0.230	0.753
3.24	2.55	2.99	2.64	1.88	1.58	3.32	4.33	2.48	2.75	1.68	1.55	4.88
0.498	0.392	0.470	0.410	0.286	0.236	0.492	0.608	0.365	0.413	0.256	0.243	0.731
3.28	2.37	2.70	2.48	2.02	2.24	2.58	2.54	2.55	2.16	1.28	0.958	2.45
0.470	0.412	0.296	0.324	0.318	0.326	0.463	0.893	0.342	0.412	0.190	0.184	0.741
1.83	1.86	2.17	2.92	4.33	2.18	6.87	2.95	2.77	1.88	1.50	8.22	4.90
1.76	1.29	1.57	1.35	1.16	3.17	0.546	3.78	0.863	1.84	0.457	0.774	3.40
0.440	0.335	0.384	0.325	0.543	0.760	0.494	0.498	0.237	0.656	0.225	0.513	0.802
0.633	0.607	0.487	0.593	0.598	0.253	1.03	0.596	0.641	0.581	0.614	0.316	0.547
0.752	0.773	0.490	0.580	0.552	0.295	0.914	0.563	0.617	0.594	0.596	0.411	0.578
0.944	0.966	0.899	0.930	0.974	0.971	0.789	0.523	0.902	0.864	0.919	1.07	0.996
1.23	0.935	0.997	0.990	0.862	0.911	0.720	0.384	0.860	0.743	0.642	0.664	0.366
1.23	0.947	1.03	0.986	0.831	0.929	0.697	0.430	0.840	0.724	0.692	0.708	0.387
2.13	2.21	1.71	2.18	3.18	3.08	2.72	3.80	2.50	2.55	2.02	1.59	2.50
2.07	2.92	2.52	2.97	5.26	7.18	3.78	5.21	4.70	3.06	4.15	5.67	3.18
0.545	0.506	0.524	0.509	0.618	2.01	0.164	0.874	0.348	0.667	0.272	0.499	0.697

Amphibolite group II					Amphibolite group III					
AY65	AC228	AC368	AY16	AC440	AY50	AY61	AC538	AY33	AC273	AC416
49.45	50.91	52.95	48.78	57.45	44.20	44.68	45.07	44.80	51.76	50.70
0.37	1.45	0.86	1.03	0.41	2.23	2.12	2.27	1.91	0.41	0.44
18.81	16.88	16.38	16.75	17.19	17.04	17.29	16.30	18.35	15.49	16.51
8.05	10.73	9.55	10.10	6.26	17.29	14.80	16.53	13.32	8.65	7.33
0.16	0.18	0.17	0.16	0.13	0.22	0.21	0.24	0.19	0.16	0.14
7.04	4.61	5.02	6.17	5.23	4.87	5.22	5.18	5.14	9.02	8.78
8.06	8.26	8.14	9.88	7.87	9.31	9.62	9.53	10.75	8.77	9.71
2.88	3.48	3.31	2.93	3.80	2.36	2.47	2.56	2.18	2.86	2.41
2.68	1.70	1.78	0.82	0.74	1.50	1.57	1.22	1.41	1.39	1.72
0.07	0.34	0.23	0.12	0.09	0.02	0.02	0.02	0.01	0.02	0.03
119	195	150	238	119	212	209	126	643	156	146
359	70.7	61.2	9.93	99.8	6.37	2.79	4.49	3.71	139	526
32.8	29.8	26.8	40.1	22.5	72.0	70.5	61.2	62.3	39.8	40.9
76.0	30.0	29.3	51.7	66.6	5.71	3.04	4.43	15.3	135	209
3.49	33.7	16.5	58.7	3.65	13.6	4.00	11.1	17.9	2.92	11.1
103	132	110	95.9	84.4	139	131	133	97.7	82.7	74.6
65.9	30.6	25.2	11.1	7.48	24.2	24.2	19.2	25.2	33.1	36.7
462	282	354	403	395	204	181	208	170	220	295
12.2	35.1	28.6	16.6	18.1	6.14	6.15	9.33	5.75	8.32	6.35
54.6	343	158	64.8	87.6	17.1	14.6	24.1	15.3	23.1	26.0
4.98	22.9	13.1	7.87	9.44	1.75	1.48	3.09	1.59	5.00	1.78
1.59	0.732	0.320	0.604	0.172	0.936	1.15	0.535	1.05	1.21	0.557
873	548	368	278	273	445	410	262	231	398	484
38.2	29.7	39.1	25.7	19.3	2.97	2.90	4.69	3.09	5.45	6.02
70.8	71.6	88.7	56.4	39.4	5.70	5.75	9.54	6.04	10.7	10.5
7.53	9.51	11.1	6.92	4.79	0.715	0.733	1.17	0.736	1.25	1.23
27.3	40.3	45.5	28.7	19.3	3.19	3.27	5.15	3.25	5.15	5.19
4.11	8.07	8.37	5.17	4.04	0.861	0.877	1.33	0.853	1.27	1.20
1.26	2.56	1.91	1.77	1.10	0.680	0.645	0.782	0.538	0.540	0.493
3.28	8.14	6.88	4.12	3.90	1.11	1.12	1.68	1.09	1.50	1.40
0.413	1.23	0.986	0.571	0.572	0.186	0.184	0.283	0.179	0.241	0.210
2.43	7.39	5.99	3.41	3.47	1.23	1.24	1.87	1.19	1.54	1.33
0.474	1.48	1.16	0.666	0.700	0.255	0.258	0.391	0.244	0.318	0.268
1.38	4.17	3.30	1.89	2.02	0.728	0.719	1.12	0.702	0.887	0.736
0.190	0.577	0.444	0.251	0.297	0.100	0.101	0.159	0.098	0.130	0.102
1.29	3.75	2.93	1.75	2.06	0.686	0.664	1.04	0.661	0.885	0.670
0.189	0.566	0.421	0.257	0.314	0.105	0.103	0.162	0.100	0.134	0.104
1.37	7.69	3.94	1.78	2.31	0.546	0.466	0.802	0.497	0.672	0.748
0.164	1.09	0.653	0.470	0.849	0.128	0.095	0.248	0.102	0.275	0.105
4.79	8.08	7.78	5.64	6.40	5.85	4.56	5.18	4.01	3.64	2.52
1.70	1.19	2.10	0.624	8.28	0.463	0.464	0.898	0.573	1.11	1.06
0.482	1.17	0.937	0.196	2.10	0.129	0.151	0.336	0.226	0.363	0.296
0.184	1.12	0.449	0.493	0.211	0.502	0.428	0.498	0.396	0.668	0.236
0.105	0.928	0.391	0.513	0.330	0.640	0.480	0.697	0.441	0.639	0.242
1.01	0.957	0.747	1.13	0.837	2.13	1.99	1.60	1.70	1.19	1.16
0.332	1.28	0.538	0.352	0.669	0.710	0.592	0.633	0.632	0.619	0.711
0.303	1.04	0.486	0.352	0.640	0.823	0.686	0.764	0.744	0.652	0.740
3.86	6.11	4.45	4.50	4.58	2.55	2.22	2.97	2.40	5.66	2.66
29.7	7.93	13.3	14.7	9.37	4.33	4.36	4.51	4.67	6.16	8.98
1.32	0.316	0.715	0.357	4.02	0.675	0.699	0.863	0.866	1.26	1.58

Table 6. Major element compositions of constituent minerals from samples of Acasta mafic rocks

	Amphibolite (no cpx)															
Sample	AC117	AC117	AC117	AC177	AC177	AC177	AC178	AC178	AC179	AC179	AC228	AC228	AC228	AC263	AC263	AC263
Mineral	hbl	pl	chl	hbl	pl	chl	hbl	pl	hbl	pl	hbl	pl	chl	hbl	pl	chl
The number of analysis	4	3	4	21	18	4	2	1	3	3	3	3	2	3	3	1
SiO_2	41.49	60.25	26.06	44.09	9.44	27.08	41.99	57.71	44.42	55.55	42.12	60.32	25.94	41.23	57.05	26.17
TiO_2	0.77	0.00	0.05	0.61	57.82	0.05	0.80	0.01	0.68	0.00	1.11	0.00	0.08	1.09	0.00	0.04
Al_2O_3	14.12	25.38	19.78	11.24	0.00	18.50	12.50	24.48	11.03	27.72	11.02	23.94	19.47	13.41	26.65	20.33
Cr_2O_3	0.01	0.00	0.03	0.06	26.12	0.18	0.05	0.00	0.06	0.01	0.02	0.00	0.05	0.02	0.00	0.02
FeO^T	19.54	0.08	27.93	17.59	0.01	27.72	18.67	0.09	17.11	0.09	18.65	0.06	27.86	18.73	0.12	25.72
MnO	0.00	0.00	0.00	0.31	0.09	0.15	0.31	0.00	0.30	0.01	0.00	0.01	0.02	0.28	0.00	0.21
MgO	6.88	0.00	13.14	9.03	0.01	11.61	7.64	0.00	8.97	0.01	8.17	0.00	12.37	7.46	0.00	14.08
CaO	10.66	6.69	0.07	11.29	0.01	0.10	10.33	6.69	11.61	10.17	11.84	6.01	0.04	11.24	8.92	0.04
Na_2O	1.12	6.59	0.03	1.09	8.05	0.06	1.08	6.69	1.03	5.40	0.98	7.27	0.00	1.35	6.01	0.00
K_2O	1.04	0.08	0.01	0.45	6.31	0.01	0.93	0.20	0.51	0.03	1.15	0.16	0.00	0.95	0.05	0.04
Si in formura	6.32			6.65			6.45		6.73		6.54			6.32		
$Mg/(Mg+Fe^{2+})$	0.46			0.54			0.51		0.51		0.46			0.46		
$Mg/(Mg+Fe^T)$			0.46			0.43							0.44			0.49
An content		0.36			0.41			0.36		0.51		0.31			0.45	
Ab content		0.64			0.59			0.64		0.49		0.69			0.55	
Almandine																
Grossular																
Pyrope																
Spessartine																

FeO^T;total Fe, assumed to be FeO.

Fe_2O_3 were calculated assuming stoichiometry

Amphiboles calculated on the basis of 23 oxygens

An = Ca/(Ca + Na); Ab= Na/(Na + Ca)

Almandine; $Fe^T/(Fe^T+ Ca + Mg + Mn)$, Grossular; $Ca/(Ca + Fe^T+ Mg + Mn)$, Pyrope; $Mg/(Mg + Ca + Fe^T+ Mn)$, Spessartine; $Mn /(Mn + Ca + Fe^T+ Mg)$

Amphibolite (no cpx)																		
AC273	AC273	AC273	AC378	AC378	AC378	AC384	AC384	AC384	AC415	AC415	AC415	AC416	AC416	AC440	AC440	AC440	AC461	AC461
hbl	pl	chl	hbl	pl	chl	hbl	pl	chl	hbl	pl	chl	hbl	pl	hbl	pl	chl	hbl	pl
4	3	3	2	1	2	3	3	1	3	3	1	2	4	3	21	1	2	2
47.63	60.81	28.10	44.83	61.31	26.79	47.32	57.90	27.33	45.76	60.10	26.65	46.93	57.83	46.61	59.50	26.96	49.24	60.45
0.51	0.01	0.03	0.61	0.02	0.00	1.02	0.01	0.04	0.78	0.01	0.05	0.66	0.00	0.61	0.01	0.04	0.34	0.00
8.93	24.83	19.33	9.87	24.53	19.27	7.59	26.44	18.56	10.16	25.69	20.35	9.18	26.30	9.88	26.47	19.56	7.59	25.00
0.05	0.00	0.13	0.12	0.00	0.18	0.07	0.02	0.06	0.08	0.01	0.15	0.08	0.01	0.07	0.01	0.01	0.31	0.02
12.49	0.03	21.43	17.71	0.16	24.99	15.03	0.25	21.03	15.77	0.06	23.00	12.51	0.07	13.59	0.06	21.18	11.24	0.06
0.27	0.01	0.20	0.00	0.00	0.01	0.00	0.00	0.00	0.28	0.01	0.32	0.26	0.01	0.33	0.01	0.28	0.27	0.00
13.09	0.00	18.01	10.02	0.00	15.77	11.62	0.01	17.27	10.73	0.00	15.70	12.75	0.01	12.37	0.01	17.55	14.25	0.00
12.06	6.46	0.11	11.08	5.94	0.06	11.00	8.31	0.06	11.93	7.43	0.17	11.81	8.34	11.89	7.64	0.08	12.25	7.10
0.80	7.50	0.03	1.01	6.93	0.01	0.84	5.68	0.00	0.86	6.94	0.03	0.80	6.29	0.93	6.57	0.02	0.79	7.19
0.63	0.11	0.00	0.94	0.15	0.00	0.61	0.09	0.02	0.70	0.07	0.03	0.86	0.13	0.56	0.21	0.02	0.58	0.14
6.98			6.73			7.08			6.78			6.94		6.83			7.17	
0.69			0.58			0.63			0.59			0.68		0.68			0.71	
		0.60			0.53			0.59			0.55					0.60		
	0.32			0.32			0.45			0.37			0.42		0.39			0.35
	0.68			0.68			0.55			0.63			0.58		0.61			0.65

Amphibolite (no cpx)																		
AC480	AC480	AC499	AC499	AC499	AC579	AC579	AY13	AY33	AY33	AY33	AY50	AY50	AY50	AY110	AY110	AY261	AY261	AY261
hbl	pl	hbl	pl	chl	hbl	pl	hbl	hbl	pl	chl	hbl	pl	chl	hbl	pl	hbl	pl	chl
3	2	3	2	3	2	2	1	11	23	4	3	3	2	6	4	3	2	1
44.23	59.23	44.08	60.69	25.36	44.70	62.30	44.81	41.47	54.98	25.16	41.73	58.43	27.25	42.84	56.11	43.87	61.44	25.67
0.67	0.01	0.79	0.00	0.02	0.49	0.00	0.71	1.02	0.01	0.09	0.96	0.02	0.05	0.50	0.00	1.07	0.00	0.03
10.42	24.38	10.13	23.95	19.08	8.85	23.87	12.06	13.10	28.44	19.34	14.03	26.42	18.33	12.20	25.59	10.17	23.97	19.67
0.05	0.00	0.04	0.02	0.10	0.02	0.01	0.03	0.01	0.01	0.01	0.02	0.02	0.00	0.07	0.01	0.29	0.00	0.29
15.84	0.01	17.06	0.16	26.30	17.24	0.19	16.75	19.01	0.10	26.85	19.81	0.07	27.56	15.10	0.08	16.69	0.10	24.06
0.36	0.02	0.00	0.01	0.01	0.48	0.01	0.00	0.27	0.01	0.22	0.00	0.00	0.00	0.00	0.01	0.40	0.02	0.45
10.27	0.00	9.65	0.01	13.39	10.12	0.01	9.71	7.78	0.01	13.69	7.02	0.01	13.69	9.85	0.00	9.36	0.01	15.25
11.39	6.39	12.13	5.99	0.07	11.72	5.41	11.42	11.54	10.50	0.06	10.64	7.97	0.03	11.64	7.88	11.81	5.83	0.07
0.93	6.93	0.88	7.28	0.01	1.11	7.93	1.05	1.31	5.05	0.13	1.28	5.80	0.02	1.02	6.31	1.02	7.72	0.00
1.08	0.20	0.92	0.17	0.01	0.86	0.12	0.36	0.97	0.10	0.07	0.86	0.09	0.02	0.36	0.04	1.14	0.13	0.00
6.70		6.72			6.81		6.62	6.31			6.31			6.56		6.72		
0.59		0.52			0.56		0.58	0.47			0.46			0.59		0.51		
				0.48						0.48			0.47					0.53
	0.34		0.31			0.27			0.53			0.43			0.41		0.29	
	0.66		0.69			0.73			0.47			0.57			0.59		0.71	

Amphibolite (with cpx)			Garnet-amphibolite (with cum)				Hornble
AC477	AC477	AC477	AY99	AY99	AY99	AY99	AC283
hbl	pl	cpx	hbl	pl	grt	cum	hbl
3	1	5	8	3	7	5	2
47.13	60.53	53.97	41.51	59.58	37.54	53.47	56.14
0.57	0.01	0.02	0.49	0.01	0.04	0.04	0.07
9.54	25.91	0.14	15.51	25.69	21.10	0.54	1.22
0.12	0.03	0.01	0.00	0.02	0.01	0.01	0.00
15.47	0.25	8.81	18.62	0.13	29.91	24.95	6.63
0.31	0.04	0.39	0.17	0.01	3.30	0.26	0.35
11.44	0.00	12.89	7.54	0.00	2.47	16.09	19.75
12.25	7.48	23.92	10.64	7.28	4.66	0.45	11.60
0.83	6.99	0.29	1.32	6.61	0.01	0.02	0.18
1.00	0.20	0.00	0.32	0.05	0.02	0.00	0.12
6.88			6.19				7.86
0.60			0.55				0.94
		0.72				0.53	
	0.37			0.38			
	0.63			0.62			
					68.55		
					13.68		
					10.10		
					7.66		

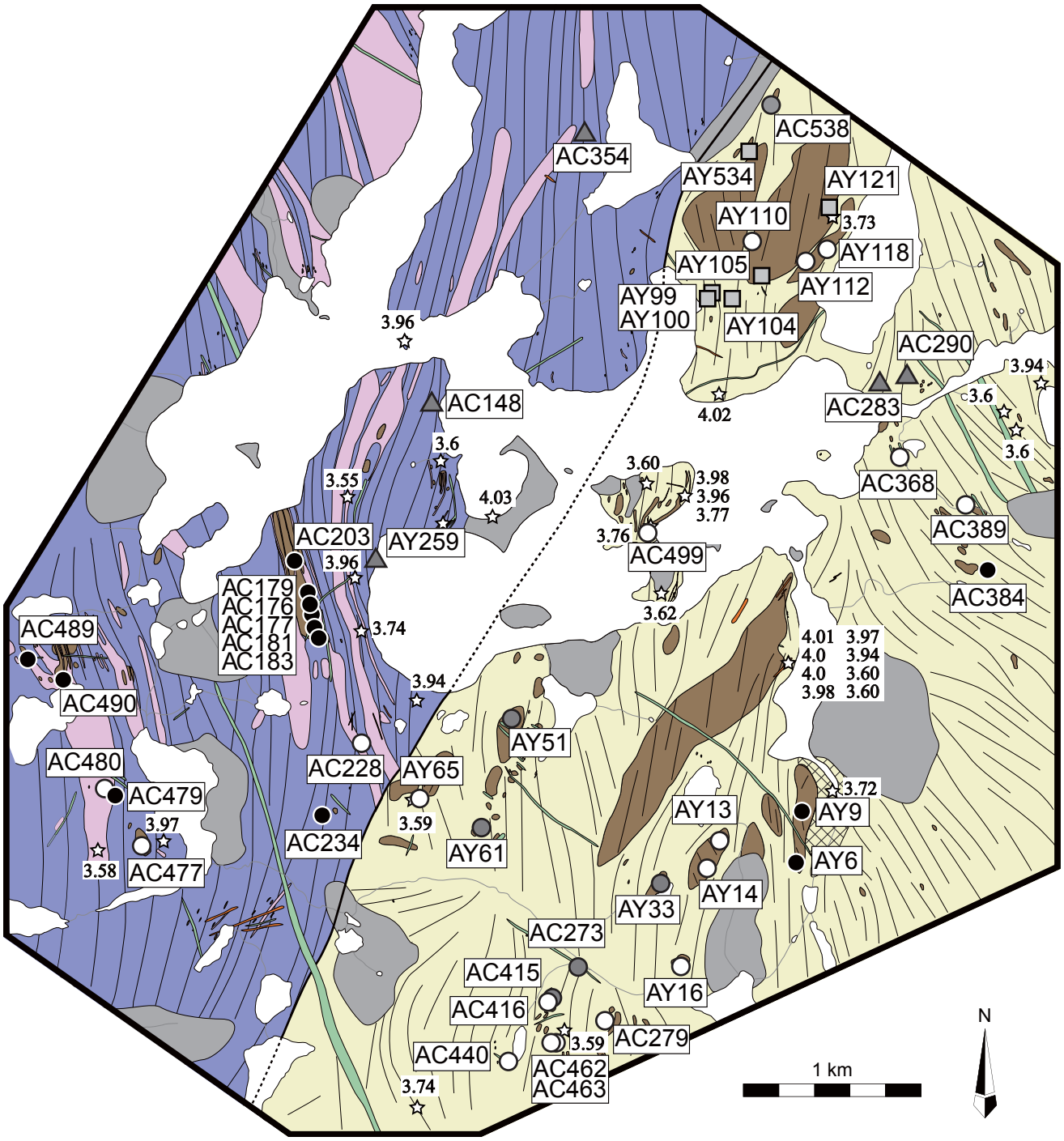
AC538
AC354
AY534
AY121
AY110
3.73
AY118
AY105
AY112
AY99
AY100
AY104
3.96
AC290
3.94
AC148
4.02
AC283
3.6
3.6
3.6
3.55
4.03
3.60
3.98
3.96
3.77
AC368
AC203
AY259
3.76
AC499
AC389
3.96
AC179
AC176
AC177
AC181
AC183
3.74
3.62
AC384
4.01 3.97
4.0 3.94
4.0 3.60
3.98 3.60
AC489
AC490
3.94
AY51
AC480
AC228
AY65
3.72
AY13
AY9
AC479
3.59
3.97
AC234
AY61
AY6
3.58
AC477
AY14
AY33
AC273
AC415
AY16
AC416
AC279
3.59
AC440
AC462
AC463
3.74
1 km
N
Quaternary
Proterozoic Sediment
Felsic Dyke
Mafic Dyke
Foliated Granite
Layered Gneiss
Felsic Gneiss
Mafic-intermediate Gneiss
Gneissosity
Fault
Sample locality
Amphibolite group I
Amphibolite group II
Amphibolite group III
Garnet-amphibolite
Hornblendite

Figure 2-1

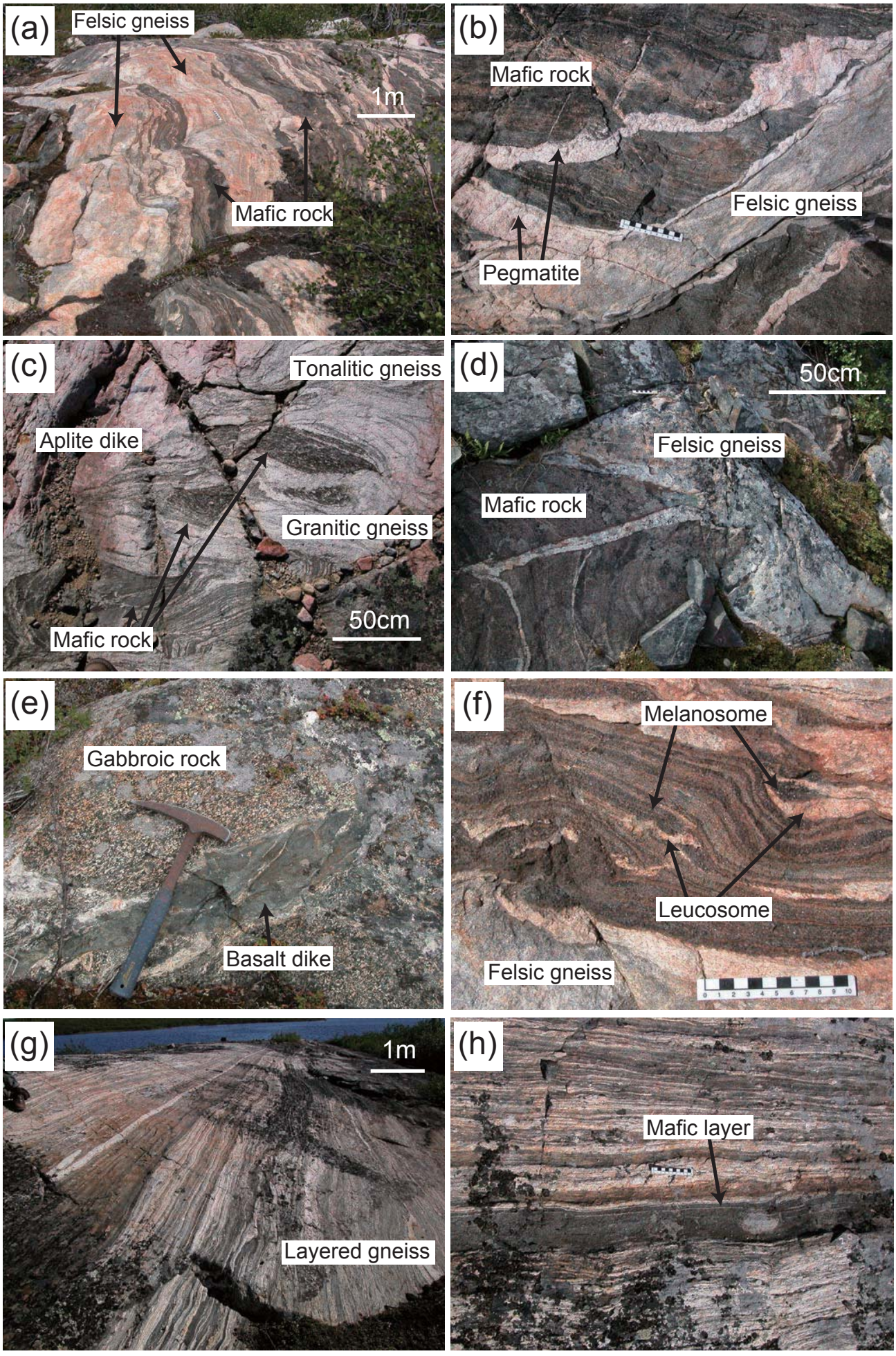
(a)
Felsic gneiss
1m
Mafic rock
(b)
Mafic rock
Felsic gneiss
Pegmatite
(c)
Tonalitic gneiss
Aplite dike
Granitic gneiss
Mafic rock
50cm
(d)
50cm
Felsic gneiss
Mafic rock
(e)
Gabbroic rock
Basalt dike
(f)
Melanosome
Leucosome
Felsic gneiss
(g)
1m
Layered gneiss
(h)
Mafic layer

Figure 2-2

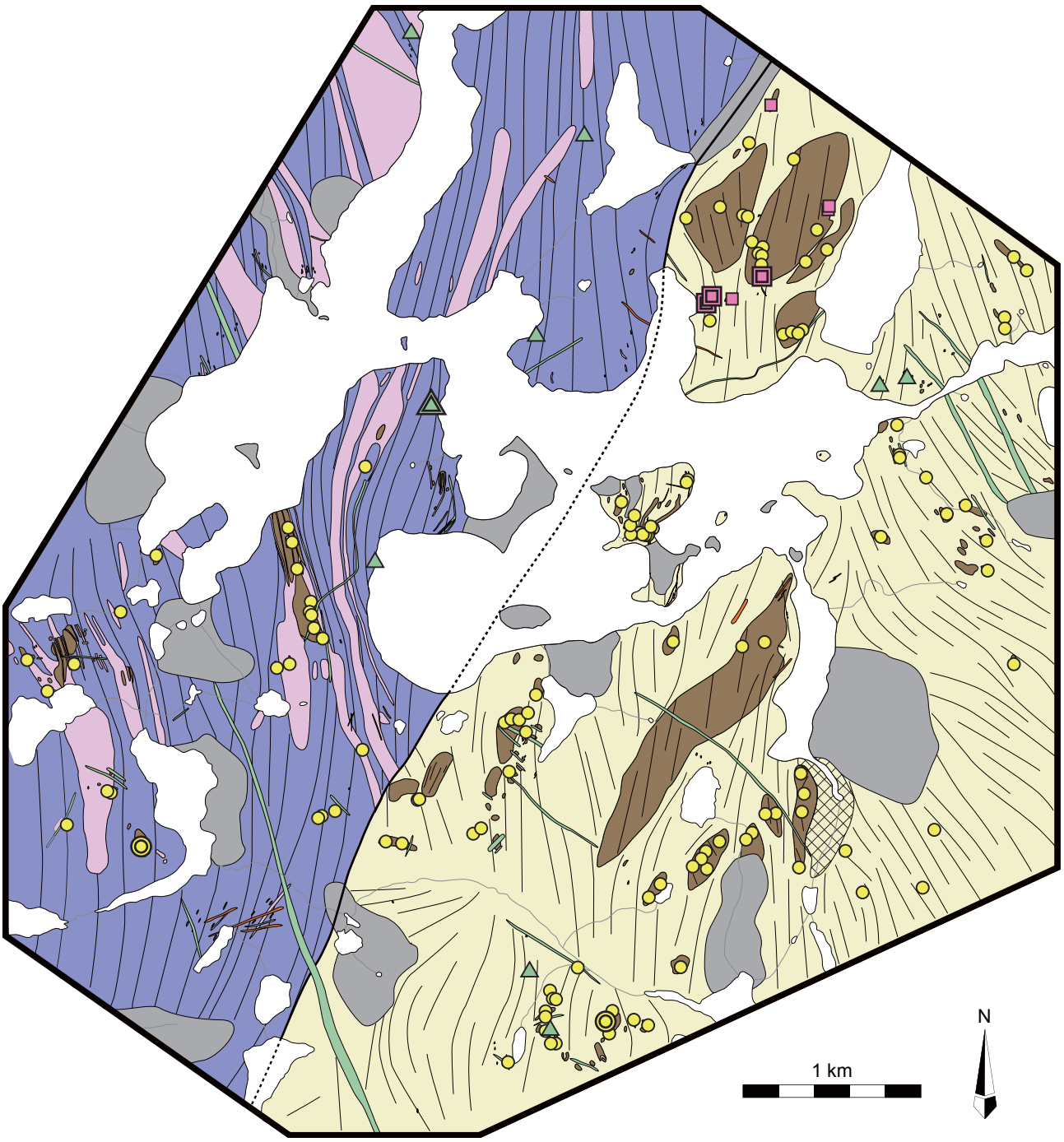
N
1 km
Quaternary
Proterozoic Sediment
Felsic Dyke
Mafic Dyke
Foliated Granite
Layered Gneiss
Felsic Gneiss
Mafic-intermediate Gneiss
Gneissosity
Fault
Sample locality
Amphibolite
Cpx-free
Cpx-bearing
Hornblendite
Cpx-free
Cpx-bearing
Garnet-amphibolite
Cum-free
Cum-bearing

Figure 2-3

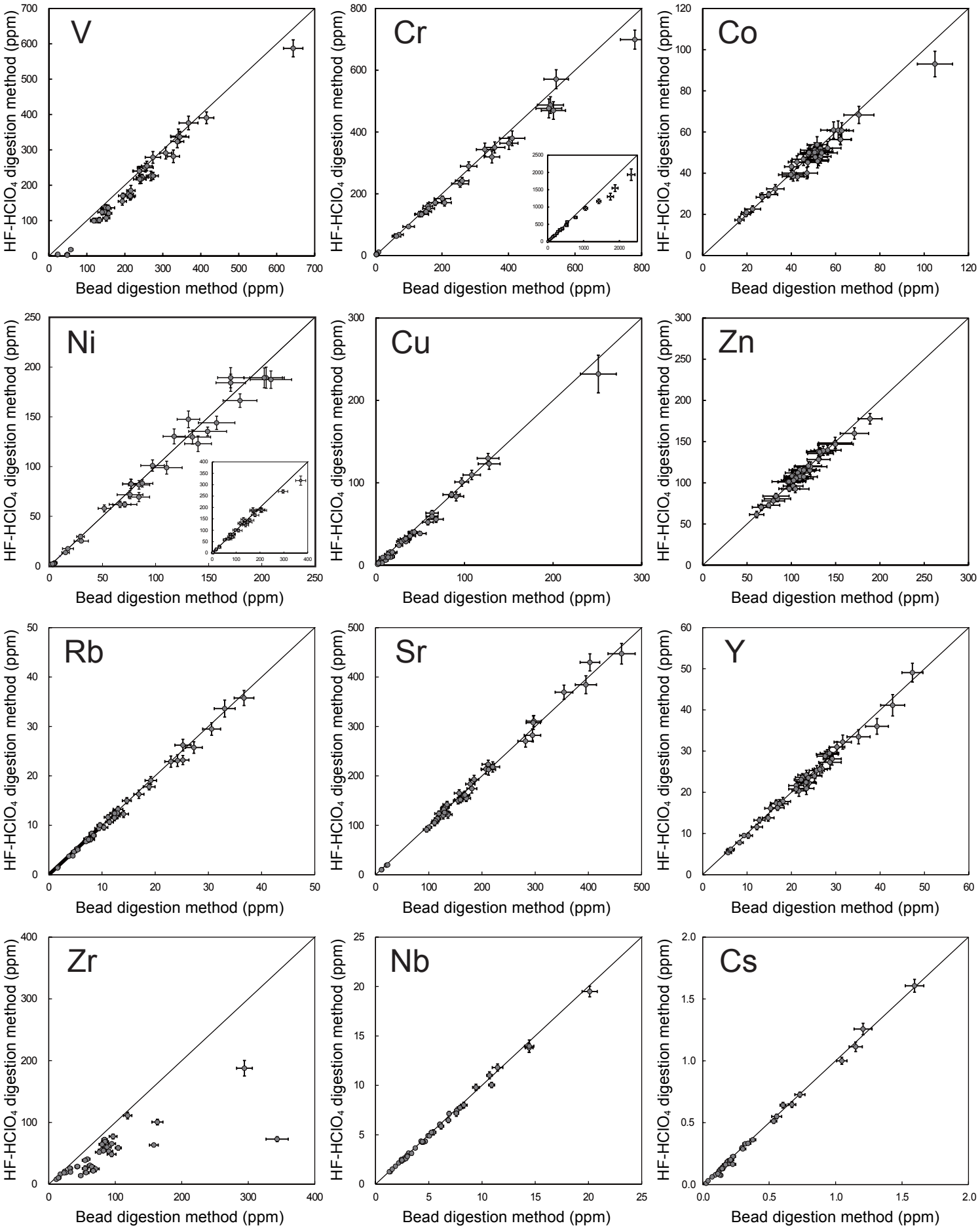
V
Cr
Co
Ni
Cu
Zn
Rb
Sr
Y
Zr
Nb
Cs
HF-HClO4 digestion method (ppm)
Bead digestion method (ppm)

Figure 2-4

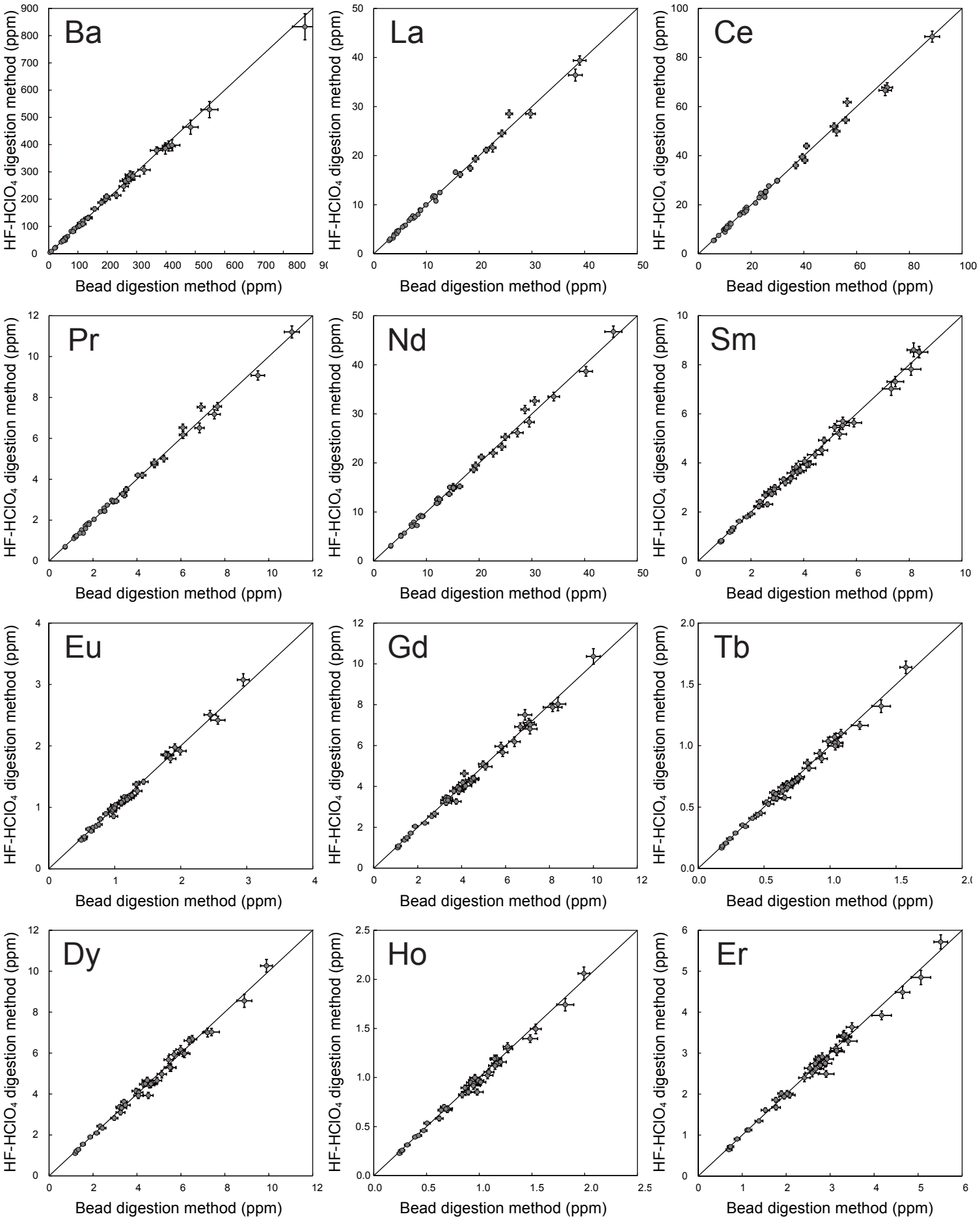
Ba
La
Ce
Pr
Nd
Sm
Eu
Gd
Tb
Dy
Ho
Er
HF-HClO4 digestion method (ppm)
Bead digestion method (ppm)

Figure 2-4

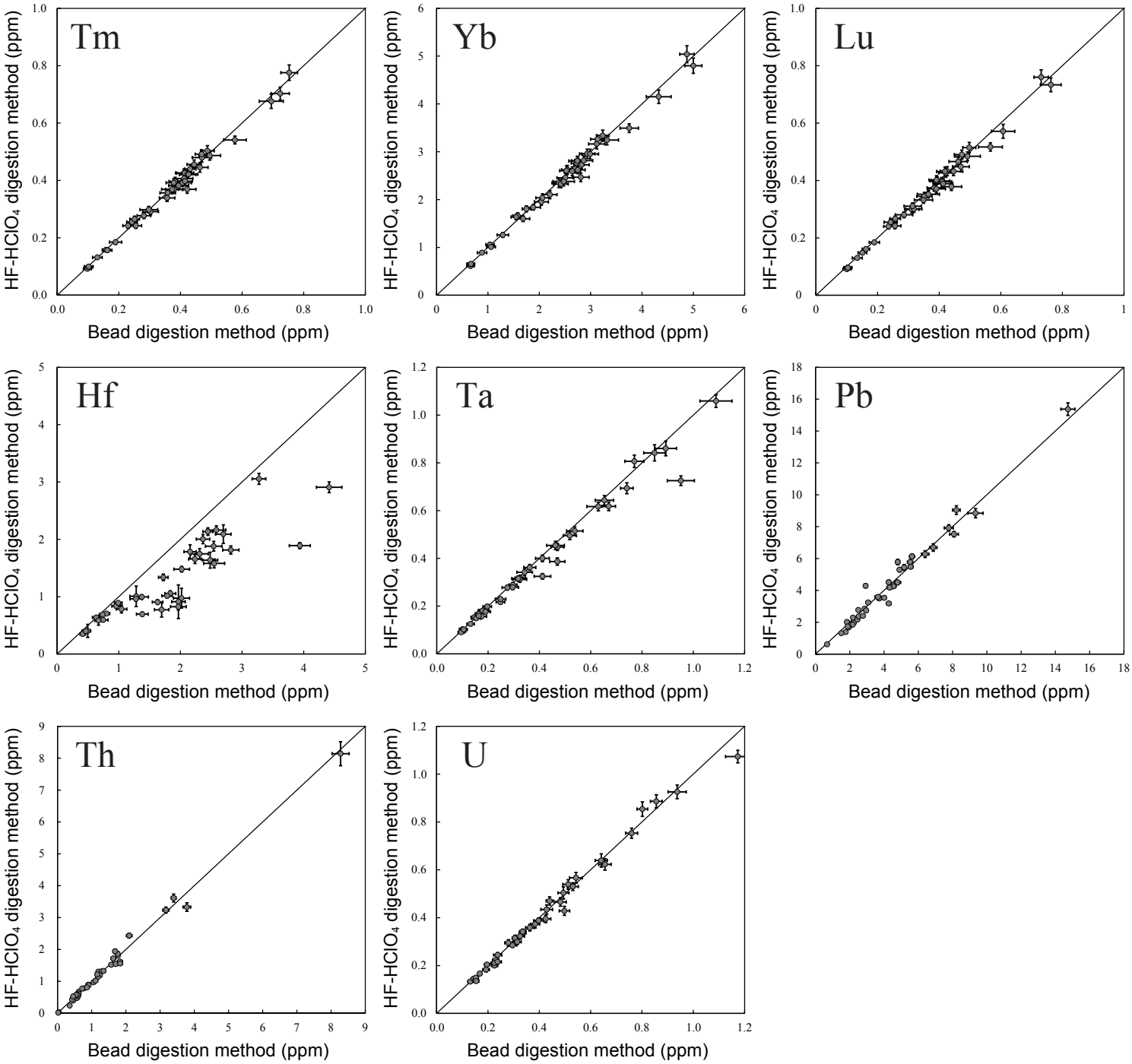
Tm
Yb
Lu
Hf
Ta
Pb
Th
U
HF-HClO4 digestion method (ppm)
Bead digestion method (ppm)

Figure 2-4

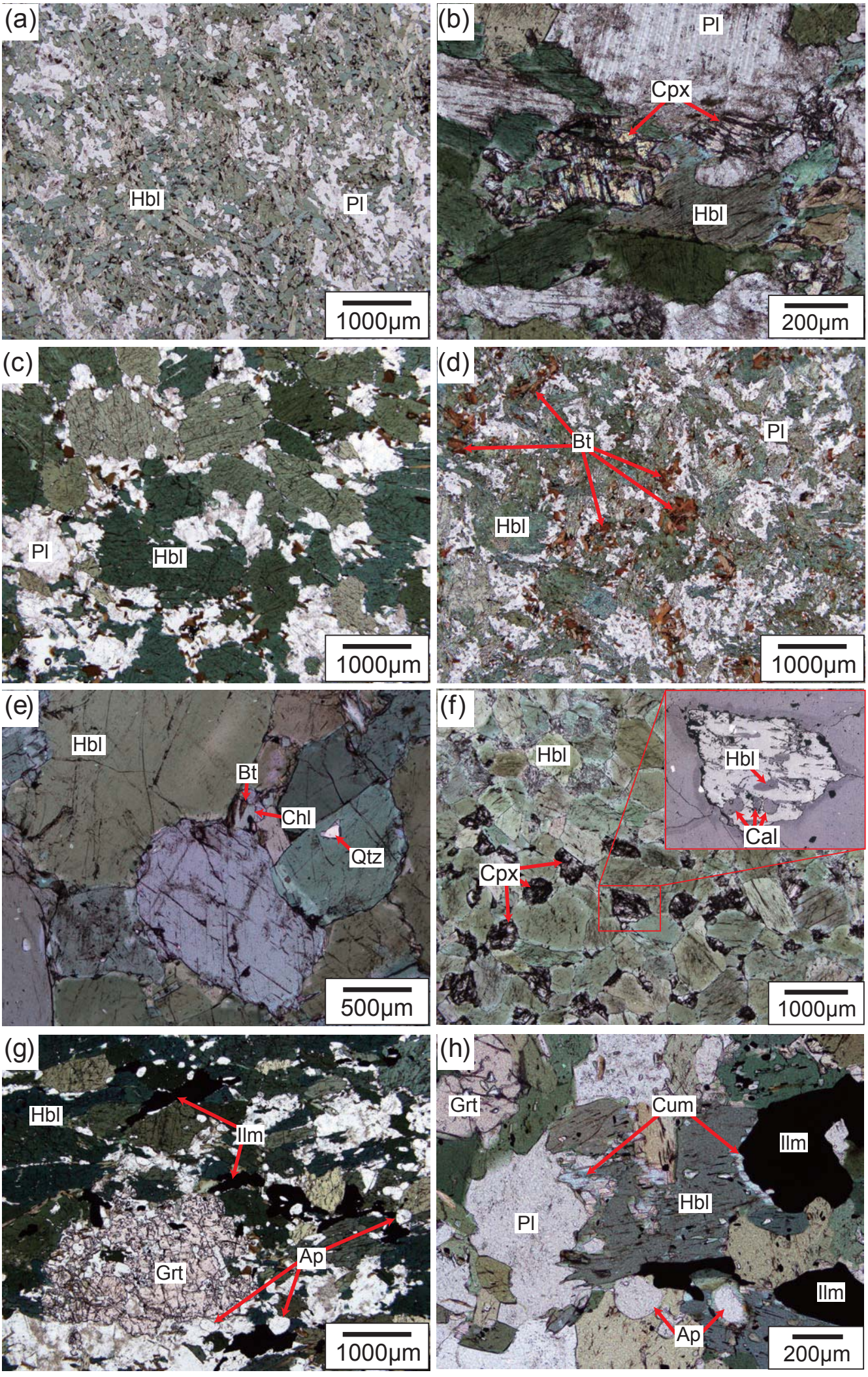
(a)
Hbl
Pl
1000μm
(b)
Pl
Cpx
Hbl
200μm
(c)
Pl
Hbl
1000μm
(d)
Bt
Pl
Hbl
1000μm
(e)
Hbl
Bt
Chl
Qtz
500μm
(f)
Hbl
Hbl
Cal
Cpx
1000μm
(g)
Hbl
Ilm
Grt
Ap
1000μm
(h)
Grt
Cum
Ilm
Hbl
Pl
Ilm
Ap
200μm

Figure 2-5

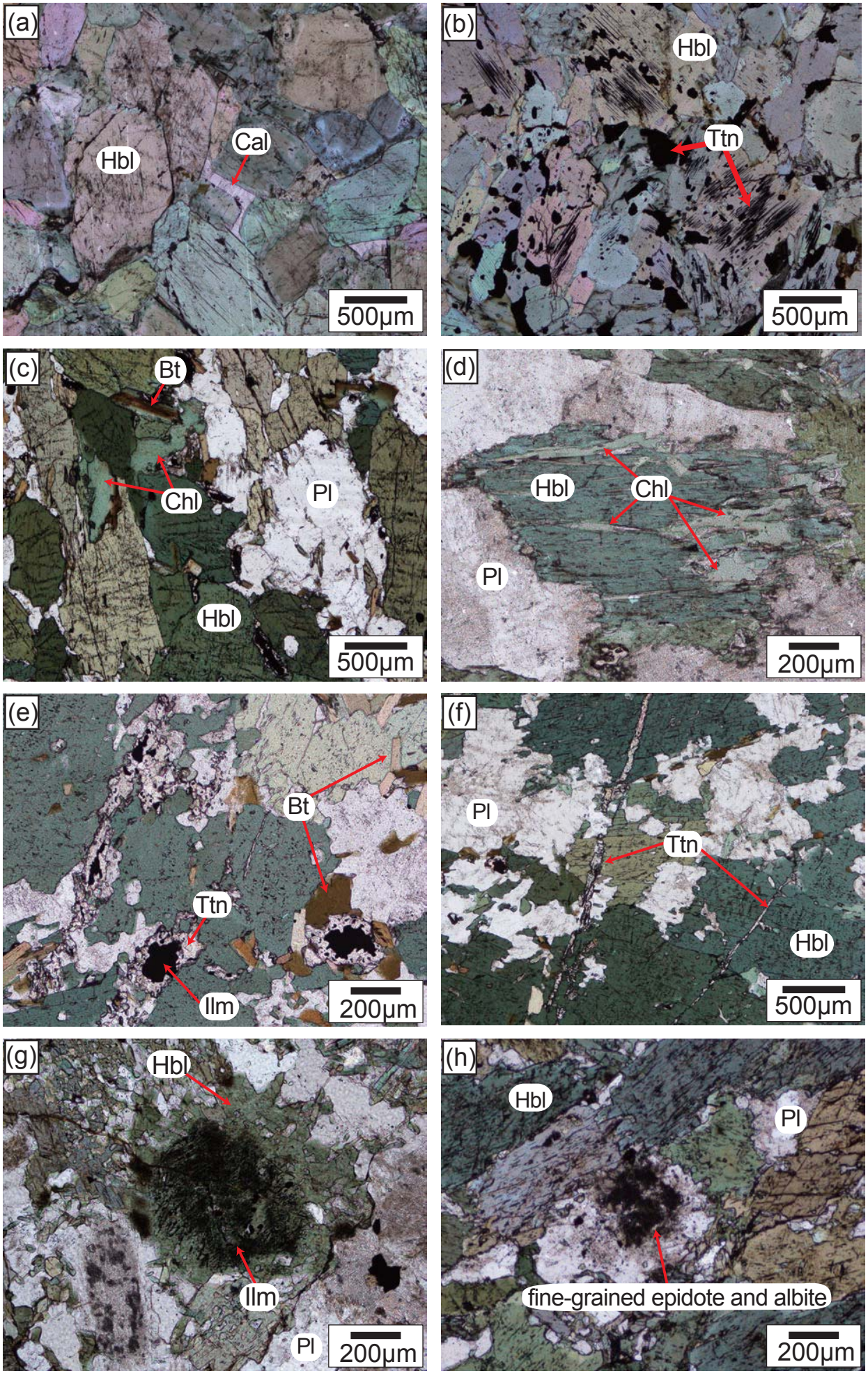
(a)
Hbl
Cal
500μm
(b)
Hbl
Ttn
500μm
(c)
Bt
Chl
Pl
Hbl
500μm
(d)
Hbl
Chl
Pl
200μm
(e)
Bt
Ttn
Ilm
200μm
(f)
Pl
Ttn
Hbl
500μm
(g)
Hbl
Ilm
Pl
200μm
(h)
Hbl
Pl
fine-grained epidote and albite
200μm

Figure 2-6

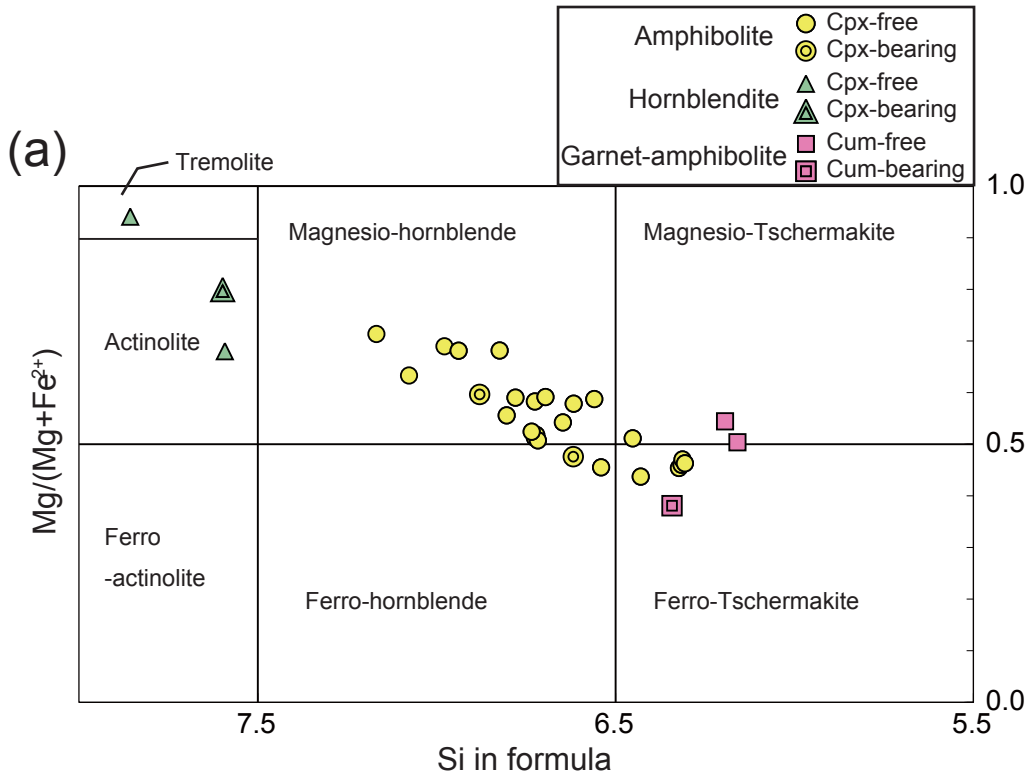
(a)
Amphibolite
Cpx-free
Cpx-bearing
Hornblendite
Cpx-free
Cpx-bearing
Garnet-amphibolite
Cum-free
Cum-bearing
Tremolite
Magnesio-hornblende
Magnesio-Tschermakite
Actinolite
Ferro
-actinolite
Ferro-hornblende
Ferro-Tschermakite
Mg/(Mg+Fe2+)
1.0
0.5
0.0
7.5
6.5
5.5
Si in formula

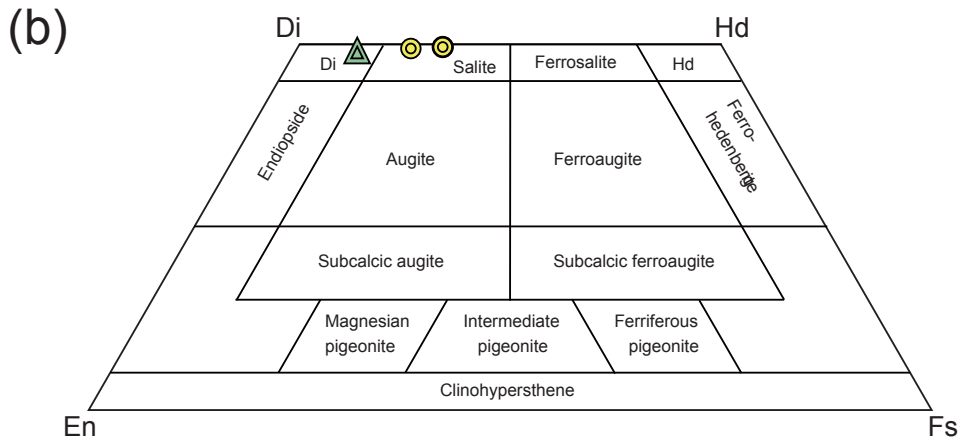
(b)
Di
Hd
Di
Salite
Ferrosalite
Hd
Endiopside
Augite
Ferroaugite
Ferro-
hedenbergite
Subcalcic augite
Subcalcic ferroaugite
Magnesian
pigeonite
Intermediate
pigeonite
Ferriferous
pigeonite
Clinohypersthene
En
Fs

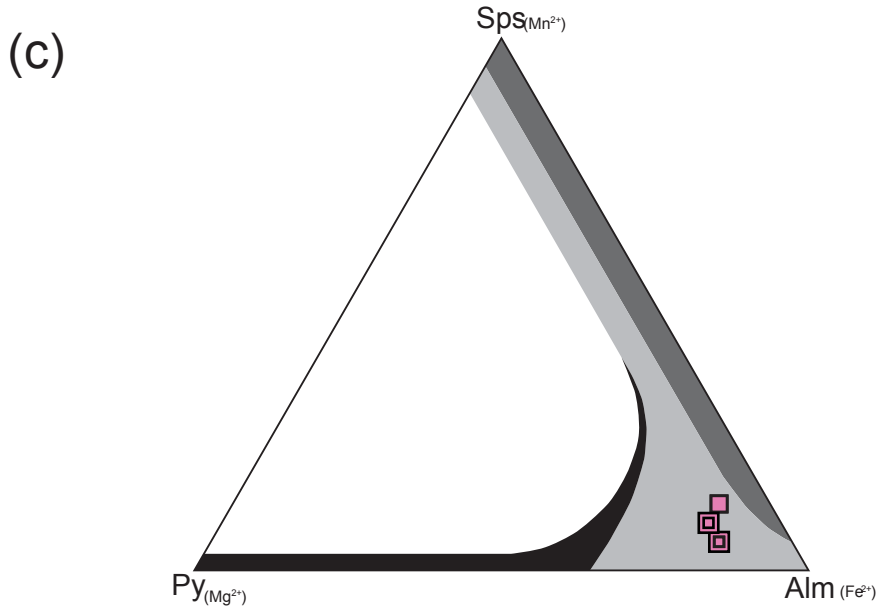
(c)
Sps(Mn2+)
Py(Mg2+)
Alm (Fe2+)

Figure 2-7

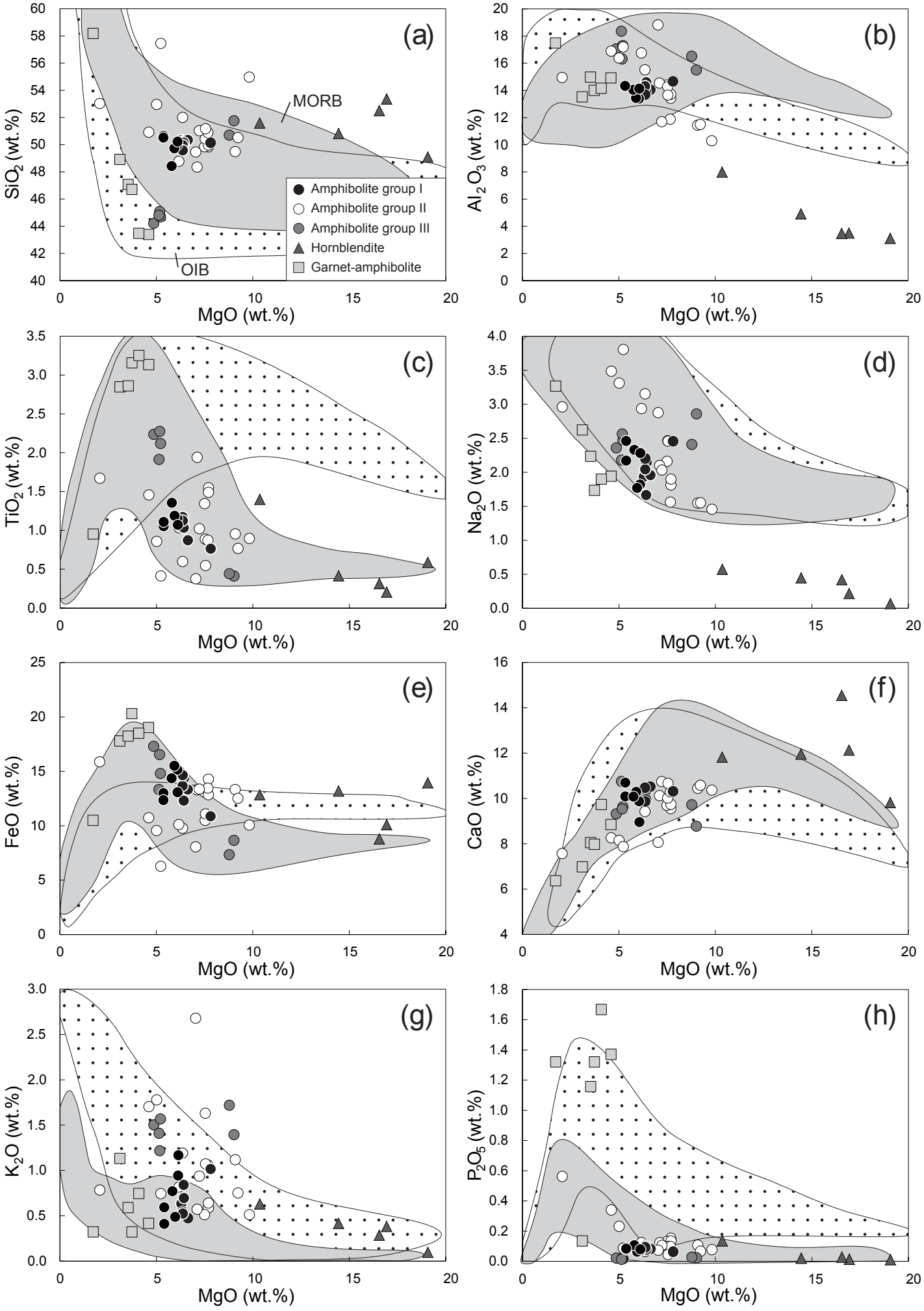
(a)
SiO2 (wt.%)
MgO (wt.%)
MORB
OIB
Amphibolite group I
Amphibolite group II
Amphibolite group III
Hornblendite
Garnet-amphibolite
(b)
Al2O3 (wt.%)
MgO (wt.%)
(c)
TiO2 (wt.%)
MgO (wt.%)
(d)
Na2O (wt.%)
MgO (wt.%)
(e)
FeO (wt.%)
MgO (wt.%)
(f)
CaO (wt.%)
MgO (wt.%)
(g)
K2O (wt.%)
MgO (wt.%)
(h)
P2O5 (wt.%)
MgO (wt.%)

Figure 2-8

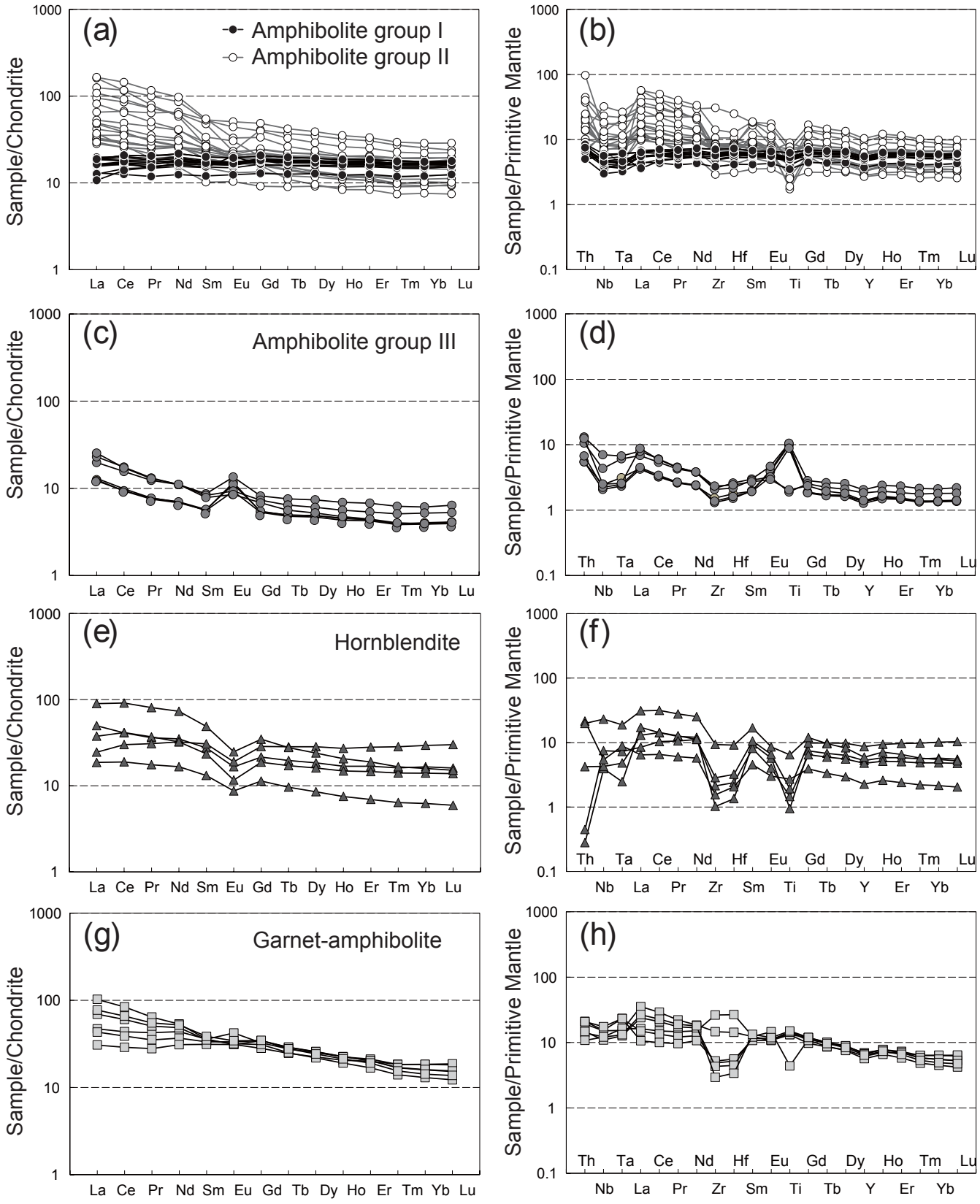
(a)
Amphibolite group I
Amphibolite group II
Sample/Chondrite
1000
100
10
1
La Ce Pr Nd Sm Eu Gd Tb Dy Ho Er Tm Yb Lu
(b)
Sample/Primitive Mantle
1000
100
10
1
0.1
Th Ta Ce Nd Hf Eu Gd Dy Ho Tm Lu
Nb La Pr Zr Sm Ti Tb Y Er Yb
(c)
Amphibolite group III
Sample/Chondrite
La Ce Pr Nd Sm Eu Gd Tb Dy Ho Er Tm Yb Lu
(d)
Sample/Primitive Mantle
Th Ta Ce Nd Hf Eu Gd Dy Ho Tm Lu
Nb La Pr Zr Sm Ti Tb Y Er Yb
(e)
Hornblendite
Sample/Chondrite
La Ce Pr Nd Sm Eu Gd Tb Dy Ho Er Tm Yb Lu
(f)
Sample/Primitive Mantle
Th Ta Ce Nd Hf Eu Gd Dy Ho Tm Lu
Nb La Pr Zr Sm Ti Tb Y Er Yb
(g)
Garnet-amphibolite
Sample/Chondrite
La Ce Pr Nd Sm Eu Gd Tb Dy Ho Er Tm Yb Lu
(h)
Sample/Primitive Mantle
Th Ta Ce Nd Hf Eu Gd Dy Ho Tm Lu
Nb La Pr Zr Sm Ti Tb Y Er Yb

Figure 2-9

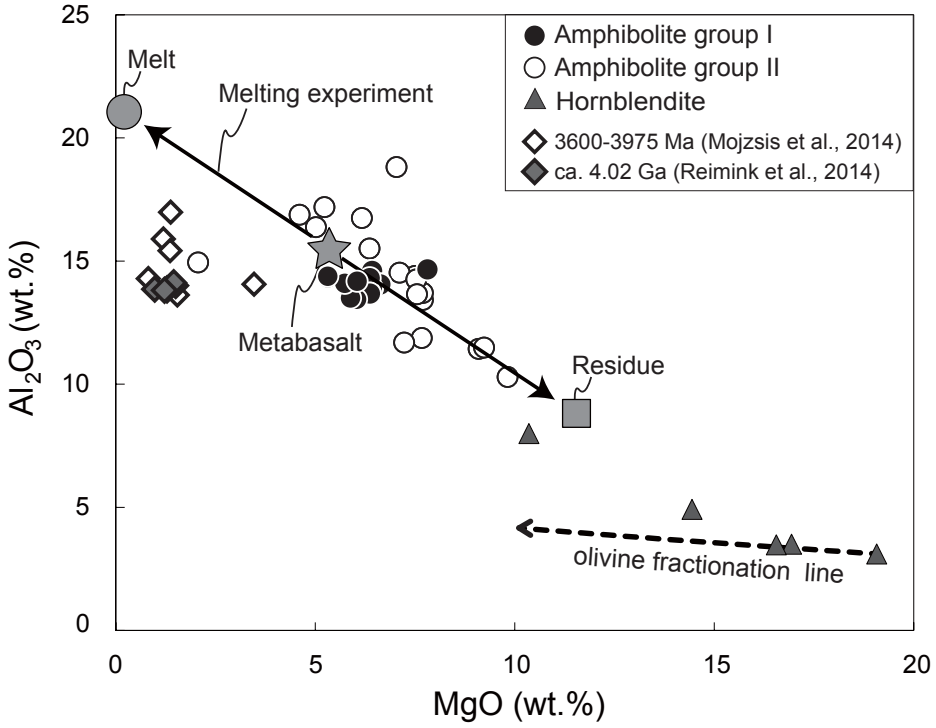
Amphibolite group I
Amphibolite group II
Hornblendite
3600-3975 Ma (Mojzsis et al., 2014)
ca. 4.02 Ga (Reimink et al., 2014)
Melt
Melting experiment
Metabasalt
Residue
olivine fractionation line
Al2O3 (wt.%)
MgO (wt.%)
0
5
10
15
20
25

Figure 2-10

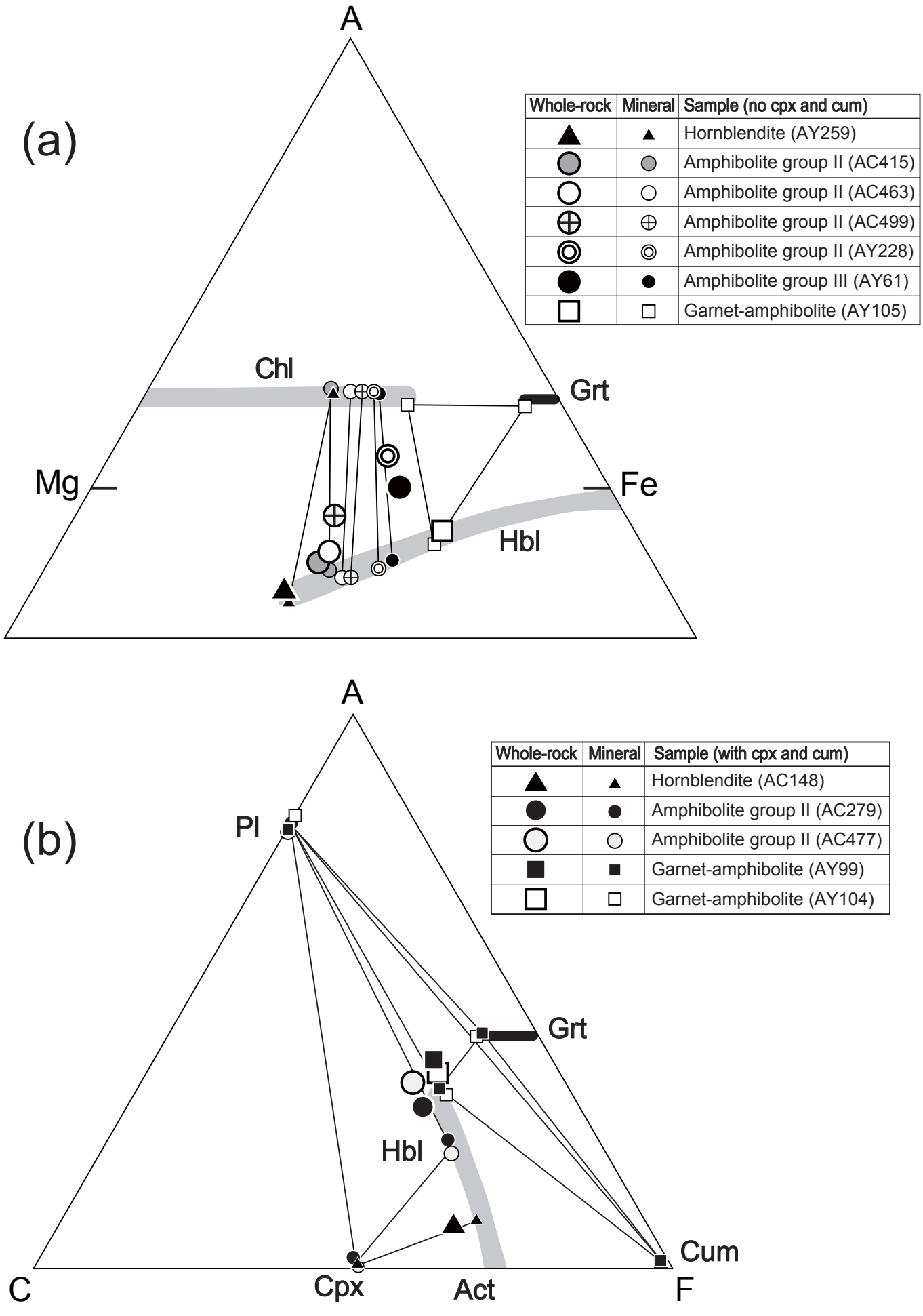
(a)
A
Chl
Grt
Mg
Fe
Hbl
Whole-rock
Mineral
Sample (no cpx and cum)
Hornblendite (AY259)
Amphibolite group II (AC415)
Amphibolite group II (AC463)
Amphibolite group II (AC499)
Amphibolite group II (AY228)
Amphibolite group III (AY61)
Garnet-amphibolite (AY105)
(b)
A
Pl
Grt
Hbl
C
Cpx
Act
Cum
F
Whole-rock
Mineral
Sample (with cpx and cum)
Hornblendite (AC148)
Amphibolite group II (AC279)
Amphibolite group II (AC477)
Garnet-amphibolite (AY99)
Garnet-amphibolite (AY104)

Figure 2-11

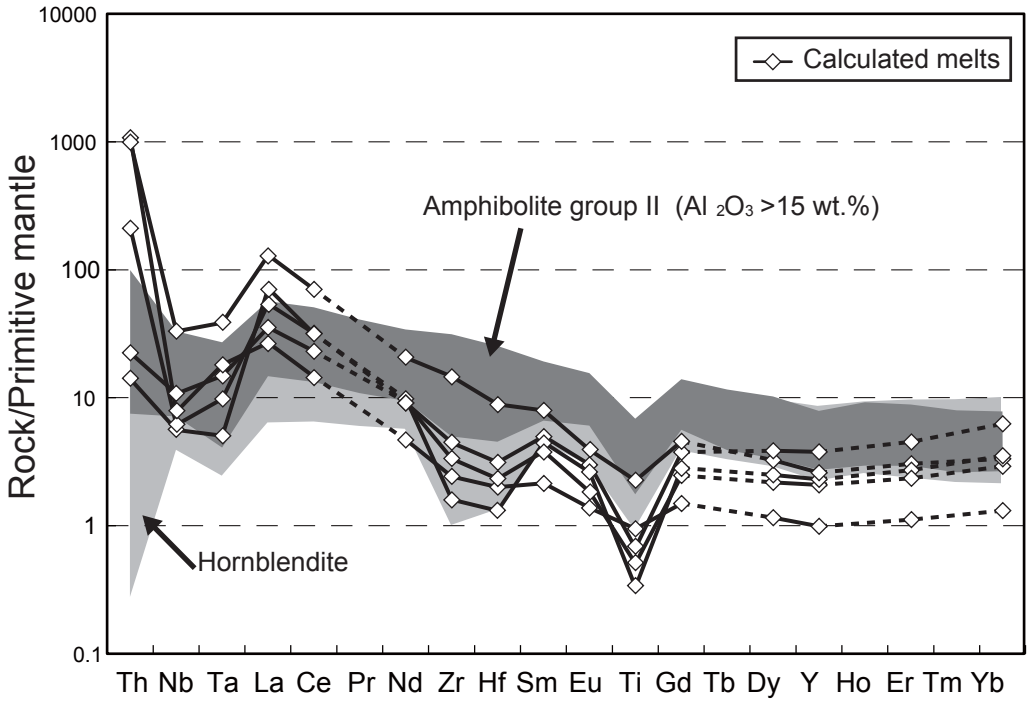
Calculated melts
Amphibolite group II (Al 2O3 >15 wt.%)
Hornblendite
Rock/Primitive mantle
10000
1000
100
10
1
0.1
Th Nb Ta La Ce Pr Nd Zr Hf Sm Eu Ti Gd Tb Dy Y Ho Er Tm Yb

Figure 2-12

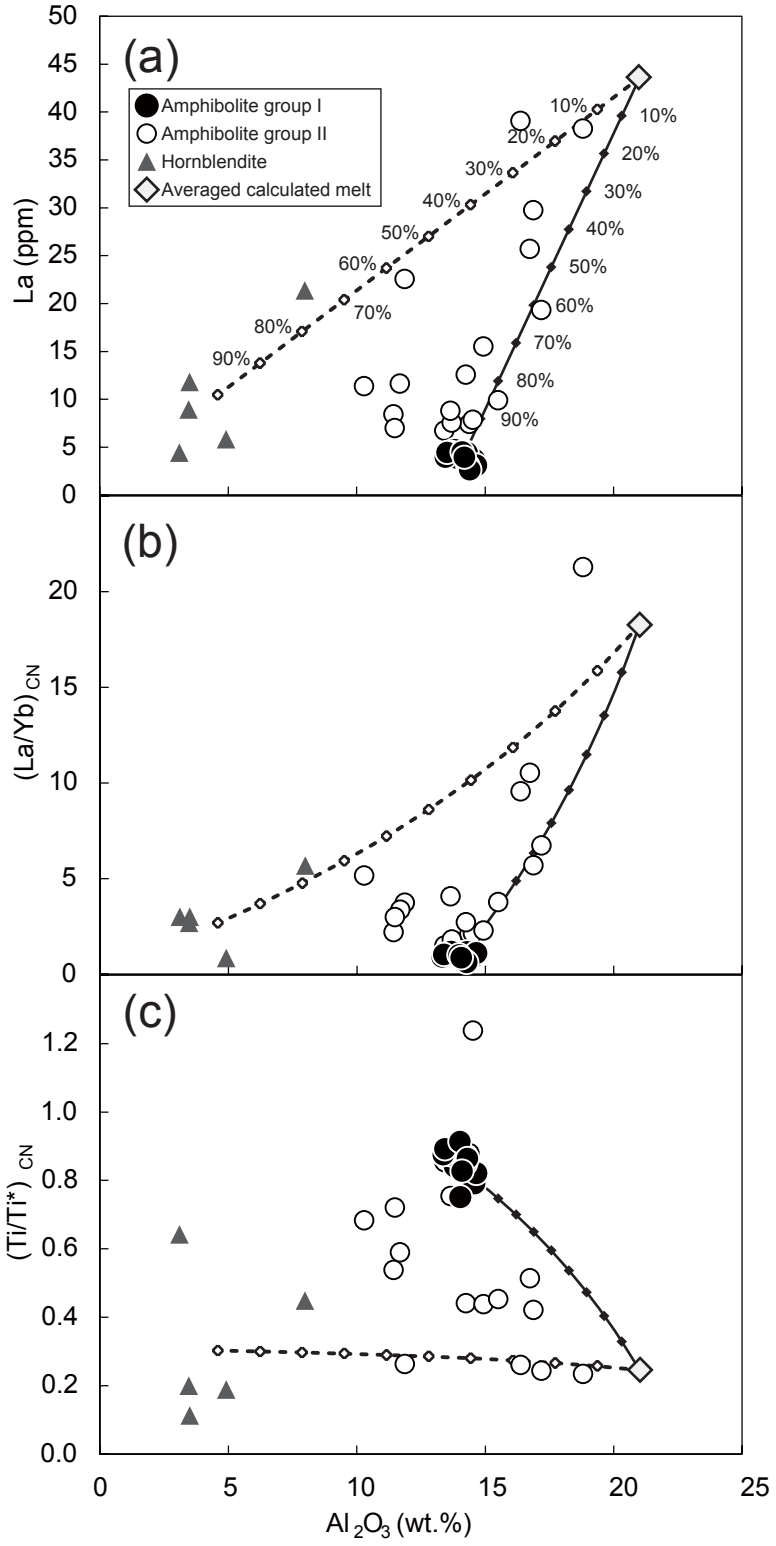
(a)
Amphibolite group I
Amphibolite group II
Hornblendite
Averaged calculated melt
La (ppm)
10%
20%
30%
40%
50%
60%
70%
80%
90%
(b)
(La/Yb)CN
(c)
(Ti/Ti*)CN
Al2O3 (wt.%)

Figure 2-13

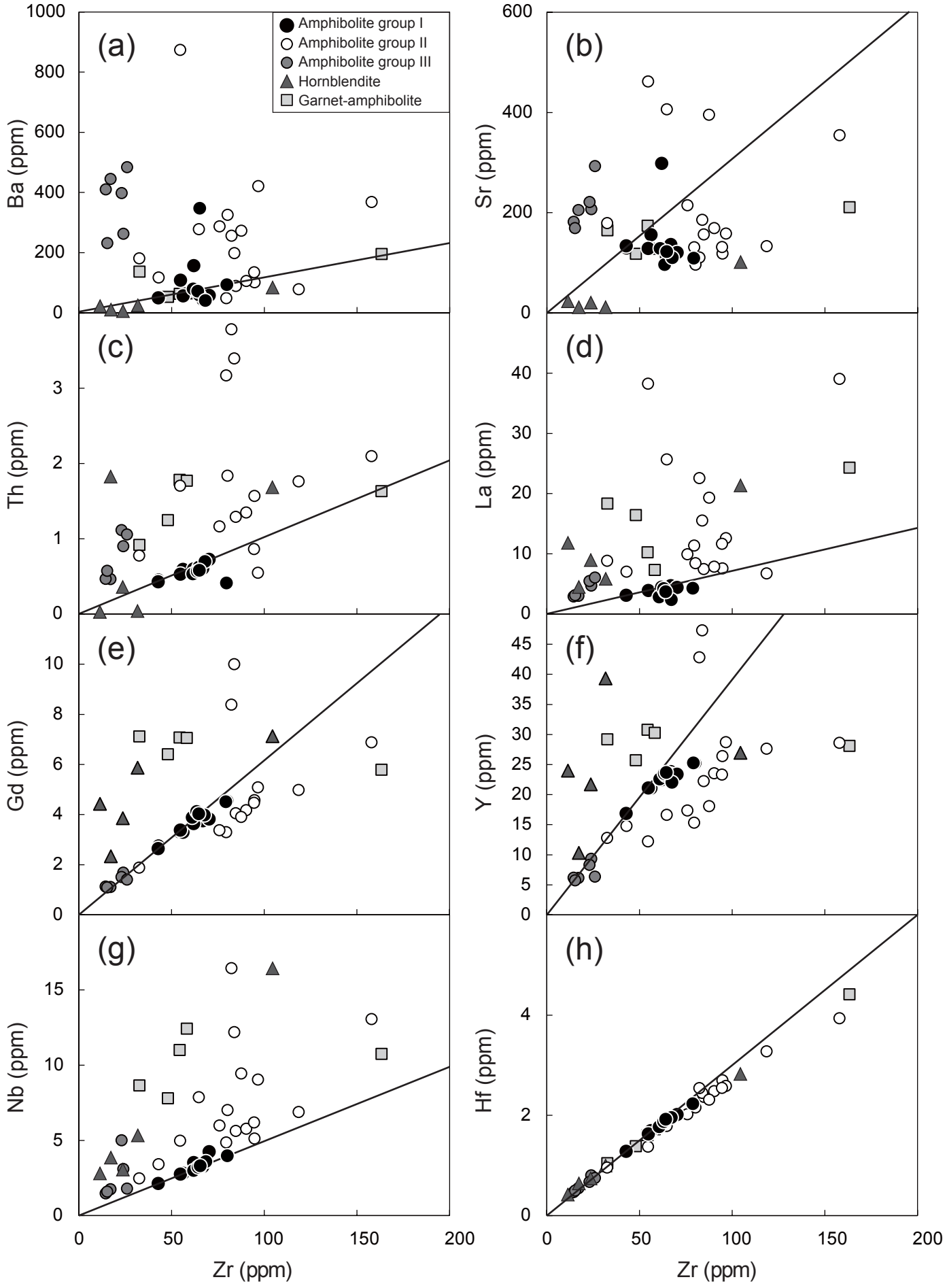
(a)
(b)
(c)
(d)
(e)
(f)
(g)
(h)
Amphibolite group I
Amphibolite group II
Amphibolite group III
Hornblendite
Garnet-amphibolite
Ba (ppm)
Sr (ppm)
Th (ppm)
La (ppm)
Gd (ppm)
Y (ppm)
Nb (ppm)
Hf (ppm)
Zr (ppm)
Zr (ppm)

Figure 2-14

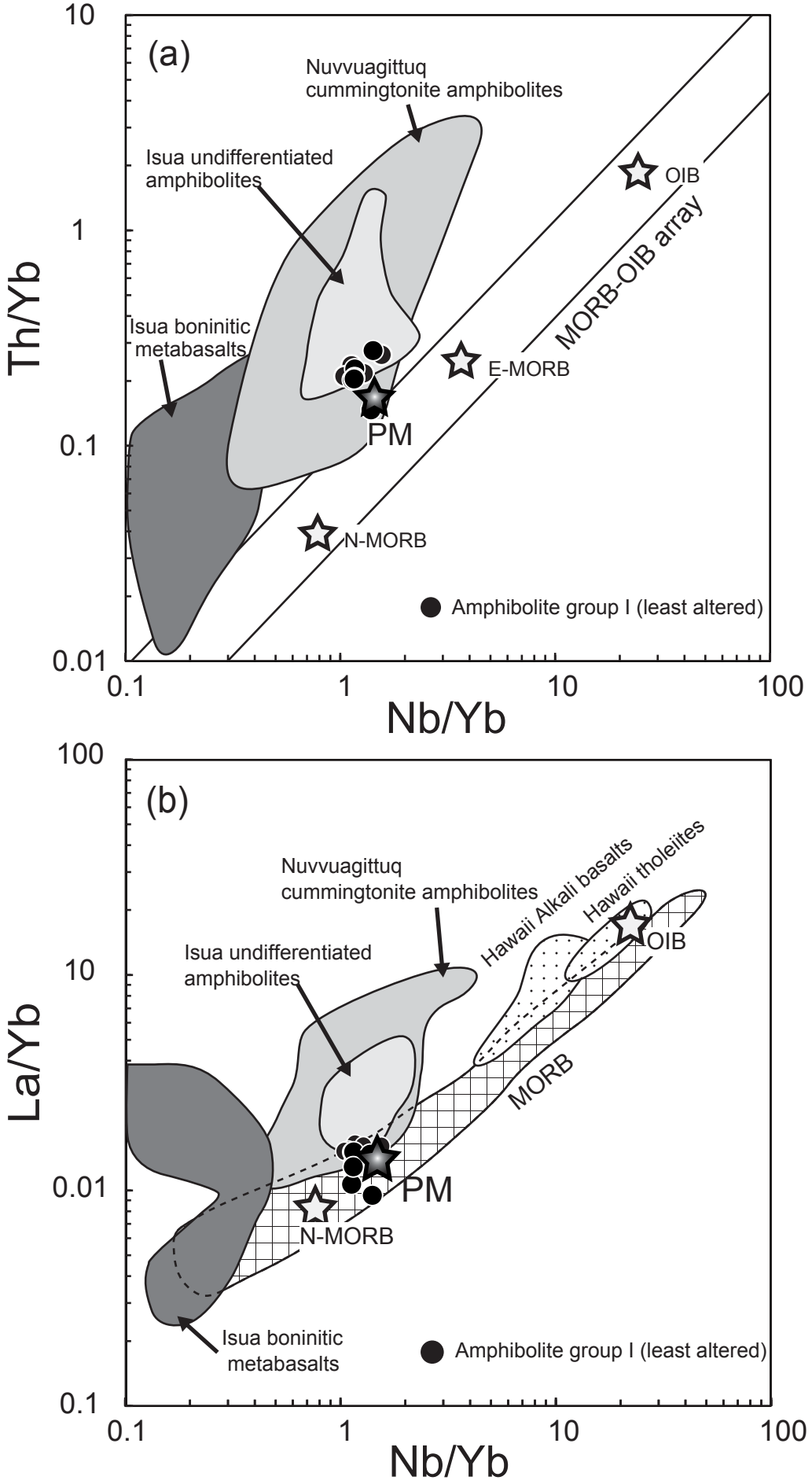
(a)
Nuvvuagittuq
cummingtonite amphibolites
Isua undifferentiated
amphibolites
Isua boninitic
metabasalts
OIB
MORB-OIB array
E-MORB
PM
N-MORB
Amphibolite group I (least altered)
Th/Yb
Nb/Yb
10
1
0.1
0.01
0.1
1
10
100
(b)
Nuvvuagittuq
cummingtonite amphibolites
Hawaii Alkali basalts
Hawaii tholeiites
OIB
Isua undifferentiated
amphibolites
MORB
PM
N-MORB
Isua boninitic
metabasalts
Amphibolite group I (least altered)
La/Yb
Nb/Yb
100
10
0.01
0.1
0.1
1
10
100

Figure 2-15

第３章
本章については、５年以内に雑誌等で刊行予定のため、非公開。

第４章
本章については、５年以内に雑誌等で刊行予定のため、非公開。

Chapter 5

General Conclusion

Many of studies about the early Earth were based on indirect samples or theoretical principles because of the scarce of old terrestrial samples. In addition, most geochronological investigations using rare relict Eoarchean geologic body focused on felsic rocks which contain abundant zircons, rather than mafic rocks. Zircon provides precise U-Pb geochronological constraint to their host granitoids. However, felsic rock is not formed by mantle melting directly. For better understanding about the early mantle evolution, it is need to study old mafic rocks which are formed by the early mantle melting. Because a mafic rock does not contain igneous zircons, ages of mafic rocks which occur in Eoarchean terrains have had been argued by cross-cutting field relations between them and felsic rocks. Acasta Gniess Complex is dominated by 4.0-3.6 Ga felsic-intermediate rocks while relatively small amount of mafic rocks are also present. Although the mafic rocks have had been suggested that they were older than surrounding felsic-intermediate gneisses from the occurrences, their ages have had not been determined because of a sever deformation and metamorphism. This study conducted a comprehensive study on Acasta mafic rocks to know origins of them.

In summary, this thesis indicated that:

(1) Mafic rocks in Acasta Gneiss Complex commonly underwent amphibolite- to uppper amophibolite-facies metamorphism and migmatization

(2) The least modified mafic rocks have chondritic trace element relative abundances, except for Nb and Ta, and modern basalt-like highly siderophile element compositions.

(3) They were formed at 4.3±0.3 Ga.

(4) Their mantle source had both chondritic Sm/Nd ratio and non-chondritic $^{142}Nd/^{144}Nd$ ratio at 4.3 Ga.

These observations lead to the following implications.

(1) Acasta mafic rocks were derived from Nb- and Ta-deficit primitive mantle which have had originated from the core formation
(2) The difference in $^{142}Nd/^{144}Nd$ ratio between modern terrestrial mantle and chondrites is due to the heterogeneity of Nd isotopes in early solar nebula.
(3) The mantle heterogeneity formed by crystallization of a magma ocean was disappeared before 4.3 Ga by rapid mantle mixing, or, the magma ocean did not reach the core-mantle boundary, remaining the primitive portion in the deep mantle.

Previous studies about the Acasta gneiss complex have had mainly focused on felsic to intermediate gneisses. Although some studies investigated mafic rocks and showed a variety of whole-rock tracer isotopes and U-Pb ages of their zircons, detailed sample descriptions were absent from them. This study carried on the comprehensive investigation of mafic rocks in the AGC and revealed the petrological and geochemical variations of them, resulting in indicating that there is mafic rock which preserves the basaltic magma composition. Their whole-rock isotope systematics showed that they were formed at 4.3 Ga. This is the first study to have determined the age of Acasta mafic rocks. Distinct from crystal accumulation which is previously recognized mafic rock at AGC, mafic rocks found in this study have trace element relative abundances similar to those of their parent magma, and possibly source material. Therefore, Acasta

mafic rocks represent the ideal target to further our knowledge of the evolution of the primordial terrestrial mantle as follows.

The Acasta mafic rocks represent the ideal place to know the Earth's mantle which has not yet been affected by the Late Heavy meteorite Bombardment (LHB) that was thought to have occurred between 4.1-3.8 Ga. Their modern basalt-like highly siderophile element compositions may simply reflect their mantle source which had a modern primitive upper mantle-like composition, suggesting that the late veneer did not relate to LHB and occurred before 4.3 Ga. In addition, considering that the accreted materials were homogenized within the mantle before 4.3 Ga, it is implied that the early mantle convection was rapid. However, we cannot rule out the scenario that source material of them was a pre-late veneer mantle because of their anomalously high initial $^{187}Os/^{188}Os$ ratio. To explore this possibility, further work is needed. For example, a study of whole rock ^{190}Pt-^{186}Os and ^{182}Hf-^{182}W isotope systematics would provide additional constraint.

Metabasalts from 3.8-3.7 Ga (or possibly 4.28 Ga) Isua Supracrustal Belt and Nuvvuagittuq Supracrustal Belt have negative to positive anomalies in $\mu^{142}Nd$ values. The majority of them have chemical features, such as fractionated or concave-upward trace element patterns with depletion of HFSEs, which are characteristic of subduction setting or crustal contamination. On the other hand, Acasta mafic rocks seem to be derived from mantle which have had not contaminated by any fluids or crusts. Therefore they would provide valuable information on a widespread characteristic of the Hadean mantle. Acasta mafic rocks are the first terrestrial samples which show a normal $\mu^{142}Nd$ values among mafic/ultramafic rocks older than 3.7 Ga. Furthermore, the consistency between trace element compositions and initial $^{143}Nd/^{144}Nd$ ratio of

them is substantial evidence to suggest their chondritic primitive mantle source. These observations imply the existence of primitive mantle extensively at 4.3 Ga and allow us to emerge new pictures about early mantle evolution: “Rapid mixing and homogenization of the Hadean mantle model” and “Undifferentiated mantle left in deep portion”. The former model is consistent with the implication from highly siderophile element composition.

ACKNOWLEDGEMENT

First of all, I would like to thank associate professor Tsuyoshi Komiya for his great support for my two years Master course and three years doctor course program. I am flattered that he gave me an opportunity to study. I am deeply grateful to assistant professor Akira Ishikawa for valuable advices on my study and experimental technique throughout my master and doctor course. The obtained results led to the discovery of the Earth's oldest rocks. I would grateful to associate professor Tetsuya Yokoyama for providing me access to Yokoyama laboratory and opportunity to analyze Sm and Nd isotopes. Thanks to Saya Kagami and Ryota Fukai for their help in the lab, I could get precise data. I am also grateful to Dr. Junichi Kimura for measuring Lu and Hf isotopes, Dr. Katsuhiko Suzuki for experiment assistance and Prof. Hikaru Iwamori and PhD. Kenta Ueki for their careful instructions in major element analysis. I thank Tsuyoshi Iizuka, Yuichiro Ueno, Ikuo Katayama, Walt Humphries, Diane Baldwin, Karen Gochnauer and Mark Senkiw for field assistance. This work also benefited from discussions with many colleagues, including Yukio Isozaki, Masaki Ogawa and other members of the Komaba Earth Science Group (Univ. Toyko). I would like to thank for them.